Universitat Politècnica de Catalunya
Escola Tècnica Superior d'Enginyeria
de Telecomunicació de Barcelona

Technische Universität Berlin
Fakultät IV - Elektrotechnik und Informatik

Master Thesis

Design and Simulation of Vertical Grating Coupler for Photonic Integrated System-in-Package

Oriol Gili de Villasante

Advisors: Prof. Dr. -Ing. Dr. -Ing. E.h. Herbert Reichl

Dr. –Ing. Tolga Tekin

Berlin, April 2010

Contents

Abstract V
Zusammenfassung VI
Acknowledgements VII

1. Introduction 1

2. System-in-Package and Silicon Photonics 3
2.1 System-in-Package 3
2.1.1 Motivation 3
2.1.2 Solutions 4
2.1.3 Applications 4
2.2 Silicon Photonics 5
2.2.1 Motivation 5
2.2.2 Solutions 6
2.2.3 Applications 6

3. SOI Waveguides 7
3.1 Introduction to waveguiding 7
3.2 Propagation theory 8
3.2.1 Polarisation 9
3.2.2 Modes in a waveguide 9
3.2.3 Effective index of a mode 9
3.2.4 Mode profiles 10
3.2.5 Quasi-TE and quasi-TM modes 11
3.3 Waveguide structures 12
3.3.1 Large single mode waveguides 13
3.3.2 Strip nano waveguides 14
3.4 Reported results 15

4. Coupling to fibre 16
4.1 Introduction to coupling 16
4.2 Coupling schemes 17
4.2.1 Horizontal coupling using tapered waveguides 17
4.2.2 Vertical coupling using a grating coupler 18
4.3 Grating coupler theory 19
4.3.1 Bragg diffraction 19
4.3.2 Reciprocity 20
4.3.3 Symmetry 20
4.3.4 Detuned gratings 21
4.3.5 Definitions 22

5. General theoretical background 24
5.1 Analytical calculations 24
5.1.1 Effective Index Method 24
5.1.2 Overlap 26
5.1.3 Interface loss 26
5.1.4 Confinement factor 27
5.1.5 Gaussian beam approximation 27
5.2 Simulation tools used in design 28
5.2.1 Film Mode Matching Method (FMM) 28
5.2.2 Finite Difference Time Domain (FDTD) 29
5.2.3 Perfectly Matched Layer (PML) 29

6. Fabrication techniques 30
6.1 Wafer fabrication 30
6.1.1 Separation by IMplanted OXygen (SIMOX) 30
6.1.2 Bond and Etch-back SOI (BESOI) 30
6.1.3 SmartCut Process 31
6.1.4 Silicon epitaxial growth 31
6.2 Waveguide fabrication 32
6.2.1 Critical dimension control 33
6.3 Grating fabrication 34
6.3.1 Optical lithography 34

6.3.2 Electron-beam direct-write lithography 34
6.3.3 Interference lithography 34
6.3.4 Dry etching 34
6.3.5 Focused Ion-Beam etching (FIB) 34

7. Review of existing grating coupler structures 35
7.1 One dimensional structures 35
7.1.1 Grating with upper index matching layer 35
7.1.2 Grating with bottom reflector 36
7.1.3 Grating with top mirror 36
7.1.4 Metal gratings 37
7.1.5 Blazed gratings 37
7.1.6 Chirped gratings 38
7.1.7 Gratings with rear reflector 38
7.1.8 Slot waveguide-based grating coupler 39
7.1.9 One-dimensional focusing gratings 39
7.1.10 Structures based on other materials 40
7.2 Two dimensional structures 40
7.2.1 Two-dimensional polarisation diversity gratings 40
7.2.2 Two-dimensional focusing grating couplers 40
7.3 Reported efficiencies 41

8. Waveguide design and simulation 42
8.1 Large single mode waveguides 42
8.1.1 Structure and simulation description 42
8.1.2 Mode mismatch loss 50
8.2 Nano strip waveguides 51
8.2.1 Structure and simulation description 51
8.2.2 Single mode region 52
8.2.3 Propagation profiles 53
8.2.4 Effective index 55
8.2.5 Confinement factor 56
8.2.6 Coupling losses 57

9. Grating coupler design and simulation 58
9.1 Structure description and design process 58
9.2 TE grating coupler 59
9.2.1 Optimal simulation period 59
9.2.2 Etch depth vary 60
9.2.3 Spectral response 61
9.2.4 Alignment tolerances 62
9.2.5 Propagation and index profiles 64
9.3 TM grating coupler 65
9.3.1 Optimal simulation period 65
9.3.2 Etch depth vary 66
9.3.3 Spectral response 67
9.3.4 Alignment tolerances 68
9.3.5 Propagation and index profiles 70
9.4 Crosstalk effects 71
9.4.1 Crosstalk effects for TE polarisation 72
9.4.2 Crosstalk effects for TM polarisation 73
9.5 Summarized results 74

10. Conclusions and future prospects 75
10.1 Conclusions 75
10.2 Future prospects 76
References 77

Abstract

As we approach the limits in operating speed of IC's predicted by Moore's Law, some alternative way of increasing velocities while reducing dimensions has to be found. In this context, optical interconnects appear to be an optimal solution that avoids the main limitations that electrical interconnects have.

To implement these optical interconnects in the already well developed CMOS integrated environment, the System-in-Package (SiP) and the Silicon on Insulator (SOI) technologies arise as a good solution to achieve these goals.

In this Thesis optical single mode strip nano waveguides and a grating coupler for vertical coupling to optical fibres are presented, designed and simulated. Their design parameters are optimized, and their performance analyzed and discussed.

Firstly, the characteristics of large single mode rib waveguides and their direct butt coupling to fibres is studied. Their performance is found to be not good enough when the dimensions were reduced to under 1 μm, with losses as high as 14.5 dB.

Therefore, nano strip waveguides are studied and simulated. They provide high light confinement and good propagation characteristics. Some performance characteristics (confinement factor, single mode region, effective index) are studied, for core widths in the range 100 – 600 nm.

The vertical coupling of these nano strip waveguides to optical fibres by means of a grating coupler is simulated with the FDTD technique. The main design parameters of this grating coupler are optimized, obtaining losses of 7 dB for TE polarisation and 8.5 dB for TM. The misalignment tolerances are also analysed.

The crosstalk effects between this grating and an hypothetical underlying waveguide are studied, showing that no light couples to the lower waveguide.

Zusammenfassung

Hinsichtlich unserer fortschreitenden Annäherung an die Grenzen der Geschwindigkeit von IC's, vorhergesagt durch das Mooresche Gesetz, muss eine alternative Methode zur Erhöhung der Geschwindigkeiten bei gleichzeitiger Verringerung der Dimensionen gefunden werden. In diesem Kontext scheinen optische Verbindungen eine optimale Lösung zu sein, welche die wichtigsten Einschränkungen elektrischer Verbindungen überwindet.

Zur Umsetzung dieser optischen Verbindungen in der bereits gut entwickelten CMOS integrierten Umgebung ergeben die System-in-Package (SiP) und Silicon on Insulator (SOI) Technologien eine gute Lösung, um diese Ziele zu erreichen.

In dieser Diplomarbeit werden optische Singlemode Strip Nanowellenleiter und ein Gitter-Koppler für die vertikale Kopplung von optischen Fasern vorgestellt, entworfen und simuliert. Ihre Design-Parameter werden optimiert und ihre Leistungen analysiert und diskutiert.

Zunächst werden die Eigenschaften von großen Singlemode Rib Wellenleitern und ihre direkte Stirnkopplung zu Fasern untersucht. Ihre Leistung wird als unzureichend befunden, wenn ihre Dimensionen unter 1 µm reduziert werden - mit Verlusten von bis zu 14,5 dB.

Daher werden anschließend Strip Nanowellenleiter untersucht und simuliert. Sie bieten eine hohe Lichtausbeute und gute Entbindungs- und Ausbreitungseigenschaften. Einige Leistungsmerkmale (Entbindungs-Faktor, Single-Mode-Region, effektiver Index) werden in Kernbreiten im Bereich von 100 bis 600 nm untersucht.

Die vertikale Kopplung dieser Strip Nanowellenleiter mit optischen Fasern durch ein Gitter-Koppler wird mit der FDTD-Technik simuliert. Die wichtigsten Design-Parameter dieses Gitterkopplers sind optimiert, mit enthaltenen Verlusten von 7 dB für die TE Polarisation und 8,5 dB für die TM Polarisation. Die Versatz-Toleranzen sind ebenfalls analysiert.

Die Crosstalk-Effekte zwischen diesem Gitter und einem hypothetisch zugrundeliegenden Wellenleiter sind untersucht und zeigen, dass kein Licht auf den unteren Wellenleiter gekoppelt wird.

Acknowledgements

I would like to thank Prof. H. Reichl for granting me the opportunity to work in his department. His experience and wisdom were very inspiring.

I am also grateful to Dr. Tolga Tekin, for his tutoring and his care in all the aspects of my work with him.

I want to thank the Erasmus Program, the Technische Universität Berlin and the Universitat Politècnica de Catalunya for giving me the opportunity of enjoying such a enriching personal experience in Berlin.

I am also thankful to Zheng Wang, with whom I work, for the clarifying conversations we had, covering all kind of subjects.

I would like to thank José Vicente Galán as well, for his kind support and helpful advice.

I am also grateful to Sesilia Kriswandhi, Remco Stoffer and Arjen Bakker, for their help and interest regarding simulation issues.

A special mention has to be given to Pablo Cavero and Juan García, for the hours we spent together working in our respective Thesises. Their friendship and companionship was very useful.

And last but not least, I want to give a special mention to my family and friends, who have always supported my decisions and helped me. To them I dedicate this.

Chapter 1

Introduction

Today's integrated chips have to meet the requirements of an rapidly growing demand for increased performance, smaller size, lower power and lower cost, and these cannot always be met with conventional packaging and interconnect technologies. There are limitations in interconnect density, thermal management, bandwidth and signal integrity that cannot be improved with conventional technology. [1]

System-in-Package (SiP) technology is perhaps the most important technology to address these limitations. However, the overall performance, cost, size, and functionality of a SiP will be limited by the interconnects. [2]

Electrical interconnects face critical tradeoffs between power consumption, interconnect area, and signal integrity, even at interconnect lengths as short as the board, module, and chip level. Physical material and structural limitations will ultimately force technology changes at the physical layer if interconnect and system performance gains are to continue well into the future.

Optical interconnects arise in this situation as the optimal solution to overcome the physical limitations of electrical interconnects. Optical technology now stands at a threshold where the integration of optical interconnections and optical functions into board, package, and chip-level electrical systems is projected in industry roadmaps. [3]

To implement these optical interconnects the Silicon-on-Insulator (SOI) technology appears to be the perfect solution. Low costs and good fabrication characteristics can be achieved, because it takes advantage of the already existing and well developed Complementary Metal-Oxide-Semiconductor (CMOS) integration technology.

In order to integrate this new photonic "layer" in the SiP, the connection with the rest of the devices in the system has to be built. This is achieved by means of some coupling techniques. These can be basically in-plane or out-of-plane coupling devices.

In this context finds this thesis its motivation. Optical waveguides are designed and simulated, as well as a grating coupler structure to perform an out-of-plane coupling.

In Chapter 2 a general overview of the System-in-Package (SiP) and Silicon Photonics technologies is given, as well as the solutions they provide and some practical applications.

Chapter 3 gives a general idea of Silicon-on-Insulator (SOI) waveguides. A general theoretical background of propagation theory is given, as well as an explanation of the waveguide structures and some references to the studies that have already been performed in this field.

In Chapter 4 the coupling problem and the main solutions are presented. The theory involving grating couplers is explained too.

Chapter 5 contains a presentation of the analytical calculations and the principal simulation methods that have been used to simulate the structures presented in this Thesis.

In Chapter 6 the most common fabrication techniques for waveguides and grating couplers are reviewed.

Chapter 7 is a review of state-of-the-art grating coupler approaches and the efficiencies that have been obtained.

In Chapter 8 the design and simulation process for the nanowaveguides object of study are presented and explained, and the obtained results are discussed in detail.

In Chapter 9 the grating coupler structure is designed and simulated for both TE and TM polarisations.

Chapter 10 contains the evaluation of results and some future prospects.

Chapter 2

System-in-Package and Silicon Photonics

In this section the System-in-Package and Silicon Photonics technologies are presented.

2.1 System-in-Package

System-in-Package is a combination of multiple active electronic components of different functionality, assembled in a single unit that provides multiple functions associated with a system or sub-system. A SiP may optionally contain passives, Microelectromechanical Systems (MEMS), optical components and other packages and devices. [2]

2.1.1 Motivation

The market demand for increased performance, smaller size, lower power and lower cost cannot be satisfied with conventional packaging and interconnect technologies. There are limitations in interconnect density, thermal management, bandwidth and signal integrity that cannot be solved with the existing technological solutions. System-in-Package technology is probably the most important technology to address these limitations. [2]

SiP has evolved as an alternative to System-on-Chip (SoC) for integration because this technology provides advantages over SoC in many market segments. SiP is not a substitute for high level, single chip, silicon integration but should be viewed as complementary to SoC. For some very high volume applications SoC will be the preferred approach. Some complex SiP products can contain SoC components. [3]

The main goal of SiP is to integrate many different components (e.g. passives, MEMS or optical components) into a single package. A long term vision for SiP is the optimized heterogeneous integration of wireless, optical, fluidic and biological sensing interfaces. This goal requires new materials and control of their interactions in the submicron scale. Figure 2.1 shows a general scheme of this integration. [1]

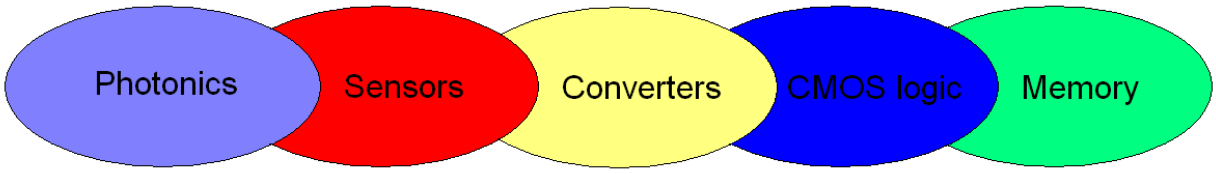

Figure 2.1: System-in-Package integration.

2.1.2 Solutions

The improvements over SoC that SiP provides are, among others, more integration flexibility, faster time to market, lower Research and Development costs and lower product cost than SoC for many applications.

The objectives of using SiPs are therefore to provide alternate and cheaper solution for SOC, as SOC sometimes take longer to fabricate and reach the market, to provide higher levels of integration and better electrical performance, and to reduce overall assembly size and weight and achieve cost effectiveness. [4]

The main advantages that SiP provides include:

- More functionality per package – each SIP may carry more modular functions,
- More capacity and higher efficiency,
- Easier board design and layout, quicker turn around and time to market,
- Higher manufacturing yield, lower cost and faster throughput,
- Better electrical performance could be achieved in most cases,
- Modular design and more interchangeable parts. [4]

However, thermal dissipation imposes the most serious limitation to the integration density that can be achieved. This issue will limit the packing density, size, cost, and performance of SiP. [3].

These limitations can be addressed with optical interconnects. This technology will be treated in more detail in the next section.

2.1.3 Applications

It is clear that SiP will be of direct application in the market sections that have to satisfy a rapidly increasing demand, such as the portable consumer electronics devices (digital cameras, video recorders, music players and mobile phones). SiPs are also moving into computing, communications and other applications in medical electronics, space and military electronics. [4]

The requirements in transmission velocity, amount of data and integration are increasing rapidly in the mentioned fields, so the possibilities that SiP offers will have to satisfy this growing necessities.

2.2 Silicon Photonics

Silicon based optoelectronics (OE's) is a wide-ranging technology that aims to take advantage of the cost-effectiveness and known performance characteristics of silicon based electronic circuits by integrating photonic components on digital and wireless silicon integrated circuits (IC's).

On-chip integrated designs is the main objective that has to be achieved in order to allow silicon-based OE's to participate in key aspects of the global photonics industry, such as the 1.3 and 1.55 μm telecommunication systems. [5]

2.2.1 Motivation

The most accepted argument in favour of silicon photonics is based on its compatibility with the well developed silicon IC manufacturing. Silicon wafers have the lowest cost and the highest crystal quality of any semiconductor material. The industry has the capability to produce microprocessors with millions of elements, all integrated onto small surfaces, and their prizes are low enough to appear in consumer electronics. Silicon manufacturing offers the best balance between technological sophistication and economics of scale.

Creating low-cost photonics for mass-market applications by exploiting the developed chip integration industry has been the traditional motivation for silicon photonics researchers. Another motivation is the availability of high-quality SOI wafers, an ideal platform for creating optical waveguide circuits. The strong optical confinement offered by the high index contrast between silicon (n ~ 3.5) and SiO_2 (n ~ 1.5) makes it possible to scale photonic devices to the submicron level. Such lateral and vertical dimensions are required for true compatibility with IC processing.

In addition, the high optical intensity arising from the large index contrast (between Si and SiO_2) makes it possible to observe nonlinear optical interactions, such as Raman and Kerr effects, in chip scale devices. This fortuitous outcome has enabled optical amplification, lasing, and wavelength conversion, functions that until recently were perceived to be beyond the possibilities of silicon. However, further investigation still has to be performed in order to obtain fully integrated and reliable silicon photonics devices.

Silicon has excellent material properties that are important in photonic devices. These include high thermal conductivity , high optical damage threshold, and high third-order optical nonlinearities. Silicon has a low absorption coefficient, which originates a low-loss wavelength window extending from 1.1 to nearly 7 μm . This makes silicon a perfect material for use in the data communication band of 1.3 - 1.55 μm. [6]

2.2.2 Solutions

Over the past 30 years, the electronics industry has improved the performance of silicon-based integrated circuits at an astounding rate. Moore's Law [2], which says that the number of transistors per IC grows exponentially in time, was formulated in the 1970's.

It seems feasible that this prediction will continue to be true, provided that some critical technological problems, which are due to the physical limitations of electrical interconnects, are solved.

These include excessive power dissipation, insufficient communication bandwidth, signal delay, high losses in the substrate dielectric, reflections and impedance discontinuities, and susceptibility to crosstalk. [1]

These critical problems that electrical interconnects have can be solved with the solutions optical interconnects provide, which include [7]:

- Reduced parasitics: the RC delay of the electrical interconnection used today increases with the reducing feature size and has become the major bottleneck in chip speed. To overcome this challenge, optical interconnection is gaining significant interest as an alternative.
- Higher transmission velocities: the capacity of an electrical connection depends on its geometrical aspect ratio, so there is a limit in this capacity that cannot be overcome. The capacity of an optical channel is essentially independent of length at the distances used within a computer because of the low losses in optical transmission
- Lower power needed: despite the benefits of scaling, new generations of CMOS usually have greater power dissipation than their predecessors. It has been shown that optics uses less energy at all distances.
- Compatible with CMOS VLSI: silicon-based optoelectronics can take advantage of the existing integrating technologies to be produced. In this thesis, we will be taking into account the Silicon-On-Insulator (SOI) technology, which should be fully compatible with the existing VLSI processes.
- Lower cost: given the previously explained points of reduced parasitic, which allows a greater scale of integration, and the CMOS compatibility, the OE devices can be produced at lower cost.

2.2.3 Applications

If we look across the range of present and potential uses of silicon photonics, we can identify applications in photonic interconnects, data communication, telecommunication, specialized signal processing, switched networks, imaging, displays, radio frequency/wireless photonics, electronic warfare, photonics for milimeter-wave/microwave/radio-frequency systems, laboratory-on-a-chip, medical diagnosis, spectrometeron-a-chip, photonic sensing of chemical/biological/physical variables, sensor fusion, neural networks, bionics, analog-to-digital conversion, optical storage, optical logic, electrooptical logic, and testing of CMOS circuits. [8]

Chapter 3

SOI Waveguides

In this Chapter a general theoretical overview of waveguiding and propagation theory is given, and the waveguide structures that are going to be used in this work are presented, as well as some results from the literature.

3.1 Introduction to waveguiding

The basic elements of silicon electronics are transistors and interconnects: the transistors perform logic operations, while the interconnects transfer digital information between these transistors.

The performance of transistors has steadily been improved by the shrinking of their dimensions. Interconnect performance, however, does not typically get better when sizes are reduced. Electrical interconnects were improved in the past by changing the technology used to fabricate the wiring layers. The ultimate limitations of electrical interconnects have physical, not technological, origins, and these limits are rapidly approaching.

The use of optical links can be the way to avoid the problems of electrical transmission. These optical interconnects are still the most promising candidate to solve the challenges imposed by electrical wiring, both for off-chip and possibly on-chip applications. [7]

The band gap of silicon (~1.1 eV) is such that the material is transparent to wavelengths commonly used for optical transport (around 1.3–1.6μm). One can use standard CMOS processing techniques to sculpt optical waveguides onto the silicon surface. Similar to an optical fibre, these optical waveguides can be used to confine and direct light as it passes through the silicon. [9]

Due to the wavelengths typically used for optical transmission and silicon's high index of refraction, the feature sizes needed for processing these silicon waveguides are on the order of 0.5 – 1 μm.

SOI single-mode rib waveguides with core dimensions comparable with single-mode optical fibres have previously been demonstrated.

In many cases, these large dimensions are needed because one uses waveguides with a low refractive index contrast. By increasing this index contrast, the confinement can be improved, but this also means that the waveguide core should be reduced in size to keep the waveguide single mode. Then, however, the geometrical features not only become very small but have to be very accurately fabricated. [10]

3.2 Propagation theory

A very simple approach to describe the propagation of guided waves in a given medium is the optical ray model, which provides a good understanding of this propagation without having to handle with the solution to Maxwell's equations. [9].

The basic law that this model uses to describe the behaviour of propagating waves in the surface between two mediums (or interface) with different refractive indexes is Snell's Law, which says that an incident field to this surface will be partly transmitted and partly reflected.:

$$n_1 \sin\theta_1 = n_2 \sin\theta_2 \tag{3.1}$$

being n_1 and n_2 the refractive indexes of the mediums, and θ_1 and θ_2 the angle of reflection and the angle of transmission, respectively.

It can be demonstrated from this law that angles smaller than a critical angle θ_c will experiment total internal reflection (TIR), which means that there is no transmitted field. This angle is given by the next expression:

$$\sin\theta_c = \frac{n_2}{n_1} \tag{3.2}$$

This law applies also in the case of ge*n*eric slab waveguides, like the one depicted in Figure 3.1. It can be shown that the propagation in such a waveguide will experiment total internal reflection in both interfaces.

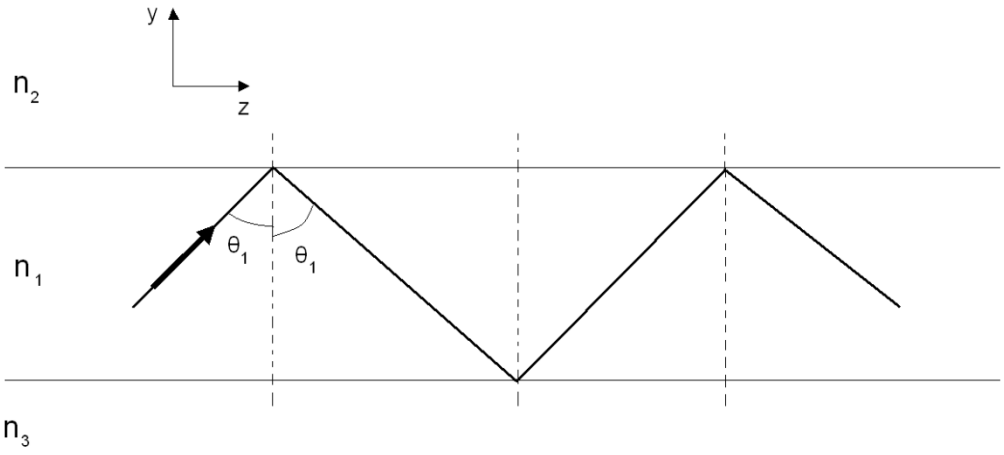

Figure 3.1: Waveguide propagation by total internal reflection (after [9]).

In general $n_1 > n_2, n_3$ to ensure propagation by total internal reflection. In the case of $n_2 = n_3$ the waveguide is called symmetrical, and asymmetrical if not.

In the following sections the basic characteristics of guided waves are described, which will be used to characterize and describe the behaviour and performance of optical devices.

3.2.1 Polarisation

The fields that can propagate in a medium are normally classified in two possible polarisations: transverse electric (TE), when the electric field is perpendicular to the plane of incidence, or transverse magnetic (TM), when the magnetic field is perpendicular to the same plane. [9]

3.2.2 Modes in a waveguide

However, light only propagates in a set of allowed discrete angles. The equation that has to be solved (for TE modes) in a generic asymmetrical waveguide is the following:

$$k_0 n_1 h \cos\theta_1 - m\pi = \tan^{-1}\frac{\sqrt{\sin^2\theta_1 - (\frac{n_2}{n_1})^2}}{\cos\theta_1} + \tan^{-1}\frac{\sqrt{\sin^2\theta_1 - (\frac{n_3}{n_1})^2}}{\cos\theta_1} \quad (3.3)$$

with $k_0 = {}^{2\pi}/_{\lambda_0}$ the propagation constant in free space and h the height of the core layer.

Every allowed angle gives place to an specific field, also called mode of propagation, and is indicated by its mode number with the index *m*. The mode with m = 0 is known as fundamental mode.

For every interface the critical angle will be different, so the angle that guarantees total internal reflection in both interfaces is the one that gives solution to this equation (the larger).

Monomode conditions can be derived from this equation. Single mode waveguides do not suffer from intermodal dispersion, which is the dispersion caused by the different velocities with which every mode travels in the waveguide. In this way the shape of the transmitted signal remains more similar after going through the waveguide. In addition, if the waveguide is multimode, the total power transmitted has to be shared by all the modes, and so the fundamental mode has lower power.

3.2.3 Effective index of a mode

The propagation constant in the z direction, k_z (or β), shows with which velocity the wave propagates in this direction.

The following equation gives the value of this constant:

$$k_z = n_1 k_0 \sin\theta_1 \quad (3.4)$$

We can define $N = n_1 \sin\theta_1$, which is known as the effective index of the mode. This would be equivalent as thinking of the mode propagating along the z direction, without reflecting in the interfaces of the waveguide.

It can be shown that $n_2 \leq N \leq n_1$, with n_2 being the refractive index of the medium that limits total internal reflection.

3.2.4 Mode profiles

The general solution to the wave equation for TE modes in planar waveguides, which is of the form [9]:

$$\nabla^2 \mathrm{E} = \mu_m \varepsilon_m \frac{\partial^2 \mathrm{E}}{\partial \mathrm{t}^2} \tag{3.5}$$

with $\mathrm{v} = {}^{1}/_{\sqrt{\mu_m \varepsilon_m}}$ the velocity of a wave.

is the following:

$$\mathrm{E_x} = \mathrm{E_c}\, \mathrm{e}^{-\mathrm{k_y y}}\, \mathrm{e}^{-\mathrm{j}\beta \mathrm{z}}\, \mathrm{e}^{\mathrm{j}\omega \mathrm{t}} \tag{3.6}$$

The $\mathrm{e}^{-\mathrm{j}\beta \mathrm{z}}$ corresponds to a propagating sinusoidal type field, while the $\mathrm{e}^{-\mathrm{k_y y}}$ represents fields propagating in the y direction through the claddings. That means that the field penetrates the cladding with a decay constant k_y, so part of the field is propagating through the cladding.

So after obtaining this solution, it is possible to plot the field distribution, $E_x(y)$, or the intensity distribution, $|E_x(y)|^2$ for the different modes, in order to have an idea of how the field propagates through the waveguide. Figure 3.2 shows these distributions:

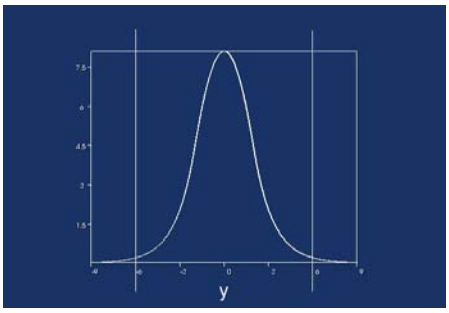

(a)

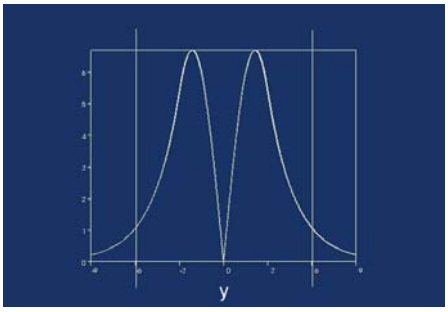

(b)

Figure 3.2: (a) Intensity distribution in the y direction for the fundamental mode (m = 0)

(b) Intensity distribution in the y direction for the first order mode (m = 1).

3.2.5 Quasi-TE and quasi-TM modes

In practice, the fields that propagate through a waveguide will not be exactly TE or TM modes, that is, they will also have field distribution in the direction perpendicular to the direction in which they are polarized. So, if considering electrical fields, TE modes is in the x direction and has some field energy in the y direction, and TM modes are normally in the y direction but have some energy in the x direction.

Therefore, a criteria has to be chosen to be able to differentiate between modes. This is the following:

For TE modes:

if $Re(E_x) >> Re(E_y)$, the mode is said to be quasi-TE or directly TE.

For TM modes:

if $Re(E_x) << Re(E_y)$, the mode is said to be quasi-TM or TM.

Figure 3.3 shows some example simulation plots of these real parts. It can be seen that the fields differ in at least an order of magnitude.

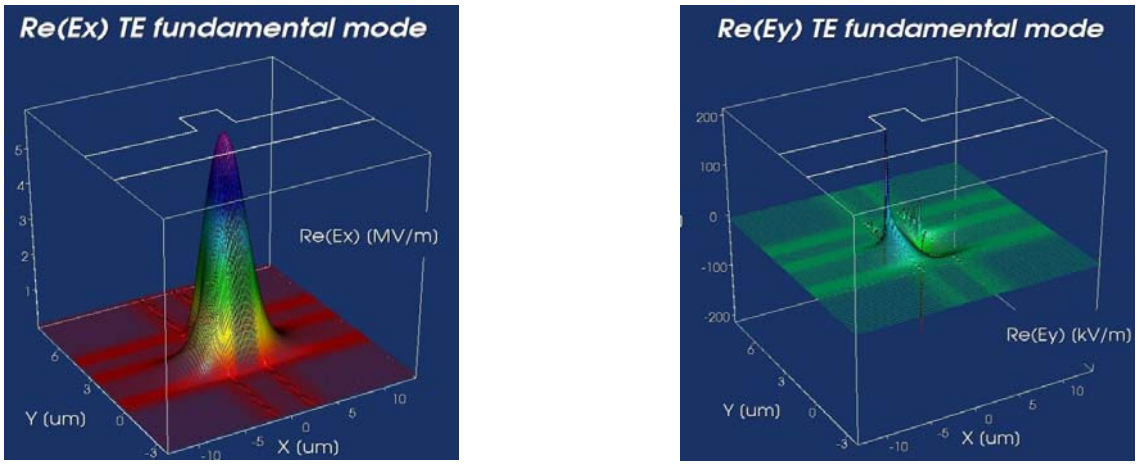

(a). (b)

Figure 3.3: (a) Real part of the electric field of the fundamental mode in the x direction

(b) Real part of the electric field of the fundamental mode in the y direction

3.3 Waveguide structures

In this section the structure of an SOI wafer and the possible waveguide structures are exposed.

The configuration of an SOI wafer is shown in Figure 3.4. A silicon dioxide layer is grown under the surface of the silicon wafer. The top layer is then used as the guiding layer.

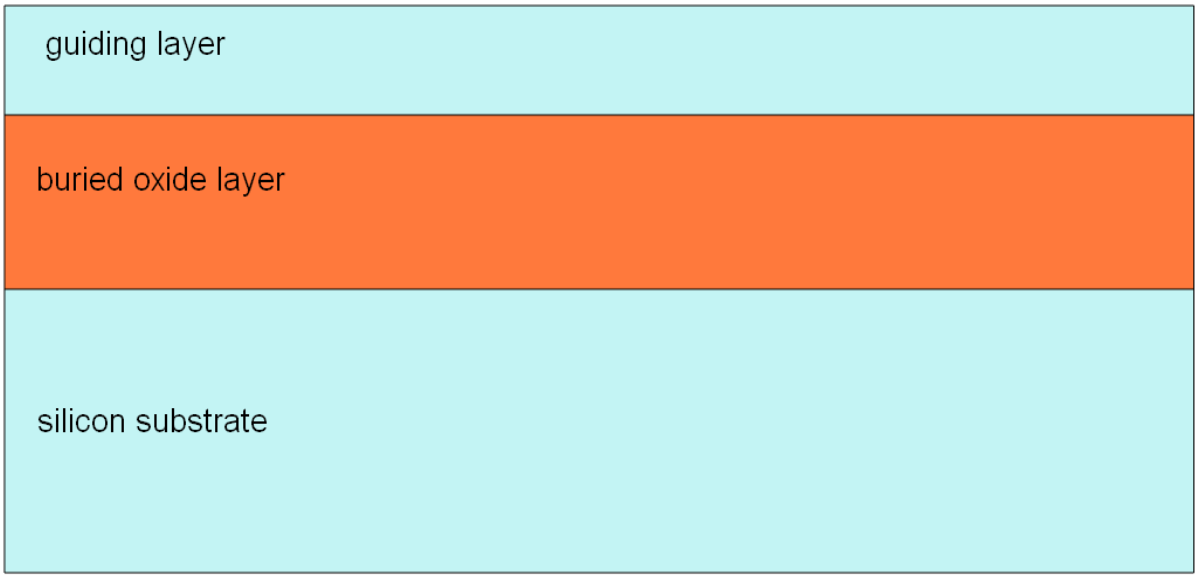

Figure 3.4: SOI wafer structure.

The purpose of the buried oxide layer is to act as the lower cladding layer, and hence prevent the field associated with the optical modes from penetrating the silicon substrate below. Therefore as long as the oxide is thicker than the evanescent fields associated with the modes it will be satisfactory. [9]

In some cases, the waveguide is transformed from an asymmetrical waveguide into a symmetrical one by the addition of a surface oxide layer. In practice, however, the refractive indices of both air *(n* = 1*)* and silicon dioxide *(n* ~1.5*)* are so different from that of silicon *(n* ~ 3.5*)* that the two configurations are very similar.

For many applications, two dimensional confinement is required. This is achieved in silicon by etching a two-dimensional waveguide. There are two main possible structures that can be etched in the silicon layer.

When the dimensions of the core width range from 1 μm to 4 μm, we talk about rib or ridge waveguide structure. The next step is to bring the dimensions of the core width to be in the order of hundreds of nanometers. This is achieved with the so called strip waveguide. Both structures will be explained in more detail in the next section.

3.3.1 Large single mode waveguides

Rib (or ridge) waveguides are composed of a core and two lateral slab regions etched on the silicon layer. The lateral confinement is achieved by means of the leakage of the higher order modes in these lateral slab regions. The cross-section of a rib waveguide is shown in Figure 3.5.

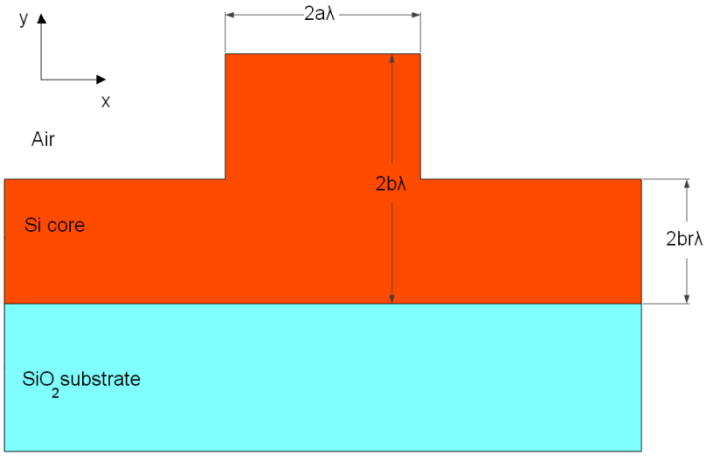

Figure 3.5: Large single mode rib waveguide cross section after [11].

The core has a width of 2aλ and a height of 2bλ, while the lateral slab regions have a height of 2brλ. The parameter r is defined as the ratio of slab height to rib height, or outer-inner ratio.

This structure has been demonstrated to be single mode when the next condition is true (in the limit of large b):

$$\frac{a}{b} \leq c + \frac{r}{\sqrt{(1 - r^2)}} \quad (for\ 0.5 \leq r \leq 1) \tag{3.7}$$

With *c* a constant that was considered to be equal to 0.3 by Soref and Petermann [11] and has been recalculated and found to be equal to –0.05 (Pogossian et al. [12])

We will restrict our consideration to rib guides with $0.5 \leq r < 1$. Having this in mind, higher-order modes in the vertical direction will be cut off because the higher-order modes in the central rib section will be coupled to the fundamental mode of the slab section, which becomes leaky for $r \geq 0.5$. This happens at $r \geq 0.5$ because the effective index of the fundamental slab mode becomes higher than the effective index of any higher-order vertical mode in the central rib region.

Intuitively speaking, the second-order modes in the vertical direction, have a double-peaked intensity distribution along the vertical axis. For $r \geq 0.5$, one of the two peaks (the lobe near the bottom of the guide) will couple out into the fundamental slab mode of the rib side regions. This lateral leakage ensures that theFirst-order modes will not propagate. That is why the condition $0.5 \leq r < 1.0$ guarantees single-mode operation of the rib in the vertical direction.[11]

In this type of structure, it has to be assured that the SiO_2 layer thickness is thick enough.The dimensions of the waveguide (width, height and slab height) are critical to define the single mode region and have to be accurately designed.

3.3.2 Strip nano waveguides

The next step towards miniaturization is bringing the waveguide to dimensions in the order of several nanometres. Recent technological advances make possible this reduction of dimensions. In this case the strip structure is used, in order to achieve higher light confinement.

Figure 3.6 shows the structure of a strip nano waveguide.

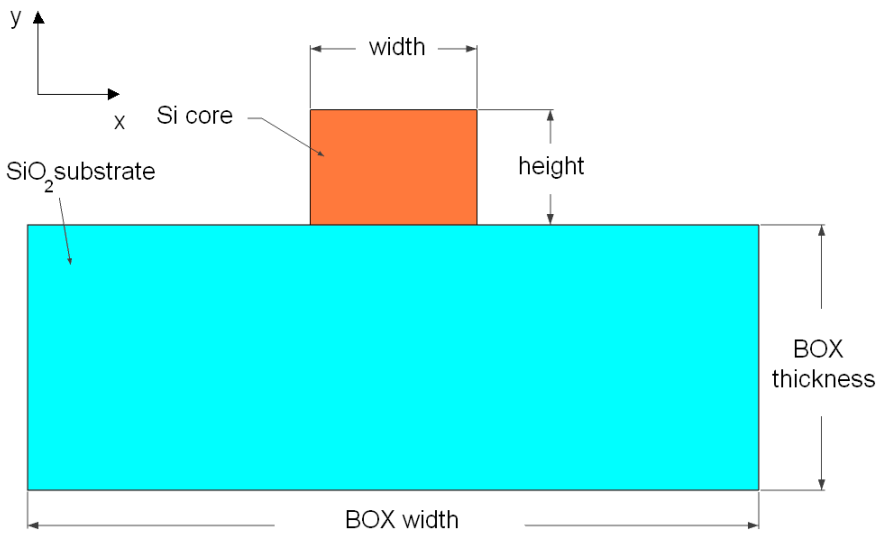

Figure 3.6: Strip nano waveguide cross section.

In this case, the core width and height define the single mode region, but the SiO_2 layer width and thickness have to be calculated to obtain good coupling conditions, because the input field is launched in the cladding and then couples to the core.

For this type of structures there is no single mode condition that has been successfully demonstrated, so results are based on measurements and simulations. Several studies in this field have been performed. They say that the single mode condition is the following [13]:

$$H < 2.109e^{-11.93W} + 0.7365e^{-1.956W} \tag{3.8}$$

For a single polarisation mode (TE or TM) the condition is modified to:

$$H < 63.13e^{-23.92W} + 0.2684e^{-0.8577W} \tag{3.9}$$

Figure 3.7 shows the single mode regions for both polarisations. A is the single mode region for TM polarisation, B is the single mode region for TE polarisation, C is single mode for both TM and TE polarisations, D is the multimode area [13].

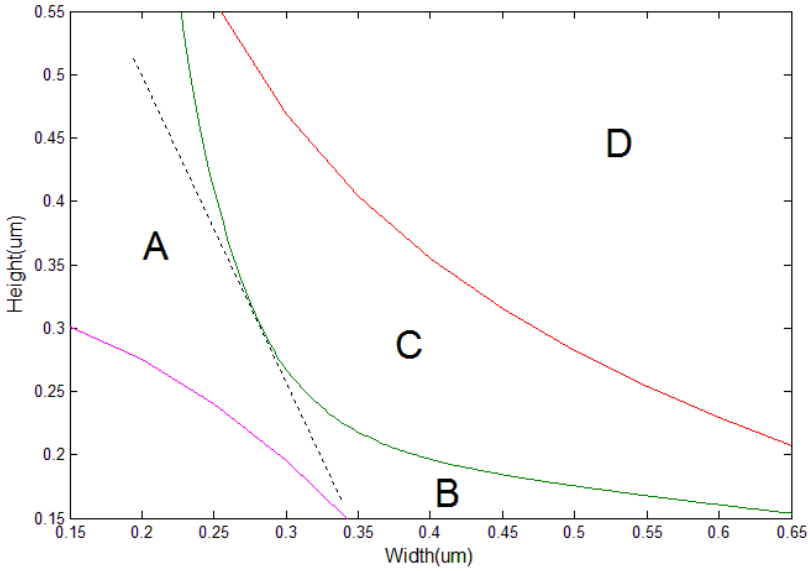

Figure 3.7: Modal regions of the strip nano waveguide.

3.4 Reported results

Many different designs and experimental approaches have been developed in order to find the optimal strip waveguide structure that provides minimal propagation losses. Table 3.1 summarizes the main ones.

	IBM [14,15]	IMEC [10]	NTT [16]	LETI [17]	Cornell [18,19]
Core height (nm)	220	220	200	200	270
Core width (nm)	460	500	400	500	470
BOX thickness (μm)	2.0	1.0	3.0	0.7	3.0
Loss (dB/cm)	3.6	2.4	2.8	6.4	5.0

Table 3.1: Strip waveguide results.

A general overview of the achievements in this field can be seen in [19].

Chapter 4

Coupling to fibre

4.1 Introduction to coupling

Efficient coupling between standard single mode fibres (SMF) and single mode waveguides is a key challenge in silicon photonics. Integrated circuits need an interface to the outside world, and that is what the coupling devices attempt to provide.

The small size of single mode silicon on insulator waveguides compared with the diameter of a single mode fibre makes coupling inefficient.

The silicon waveguide is extremely small, with a core cross sectional area of approximately 0.1 μm², which correspond to core heights and widths around 0.4 μm. By comparison an optical fibre has a core with a cross sectional area of around 250 μm² (with a radius of 8-10 μm), three orders of magnitude larger.

Thus, coupling light from an optical fibre into a silicon waveguide is like pouring water from a fire hose into a straw – most of the light will spill around the edges and be lost. So, it is important to be able to focus the light from a fibre down to the spot size of the silicon waveguide. Traditional approaches to this challenge are costly and require difficult and accurate alignment. [20]

There are some approximations to the solution of this problem which have better performance as the simple butt coupling between the fibre and the waveguide, due to the elevated coupling losses that this method presents. These solutions are presented in the following section. Figure 4.1 shows the dimension differences between a SMF fibre and a silicon single mode waveguide.

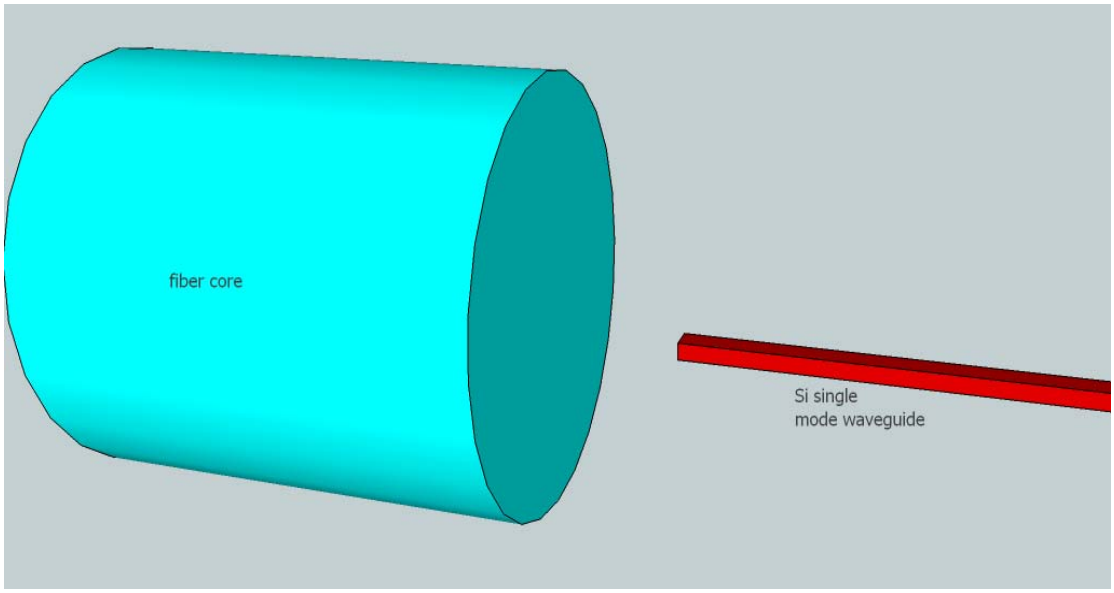

Figure 4.1: Fibre butt coupling to waveguide.

4.2 Coupling schemes

There are two basic fibre to waveguide coupling schemes: in-plane and out-of-plane couplers. Their coupling schemes and operating characteristics are presented in the following sections.

4.2.1 Horizontal coupling using tapered waveguides

Tapers that attempt to improve the coupling efficiency by reducing the mode dimensions of the field coming out of a SMF fibre to fit them into the waveguide dimensions have been suggested. However, to avoid excessive coupling to radiation modes in the taper, the required typical taper length must be of the order of millimeters. In addition, these tapers suffer from strong back reflections at the facet of the coupler.

Inverse tapers, from the waveguide dimensions to the dimensions of a small tip, have been proposed for coupling laser diodes to optical fibres. These structures rely on the evanescent field at the tip to increase the mode size of the waveguide to that of the fibre. However, these structures are hundreds of micrometers long. [21]

Figure 4.2 shows the inverse taper and the alignment to the fibre. These kind of structures offer a robust coupling to fibre. An example of inverse taper design is in [22].

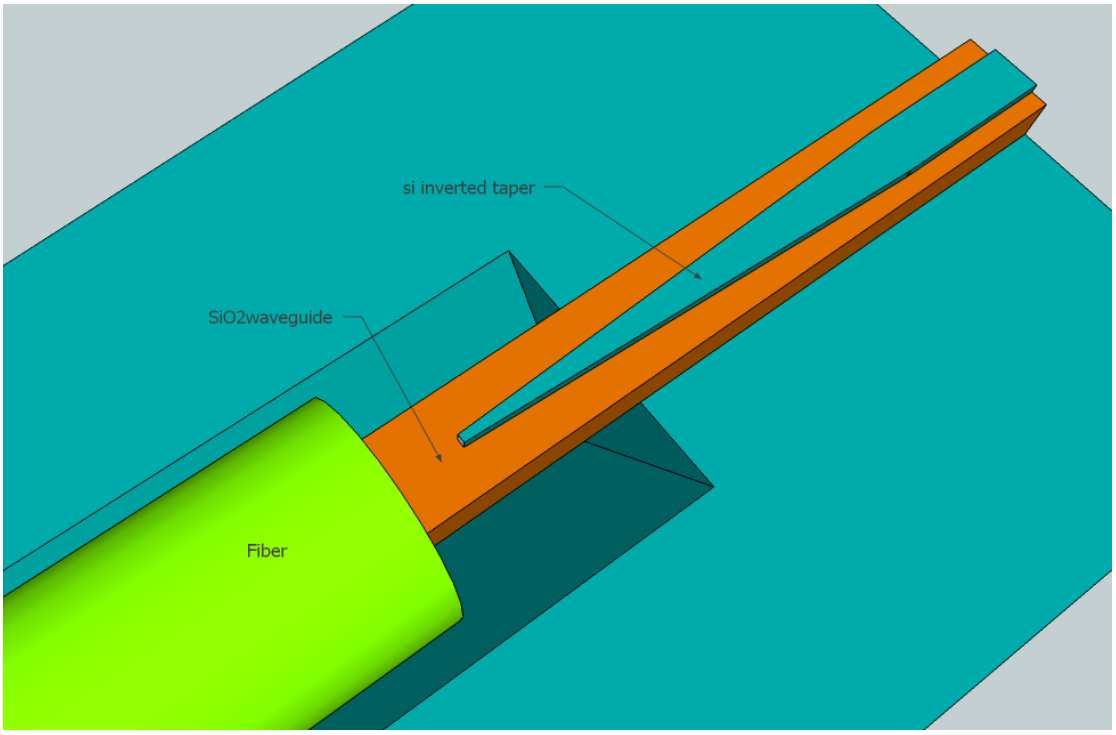

Figure 4.2: Coupling to fibre using an inverse taper after [22].

4.2.2 Vertical coupling using a grating coupler

Another solution is to use grating couplers followed by a taper to adjust the lateral size of the incident beam to the sub-micrometer waveguide width.

These devices take advantage of the Bragg diffraction phenomenon to couple the light coming from a fibre. Several developments of this initial idea have been proposed to reduce the losses, but not all of them are regarded to be fully CMOS compatible.

Figure 4.3 shows the coupling scheme to fibre. These kind of structures are not so robust, but have the advantage that couple light from standard, non-lensed single mode fibres.

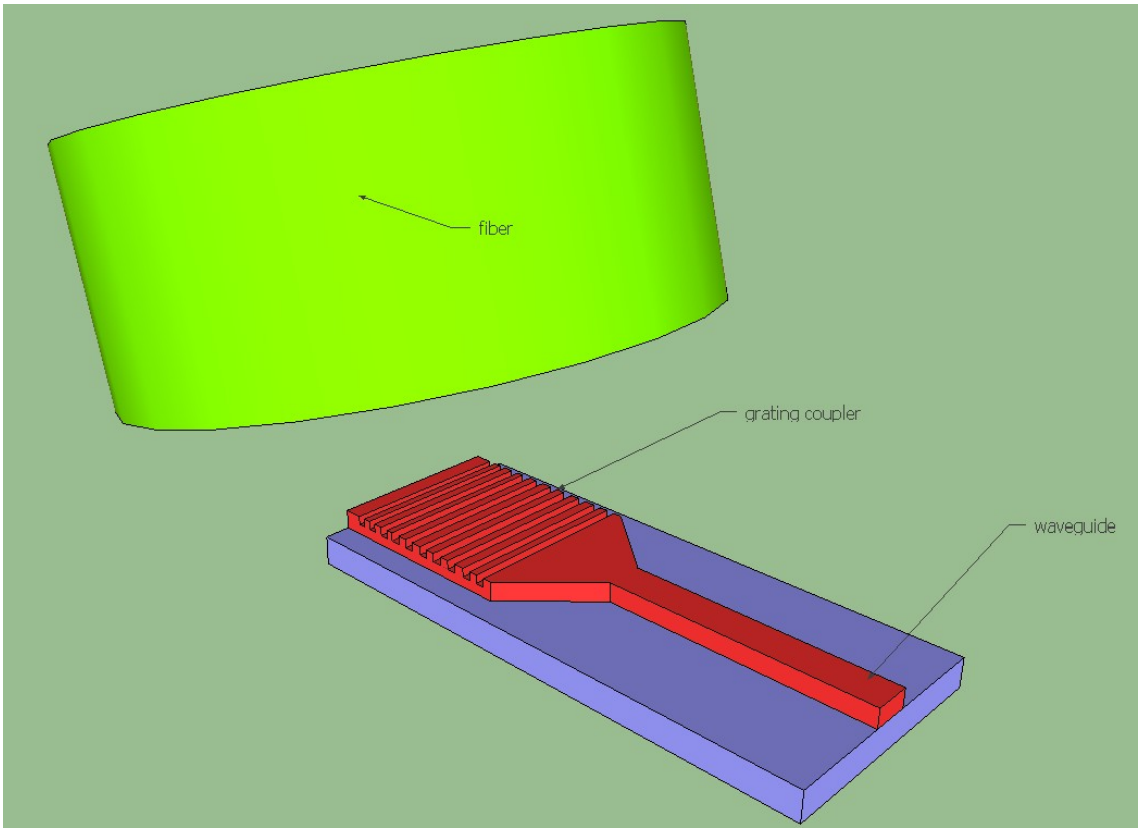

Figure 4.3: Coupling to fibre using a grating coupler.

4.3 Grating coupler theory

In this section the theoretical issues that are necessary to understand the grating coupler are explained, as well as the parameters that take part in the design process.

4.3.1 Bragg diffraction

When the incident light comes to the surface of a periodic structure, it will be diffracted. The Bragg condition describes the relation between the wave-vectors of the incident and diffracted waves. When there is no grating at the interface between the two materials, the Bragg condition is the same as Snell's Law, which describes refraction at the interface between two materials.

For grating couplers, the Bragg condition can be written as follows, for the first order diffraction:

$$k_{in} \sin\theta + \frac{2\pi}{\Lambda} = \beta \tag{4.1}$$

With $\beta = \frac{2\pi}{\lambda_0} n_{eff}$ the propagation constant of the guided mode, λ_0 the desired wavelength and n_{eff} the effective index of the fundamental mode, $k_{in} = \frac{2\pi}{\lambda_0} n_{top}$ is the wave vector of the incident wave, n_{top} the refractive index of the background, θ is the incidence angle, and Λ is the grating period. [24]

The Bragg condition is only exact for infinite structures. In finite structures there is a finite range of k vectors around the predicted one in which diffraction occurs. Figure 4.4 shows a simplified representation of the wave diffraction on the surface of the grating.

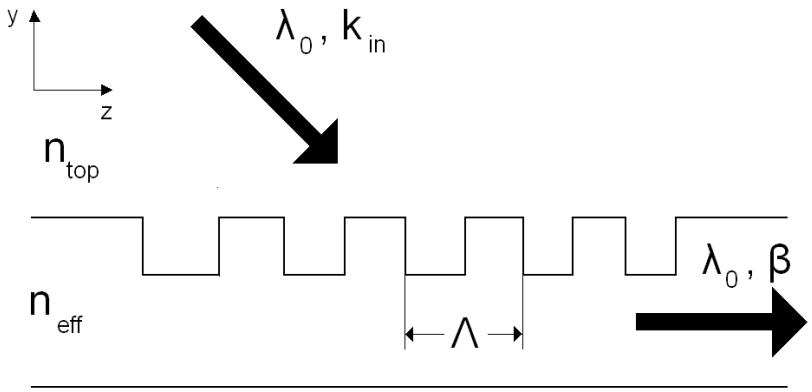

Figure 4.4: Bragg diffraction on the grating surface.

4.3.2 Reciprocity

In electromagnetic theory, it can be shown that, when the materials in a system are reciprocal, the scattering matrix, which describes the relations between the inputs and the outputs, is symmetrical. This is known as the reciprocity or symmetry theorem. Then, the elements of this matrix follow the following relation [23]:

$$S_{ij} = S_{ji} \tag{4.2}$$

This can also be applied to systems in which energy leaks out.

In our case this is very useful, because it means that we can either simulate the coupling from fibre to waveguide or from waveguide to fibre. Since we are using single-mode waveguides and fibres, the coupling efficiency will be the same in both cases.

4.3.3 Symmetry

If the optical fibre is vertically coupled to the grating, as shown in Figure 4.5, half of the power will couple in one direction and the other will couple in the other, so the coupling efficiency will always be less than 50%.[23]

To avoid this issue, symmetry has to be broken somehow. This has been achieved by using an asymmetrical grating or by coupling the fibre not exactly vertically, but with a certain angle (8 to 10 degrees). In this work the second option is used.

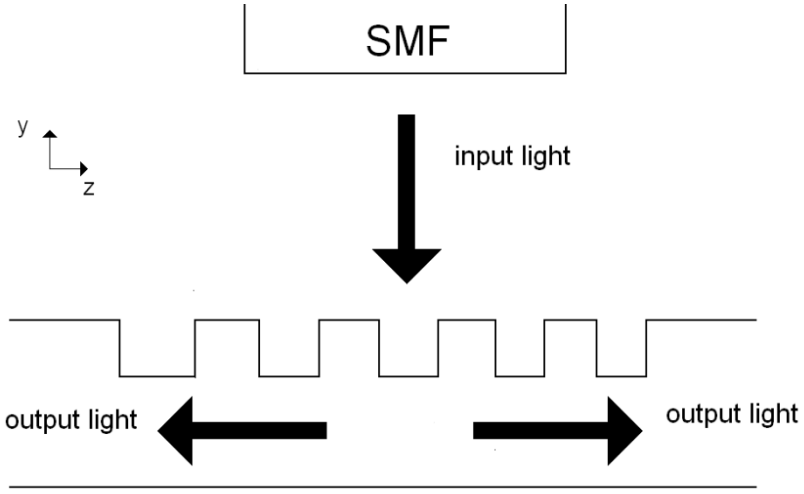

Figure 4.5: Perfectly vertical coupling.

4.3.4 Detuned gratings

In order to break the symmetry existing in the case of perfectly vertical coupling, the fibre has to be coupled in an angle close to the vertical. This grating is called detuned grating. These angle can be either positive or negative, so the coupling scheme will change for every possibility, as shown in Figure 4.6. If the angle is positive, the grating is called positively detuned, and if the angle is negative the grating is called negatively detuned.

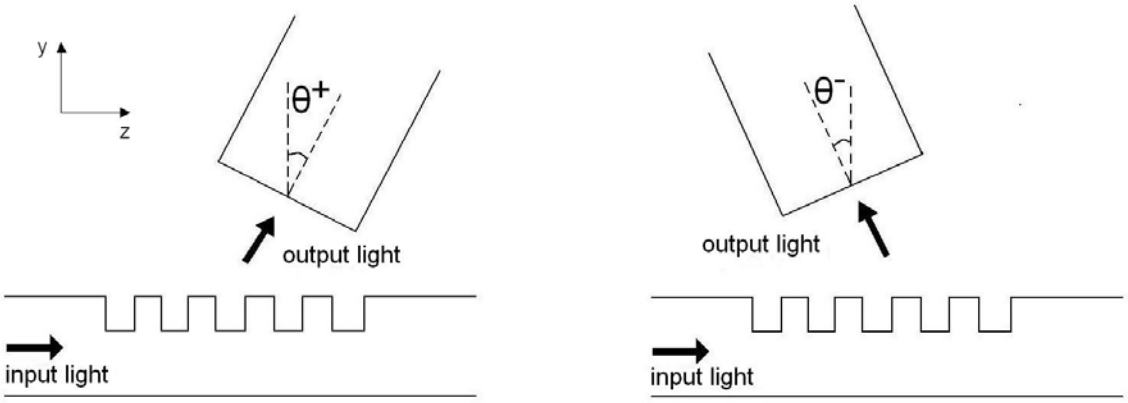

Figure 4.6: Positively and negatively detuned gratings.

In a negatively detuned grating, the grating period is smaller or the wavelength is longer compared to the case of vertical coupling. In a positively detuned grating, the grating period is larger or the wavelength is shorter compared to the case of vertical coupling. [23]

In this thesis a positively detuned grating will be designed and simulated, because this setup would make the experiments and measurements easier, since this kind of structures are measured by placing a grating coupler at both ends of a waveguide. Positively detuned gratings also have a bigger period, and so its fabrication is easier. [23]

4.3.5 Definitions

The grating coupler structure is three-dimensional, but it can be approximated by a 2D structure, because its width is much bigger than the wavelength and the core height. In this way the structure can be simulated only in a plane, what makes the calculations feasible and much easier.

The basic design parameters are shown in Figure 4.7.

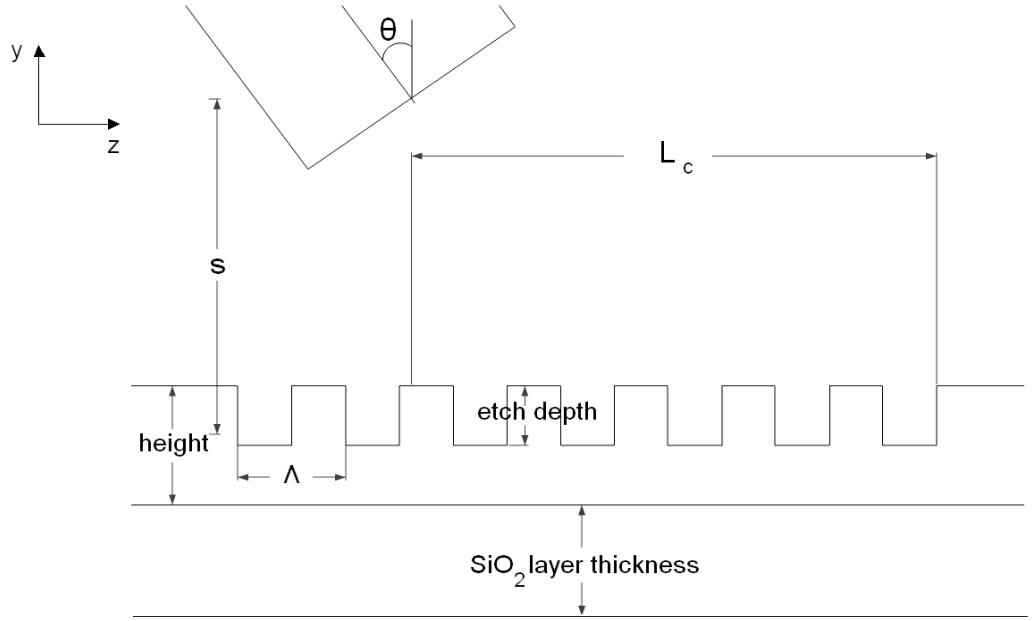

Figure 4.7: Lateral view of the grating coupler and parameters of design.

- Etching depth (ed): depth with which the guiding silicon layer is etched, i.e. the depth of the grating grooves
- Height: the height of the silicon guiding core.
- SiO_2 layer thickness: the thickness of the buried oxide cladding layer.
- θ: incidence angle of the launched field (usually ~9º)
- Coupling length in the y direction (s): vertical distance between the fibre core centre and the waveguide centre.
- Coupling length in the z direction (L_c) : it can be demonstrated that the length in the z direction between the fibre core centre and the beginning of the grating that provides maximal power at the output (expressed as $L_{c,\,opt}$) is equal to [25]:

$$L_{c,\,opt} = \frac{w_0}{1.37 \cos\theta} \tag{4.3}$$

With w_0 half the width (MFD) of the Gaussian incident beam, and θ the incidence angle.

- Grating period (Λ): its theoretical value is obtained from (4.1) [16,23,25] :

$$\Lambda_{theor} = \frac{\lambda_0}{n_{eff} - n_{top} \sin\theta} \tag{4.4}$$

With n_{eff} the effective index of the guided mode, and n_{top} the refractive index of the background (normally air or silicon dioxide)

- Filling factor (ff): relation between the widths of the etched sections and the sections without etching
- Number of periods (N): enough to make sure the surface of the grating is properly illuminated by the fibre.
- Effective index (n_{eff}): in order to find the optimal coupling length and the theoretical optimal grating period, the effective index of the structure has to be found by means of equations 4.3 and 4.4. The structure has to be divided in two sections, corresponding to the etched grooves and the sections without etching, and then the average effective index is found. The process is shown in Figure 4.8.

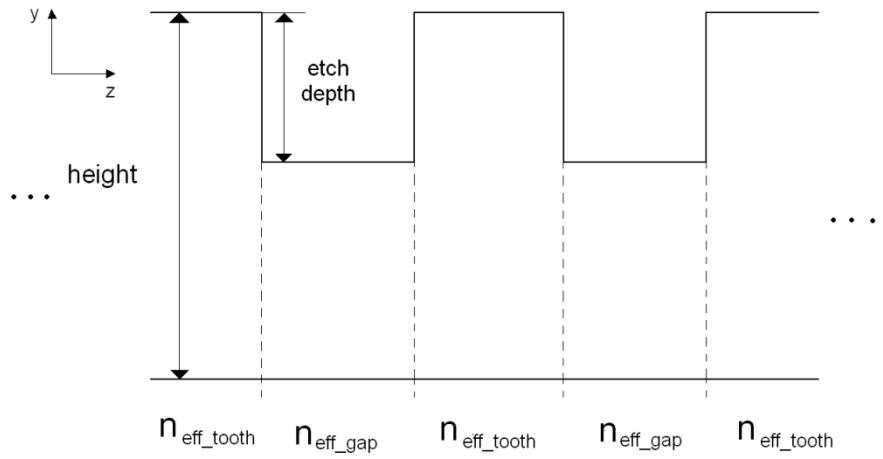

Figure 4.8: Effective index calculation.

The effective index of the etched sections, n_{eff_gap}, and the sections without etching, n_{eff_tooth}, are found using the conventional Effective Index Method explained in Chapter 5. As there is the same number of sections with and without etching, the global effective index can be found as the ratio of these two effective indexes related to the filling factor:

$$n_{eff} = (1 - ff) \cdot n_{eff\_gap} + ff \cdot n_{eff\_tooth} \tag{4.5}$$

Chapter 5

General theoretical background

5.1 Analytical calculations

5.1.1 Effective Index Method

The effective index is used to find approximate solutions for the propagation constants of two-dimensional waveguides. This is done without dealing directly with the electric fields within the waveguide, and so this method, known as the effective index method, is very simple. [9]

The approach to finding the propagation constants for the waveguide shown as an example in Figure 5.1 is to regard it as a combination of two planar waveguides, one horizontal and one vertical, shown respectively in Figures 5.2 and 5.3. We then successively solve the planar waveguide eigenvalue equations first in one direction and then the other, taking the effective index of the first as the core refractive index for the second.

So, when considering, for example, the previously defined strip waveguide, with the index distribution shown in Figure 5.1, and considering a TE mode.

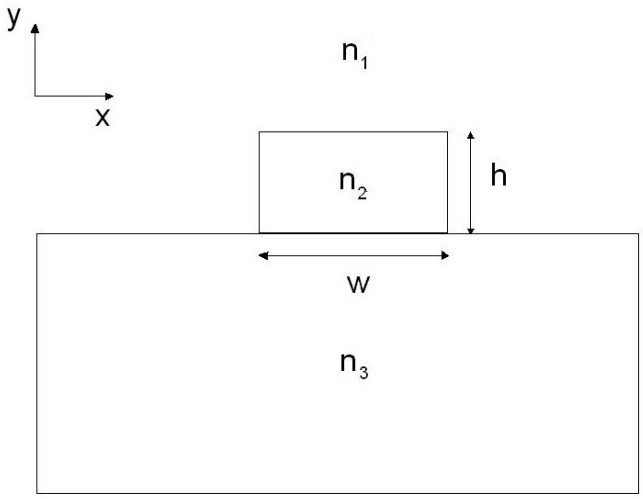

Figure 5.1: Waveguide cross section and index distribution.

We start by calculating the effective index in the y direction, and obtain the effective index in this direction, n_{eff} , as shown in Figure 5.2.

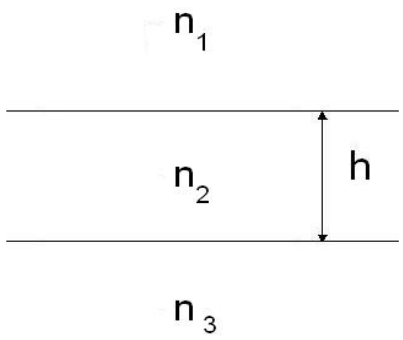

Figure 5.2: Vertical calculation of the effective index.

And then use this index we obtained as the core for the waveguide in the x direction, as seen in Figure 5.3.

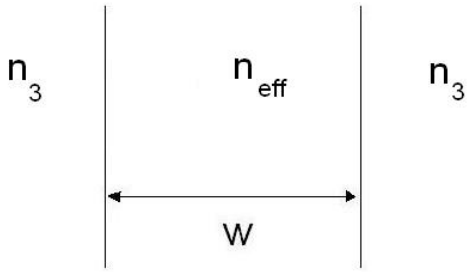

Figure 5.3: Horizontal calculation of the effective index.

For the first decomposition of the waveguide, equation 3.3 for TE modes, has to be solved in order to obtain the propagation angle θ_1.

Then, from the definition of the effective index of the mode, we obtain that:

$$n_{eff} = n_1 \sin\theta_1 \tag{5.1}$$

Then the analogous equation for TM modes has to be solved for the other decomposition in order to find the effective index of the mode.

The polarisation has to be chosen carefully. If we are considering an electric field polarized in the *x* direction (TE polarisation), then when solving the three-layer planar waveguide in the *y* direction we use the TE eigenvalue equation. However, when we subsequently solve the vertical three-layer planar waveguide, we must use the TM eigenvalue equation because, with respect to this imaginary vertical waveguide, the field is polarised in the TM direction.

More complex structures can be divided in “slices” with the same index distribution and the effective index for every slice is then calculated in the same way.

5.1.2 Overlap

The overlap integral is used to calculate how similar are the shapes of two fields. This expression is going to be used to calculate the mode mismatch loss in waveguides.

Its analytical form is the following [9]:

$$\text{overlap} = \frac{\iint_{-\infty}^{\infty} \mathrm{E}_1 \mathrm{E}_2 \, \mathrm{dx}\,\mathrm{dy}}{(\iint_{-\infty}^{\infty} \mathrm{E}_1^2 \, \mathrm{dx}\,\mathrm{dy} \iint_{-\infty}^{\infty} \mathrm{E}_2^2 \, \mathrm{dx}\,\mathrm{dy})^{\frac{1}{2}}} \tag{5.2}$$

Where E_1 and E_2 are the overlapped fields.

This overlap can also be expressed as a power loss in dB:

$$\mathrm{Loss(dB)} = -10 \log \left(\frac{\iint_{-\infty}^{\infty} (\mathrm{E}_1 \cdot \mathrm{E}_2)^2 \, \mathrm{dx}\,\mathrm{dy}}{\iint_{-\infty}^{\infty} \mathrm{E}_1^2 \, \mathrm{dx}\,\mathrm{dy} \iint_{-\infty}^{\infty} \mathrm{E}_2^2 \, \mathrm{dx}\,\mathrm{dy}} \right) \tag{5.3}$$

5.1.3 Interface loss

Overall losses in waveguides are composed of other factors, apart from the mode mismatch losses explained in the previous section. If the materials are considered ideal, there are still interface losses due to the reflections at the input and output facets of the waveguide.

The general formula to obtain these losses is:

$$\text{interface loss } (dB) = 10 \log[(1 - r_1)(1 - r_2)] \tag{5.4}$$

where r_1 is the reflection coefficient at the interface between waveguide and air, and r_2 is the reflection coefficient at the interface between fibre and air. Both are calculated as follows:

$$\mathrm{r}_1 = \frac{\mathrm{n}_{\mathrm{eff\_wg}} - \mathrm{n}_{\mathrm{air}}}{\mathrm{n}_{\mathrm{eff\_wg}} + \mathrm{n}_{\mathrm{air}}} \tag{5.5}$$

$$r_2 = \frac{n_{eff\_fiber} - n_{air}}{n_{eff\_fiber} + n_{air}} \tag{5.6}$$

with n_{eff_wg} the effective index of the waveguide, n_{air} the refractive index of air, and n_{eff_fibre} the effective index of the fibre.

5.1.4 Confinement factor

Not all of the power propagating in a waveguide mode is contained inside the core of the waveguide. Knowing how much power is inside the core can be useful, and also enables comparisons between waveguide modes and waveguide technologies. Defining a confinement factor is one way of quantifying the confinement. The confinement factor, Γ, is usually defined as a mathematical expression of the proportion of the power in a given mode that lies within the core [9]:

$$\Gamma = -10 \log \left(\frac{\int_{-h/2}^{h/2} E_x^2(y)\, dy}{\int_{-\infty}^{\infty} E_x^2(y) dy} \right) \tag{5.7}$$

Where E_x is the propagating mode.

The modal confinement is a function of polarisation, of the refractive index difference between core and claddings, of the thickness of the waveguide (relative to the wavelength), and of the mode number.

5.1.5 Gaussian beam approximation

The mode that is launched from the fibre to be coupled into the grating can be approximated by a Gaussian profile, which expression is as follows, assuming a circularly symmetrical beam [9]:

$$E = E_0 \, e^{-\frac{x^2+y^2}{{w_0}^2}} \tag{5.8}$$

The parameter w_0 is called spot size or mode field radius and corresponds at half the width of the function at an amplitude 1/e of the peak value, E_0. This parameter relates to the mode field diameter (MFD), so MFD = $2w_0$. The MFD shows in which extent the field penetrates in the cladding of the fibre.

The field distribution of this Gaussian beam is shown in Figure 5.4, and the MFD and beam waist are also indicated

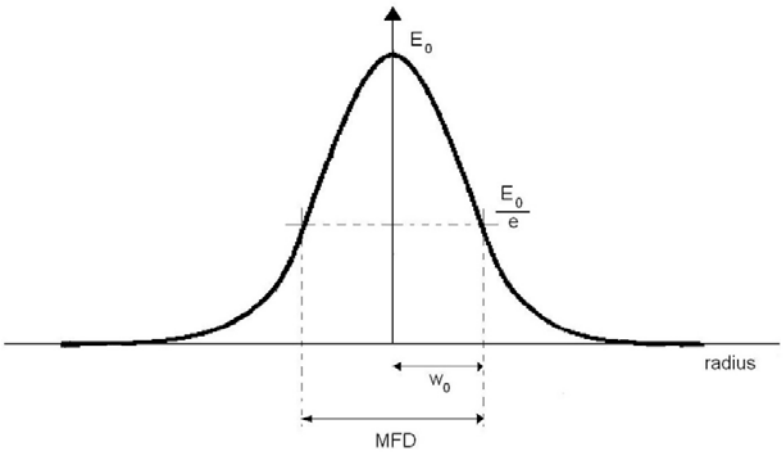

Figure 5.4: Gaussian beam field distribution.

5.2 Simulation tools used in design

In order to properly design the photonic devices that are studied in this thesis, a number of simulation tools and algorithms have been used, which the are Film Mode Matching (FMM) method, for waveguide cross sections, and the Finite Difference Time Domain (FDTD) technique for the grating coupler.

5.2.1 Film Mode Matching Method (FMM)

The Film Mode Matching Method is used to analyze and simulate waveguide cross sections with a small number of homogeneous rectangles.

The waveguide cross-section is considered as a sandwich of slices. Each slice corresponds to a multi-layer film structure. The waveguide mode field is expanded into a superposition of the TE and TM film modes of the planar slab waveguide in each

slice. Then the mode amplitudes are obtained by matching the field distributions and their normal derivative at each interface between the two adjacent slices. [26]

The grid structure used in the method is shown in Figure 5.5.

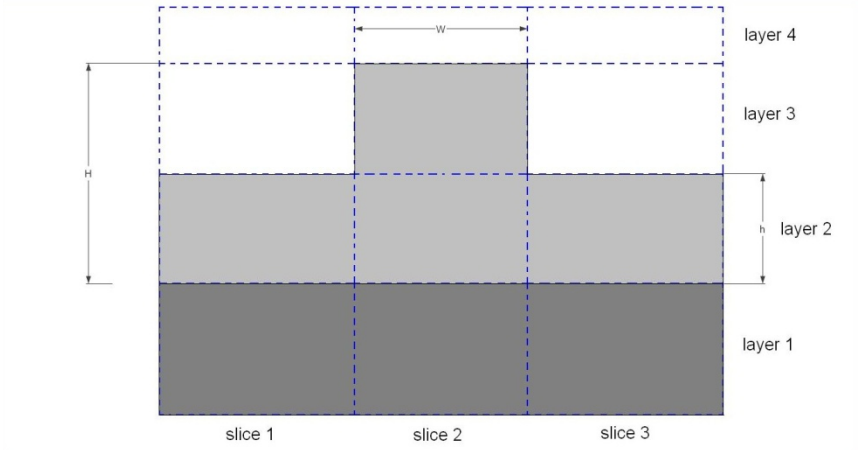

Figure 5.5: Slices and layers used in the Film Mode Matching method.

These film modes can be obtained from the wave equation of a multilayer slab dielectric waveguide in the vertical direction, and are discretized by the perfect electrical or magnetic wall boundary condition at the bottom and top boundaries.

The mode profile in each rectangle is of the form $\sum_i f_i(x)g_i(y)$ where $f_i(x)$ and $g_i(y)$ are either sinusoidally oscillatory or exponentially attenuated functions. Only those modes with well-confined (sinusoidally oscillatory) fields in the waveguide core regions and evanescent fields in the outer spaces other than the core are guided.

It is possible to know if a mode will be guided only by looking at its effective index. If this effective index is bigger than the effective index of the outer slab region, the mode will be guided. [27]

This method is full-vectorial, so it takes the coupling of different polarisations into consideration. The simulated waveguide modes might be quasi-TE or quasi-TM.

5.2.2 Finite Difference Time Domain (FDTD)

The FDTD method belongs in the general class of grid-based differential time-domain numerical modeling methods. The time-dependent Maxwell's equations are discretized using central-difference approximations to the space and time partial derivatives. The resulting finite-difference equations are solved in either software or hardware in a leapfrog manner: the electric field vector components in a volume of space are solved at a given instant in time; then the magnetic field vector components in the same spatial volume are solved at the next instant in time; and the process is repeated over and over again until the desired transient or steady-state electromagnetic field behaviour is fully evolved.This method does not use any approximation and is adequate to simulate complex structures which involve multiple reflections, such as grating couplers.The amount of required memory is enormous for 3D structures, but the method is applicable to 2D structures.

The time-dependant Maxwell equations are [28]:

$$-\mu_0 \frac{\partial \mathbf{H}}{\partial t} = \nabla \times \mathbf{E} \tag{5.9}$$

$$\varepsilon_0 \varepsilon_r \frac{\partial \mathbf{E}}{\partial t} = \nabla \times \mathbf{H} \tag{5.10}$$

For a given spatial discretisation, or grid size, $\Delta x, \Delta y, \Delta z$, and a time step, Δt, we can discretize these equations in the following way:

$$F^n(i,j,k) = F(i\Delta x, j\Delta y, k\Delta z, n\Delta t) = F(x,y,z,t) \tag{5.11}$$

The time step size is defined by the spatial grid size, and for the simulation to be stable, the following condition has to be true:

$$\Delta t \leq \frac{1}{v}\left(\frac{1}{(\Delta x)^2} + \frac{1}{(\Delta y)^2} + \frac{1}{(\Delta z)^2}\right)^{-1/2} \tag{5.12}$$

with $v = {}^{c}/_{n}$ the speed of light in that medium, and c the speed of light in vacuum, and n the effective index of the media.

5.2.3 Perfectly Matched Layer (PML)

One of the inconveniences of the FDTD method lies in the fact that the Maxwell equations have to be solved in a discretised domain whose sizes need to be restrained. Nevertheless, open problems involving theoretically boundless space extension can be solved when applying special conditions on the boundaries of the computational domain, in order to absorb the outgoing waves. Such a need of free-space simulation happens in many problems and especially in wave-structure interactions.

This technique is based on the use of an absorbing layer, a matched medium that is especially designed to absorb without reflection the electromagnetic waves. With this medium the theoretical reflection factor of a plane wave striking a vacuum-layer interface is null at any frequency and at any incidence angle [31]. So, the layer surrounding the computational domain can theoretically absorb without reflection any kind of wave travelling towards boundaries, and it can be regarded as a perfectly matched layer.

Chapter 6

Fabrication techniques

6.1 Wafer fabrication

As it has already been said in the previous sections, the SOI wafer is composed of a uniform layer of SiO_2, which is sandwiched between a thick (hundreds of microns) silicon substrate and a thin surface layer of crystalline silicon. This structure forms a waveguide structure. The waveguide can be made symmetrical by oxidation of the silicon surface.

In this section we will take a look at the most common methods for the fabrication of silicon waveguides in SOI wafers.

The first step to producing the waveguides is obtaining the SOI wafer structure from a silicon wafer. The three most relevant methods are explained in this section.

6.1.1 Separation by IMplanted OXygen (SIMOX)

In this fabrication method, a large number of oxygen ions are implanted under the silicon surface to form the SiO_2 layer.

The oxygen ions are implanted into crystalline silicon at an energy of up to 200 keV.

This energy subsequently determines the depth of the SiO2 and hence the thickness of the silicon overlayer. The silicon substrate is maintained at a temperature of approximately 600 ºC during implantation, to avoid the formation of an unwanted amorphous silicon overlayer. [9]

Several parameters that are critical for the waveguide performance, such as the crystal

dislocations which could influence the optical propagation properties and interface

micro-roughness have been improved through the years, so SIMOX has proved the most popular method for the fabrication of large volumes of SOI material.

An analysis of a waveguide fabricated using this technology can be found in [32].

6.1.2 Bond and Etch-back SOI (BESOI)

This method takes advantage of the fact that bringing two hydrophilic surfaces (such as SiO_2) into intimate contact can result in the formation of a very strong bond.

In general, the wafers are brought into contact at room temperature, at which point an initial bond is formed. The bond strength is increased to that of bulk material via subsequent thermal processing to temperatures as high as 1100 ºC. The production of BESOI has three steps shown in Figure 6.1.

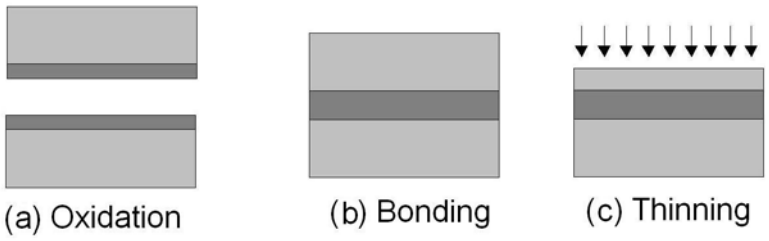

Figure 6.1: BESOI steps of fabrication: (a) oxidation of two wafers to be bonded; (b) formation of the chemical bond; (c) etching of one of the wafers. [8]

An example of the analysis of a waveguide fabricated on this kind of wafer is found in [33].

6.1.3 SmartCut Process

A process which possesses steps from the SIMOX and BESOI processes is SmartCut.. First, a wafer is oxidized to create the buried oxide layer. Then, hydrogen ions are implanted at a well controlled depth, creating a Smart Cut. This wafer is bonded to a clean silicon wafer. The substrate of the first wafer can now be separated along the Smart Cut interface and then annealed and polished. The process is shown schematically in Figure 6.2. [34]

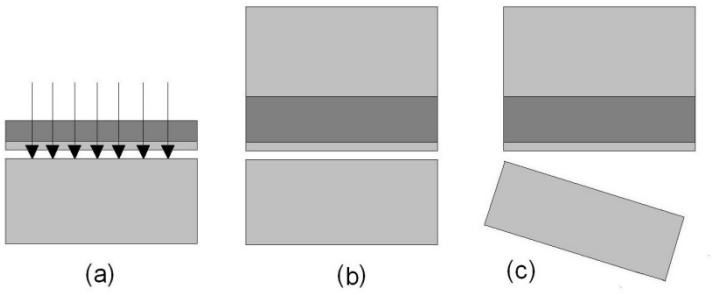

Figure 6.2: The SmartCut process: (a) oxidised wafer is implanted with a high dose of hydrogen. (b) A second wafer is bonded to the first as in the BESOI process. (c) Split the implanted wafer.

The flexibility, high quality and efficient use of silicon offered by this process makes it an excellent platform for the development of low-cost silicon photonics.

6.1.4 Silicon epitaxial growth

As the SIMOX and Smart Cut processes do not usually provide enough silicon overlay thickness, an extra thickness has to be grown on the wafer to achieve the required thickness. This is done by means of an epitaxial growth of silicon. This process deposits a solid film on the surface of a silicon wafer by the reaction of a gas mixture at that surface.

6.2 Waveguide fabrication

The previously explained wafer layer structure defines a slab waveguide itself, but without defining features that provide lateral light confinement, this slab waveguide is of no practical use in silicon photonics.

The main steps of the process of fabrication of silicon waveguides is described in Figure 6.3.

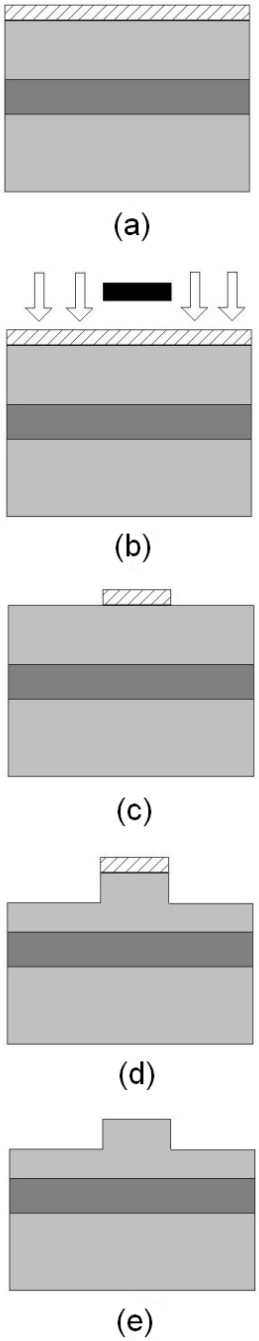

(a) In first place, a photoresist is applicated all over the surface of the SOI wafer., which has been previously cleaned and dried.

(b) The wafer is then aligned with the mask with sub-micron precision and exposed to UV light, so the photosensitive elements of the resist are activated. This process is called photolithography.

(c) The exposed parts are removed with the exposition of the wafer to a developing solution.

(d) The silicon upper layer is etched to the desired thickness.

(e) The remaining photoresist is removed.

Figure 6.3: Steps of the fabrication of waveguides.

The silicon etching can be wet or dry, but the dry etching, the requirement for flexible process capability, tight tolerances and reproducible production, dry etching is regarded as the most suitable solution. It uses chemically reactive plasma to remove the silicon of the upper layer. The plasma is generated under in the vacuum by an electromagnetic field. High-energy ions from the plasma attack the wafer surface and react with it. Reactive Ion Etching (RIE) is an example of dry etching that is used for etching effectively vertical walls. [35]

This asymmetrical waveguide may be converted to a symmetrical one with the deposition or growth of a SiO_2 upper layer.

6.2.1 Critical dimension control

A very important issue in the fabrication of waveguides is the control of the critical dimensions, that is, with which resolution can the dimensions that rule the performance of the waveguide be fabricated.

These critical dimensions are shown in Figure 6.4, for a general rib waveguide.

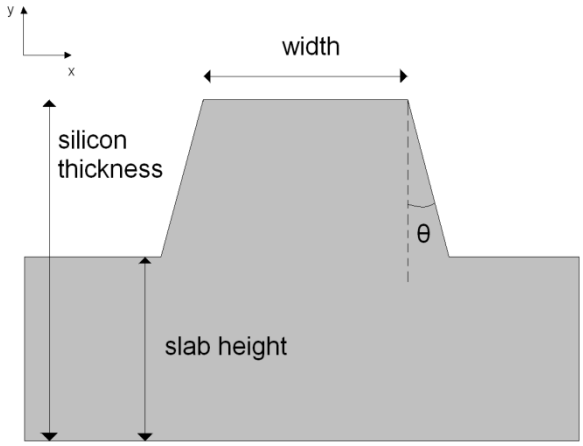

Figure 6.4: Rib waveguide corss section and critical dimensions.

The silicon overlayer thickness is determined by the process used to define the SOI wafer waveguiding layer. IN SIMOX, this accuracy is 3 nm, and in BESOI it is of 500 nm.

The rib width and the rib wall angle (θ) depend on the photolithography and removal process and the etching process.

The slab height is determined by the silicon etch process.

The minimum critical dimension control (according to the *International Technology Roadmap for Semiconductors*) is 10 nm, with minimum feature sizes lower than 100 nm. These characteristics should allow the production of submicron waveguides as well, provided that some critical features in this field are improved, such as minimum SiO_2 thickness, and interface and sidewall roughness. [36, 15]

6.3 Grating fabrication

Grating couplers are structures that are much more complicated to produce than straight waveguides, because the dimensions are much smaller and require higher accuracy. These accuracies will be exposed here.

The process of fabrication is essentially the same that has already been exposed for waveguides. First a photoresist is applicated on the surface of the SOI wafer to define the shape of the element (lithography), and then this shape is etched on the silicon upper layer.

There are a couple of lithography and etching techniques that are specially suited for this kind of structures. [23]

The three main lithography techniques are explained in this section: optical lithography (or photolithography), electron-beam direct-write lithography and interference lithography. Two etching techniques (Dry etching and Focused Ion Beam etching) are exposed as well.

6.3.1 Optical lithography

This technique uses light to image a pattern on the photoresist. The resolution depends mainly on the used wavelength. The highest resolutions can be achieved for the so-called deep UV lithography (DUV), which uses $\lambda = 248$ or 193 nm, and are < 200 nm.

6.3.2 Electron-beam direct-write lithography

In this technique, a focused electron beam scans all the surface of the photoresist and writes the pattern directly on it, so no mask is needed. This system is highly flexible and the spot-size of the beam can be as small as 5 nm. However, it is quite slow and not suitable for mass production.

6.3.3 Interference lithography

In this technique, two coherent light beams coming from a laser are combined, resulting in a periodic intensity pattern. The angle between the two beams determines the grating period. Grating periods of about 250 nm can be defined.

6.3.4 Dry etching

As in waveguides, a dry etching process such as RIE can be used. Different etching depths can be achieved by controlling the etch depth, and the error in this depth can be under 5 nm if the fabrication environment is well controlled.

6.3.5 Focused Ion-Beam etching (FIB)

The technique used in Focused Ion-Beam etching is similar to the electron-beam lithography technique, but heavy ions are used instead of electrons to etch the silicon directly. This process can be quite slow, but high accuracy can be achieved.

Chapter 7

Review of existing grating coupler structures

There are improvements that have already been applied to grating coupler structures to enhance their performance. They are either one-dimensional or two dimensional solutions. In this section we review some of them.

7.1 One dimensional structures

7.1.1 Grating with upper index matching layer

Sometimes, the entire structure is surrounded in silica index matching glue so that fibre facet reflections are minimized, and in this way efficiency is enhanced. The structure is schematically drawn in Figure 7.1.

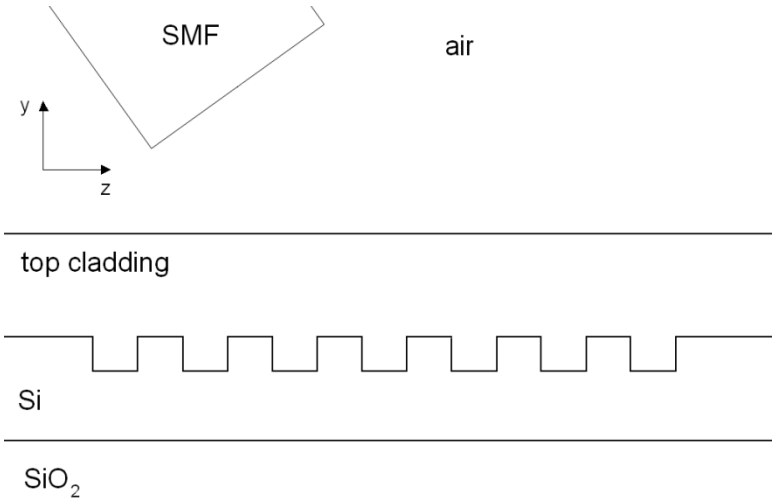

Figure 7.1: Grating coupler with index matching layer.

7.1.2 Grating with bottom reflector

The main limitation to the efficiency of the grating couplers is the leakage to the substrate. A bottom reflector can further improve this ratio and the coupling efficiency to fibre. This bottom reflector can be a multi-layer dielectric mirror or a metal mirror.

It is important to choose the buffer thickness correctly. Depending on which material is used for this bottom mirror, the structure may not be CMOS compatible, and thus not commercially available. Figure 7.2 shows an example of bottom mirror.

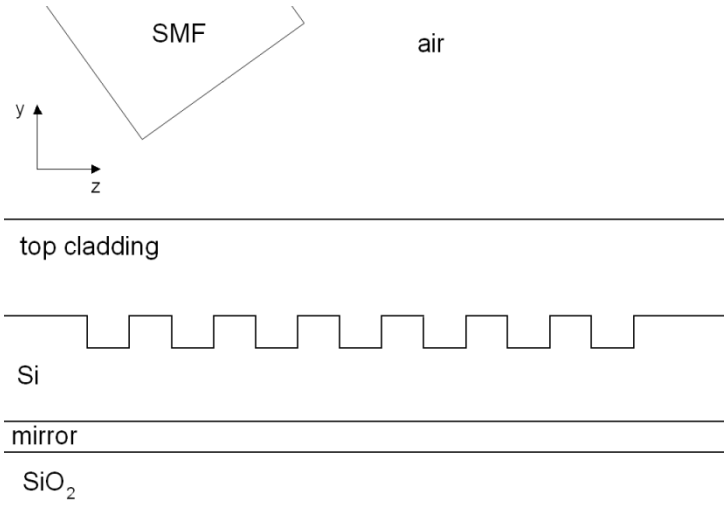

Figure 7.2: Grating coupler with bottom mirror.

7.1.3 Grating with top mirror

The characteristics of a grating coupler can also be changed by adding dielectric layers on top of the grating, in what is called a dielectric stack. The interfaces control the power distribution around the grating ensuring maximal coupling into the guided mode and destructive interference in all unwanted modes. This structure is shown in Figure 7.3.

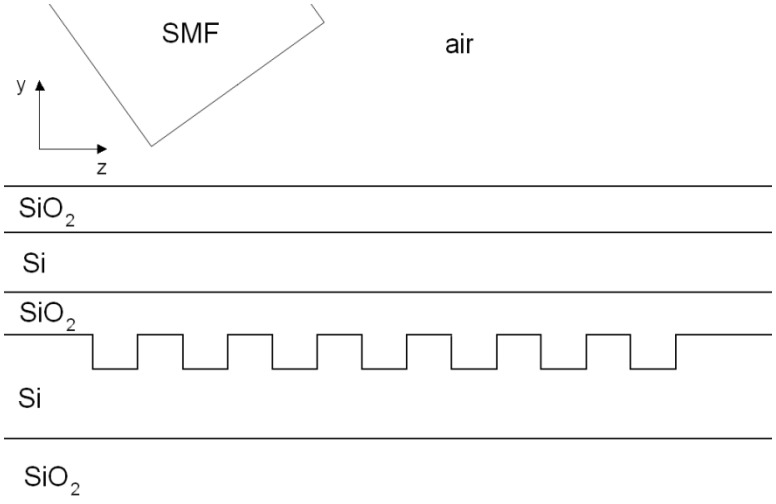

Figure 7.3: Grating coupler with top mirror.

7.1.4 Metal gratings

Metal gratings, fabricated in gold, silver, aluminium or copper, and placed on top of the SOI layer structure can also provide better performances and efficiencies. Although a metal and thus lossy material is introduced, very high efficiencies are obtained due to the strong scattering on a small length scale. There is a very high refractive index contrast between the metal teeth and their surroundings. The coupling scheme is shown in Figure 7.4.

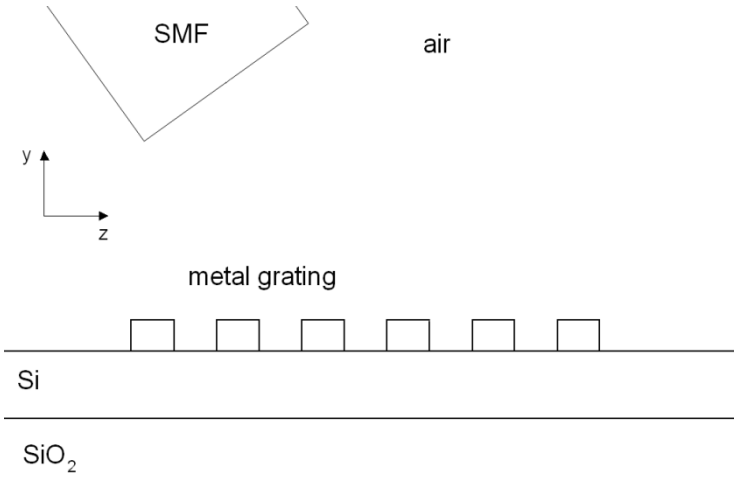

Figure 7.4: Metal grating coupler.

7.1.5 Blazed gratings

In some cases, a special tooth shape (parallelogram or triangular) is used, in order to suppress the second order reflection or enhance the directionality of the structure.

It has been shown that the best shape to achieve these enhancements is the parallelogram shape. The fabrication of these shapes is more complicated, because special etch processes have to be performed on them in order to shape the silicon layer. Figure 7.5 shows this structure.

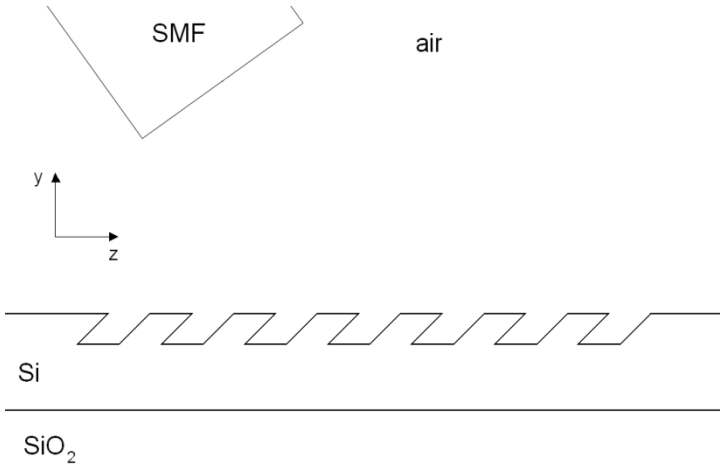

Figure 7.5: Blazed grating coupler.

7.1.6 Chirped gratings

In this kind of structures, the tooth width varies according to some defined relation to minimize back reflection into the waveguide. This variation is normally performed only on one part of the structure, while the other is kept unaltered. This variation can be seen in Figure 7.6.

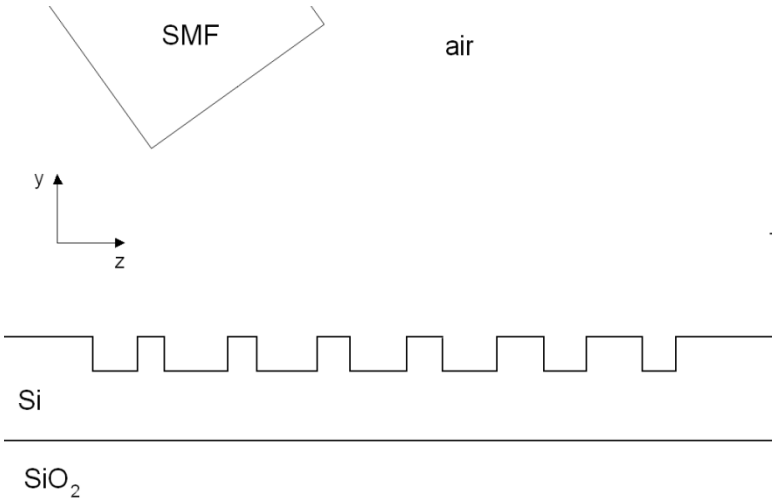

Figure 7.6: Chirped grating coupler.

7.1.7 Gratings with rear reflector

In the case of vertical coupling and a symmetrical structure, the efficiency can never be bigger than 50%, due to the symmetry. In order to break this symmetry, a second grating can be introduced next to the first one.

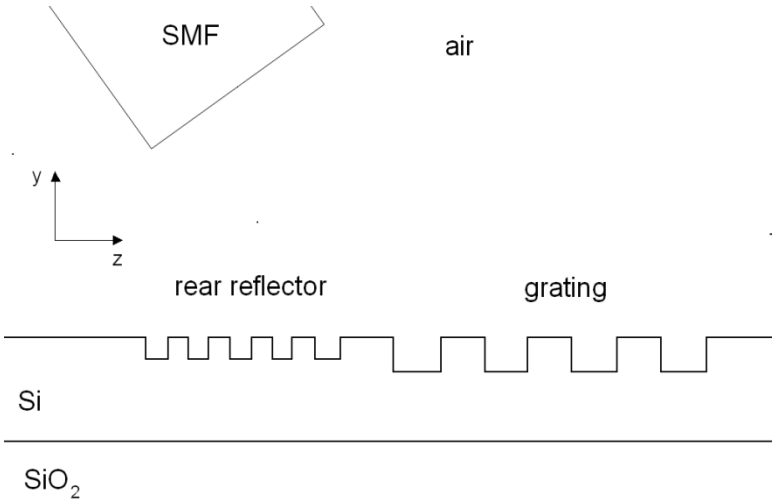

Figure 7.7: Grating coupler with rear reflector.

7.1.8 Slot waveguide-based grating coupler

One novel promising CMOS compatible material is silicon nanocrystals (Si-nc) embedded in silica (SiO_2). In this grating structure configuration, a Si-nc slot is included in the grating, to enhance silicon nonlinearities. This complex structure is shown in Figure 7.8.

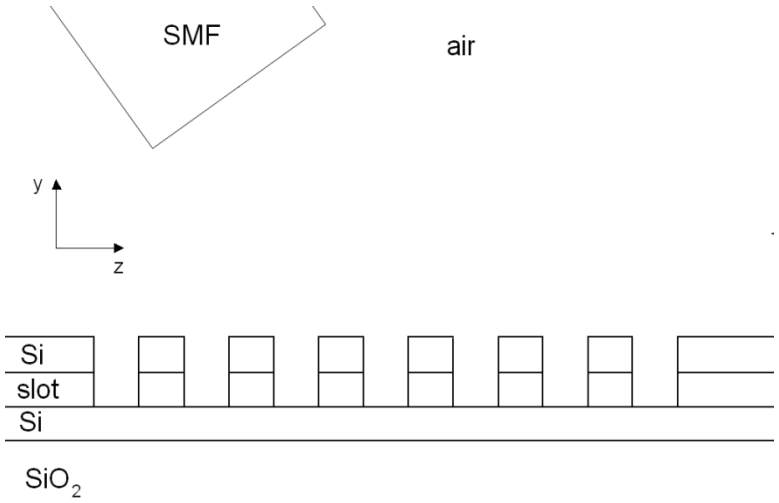

Figure 7.8: Slot waveguide based grating coupler.

7.1.9 One-dimensional focusing gratings

Normally grating couplers need to be followed by an horizontal taper that performs the mode size conversion in this direction, in order to fit it in the waveguide. An alternative to this system are focusing gratings, which perform the mode size conversion at the same time, by means of the structure that is showed in next Figure.

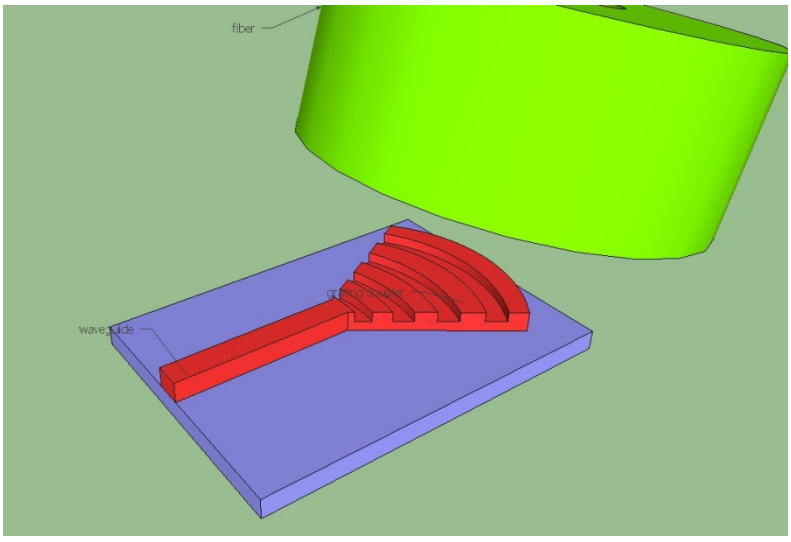

Figure 7.9: 1D focusing grating coupler.

7.1.10 Structures based on other materials

Other solutions include structures which use other materials, such as Ta_2O_5 or Si_3N_4, in the waveguide core. These cannot be regarded as fully CMOS compatible.

Examples of this kind of structures are [47, 48].

7.2 Two dimensional structures

7.2.1 Two-dimensional polarisation diversity gratings

The light from the fibre has an unknown polarisation which also changes over time, while the nanophotonic components on the SOI-chip are often very polarisation

Sensitive. 2-D polarisation diversity grating couplers consist of a 2-D grating at the intersection of two orthogonal waveguides. For symmetry reasons, the two orthogonal polarisation components coming from a vertical fibre couple to their own waveguide, in which the polarisation is the same. A 3D view of this kind of coupler is shown in Figure 7.10.

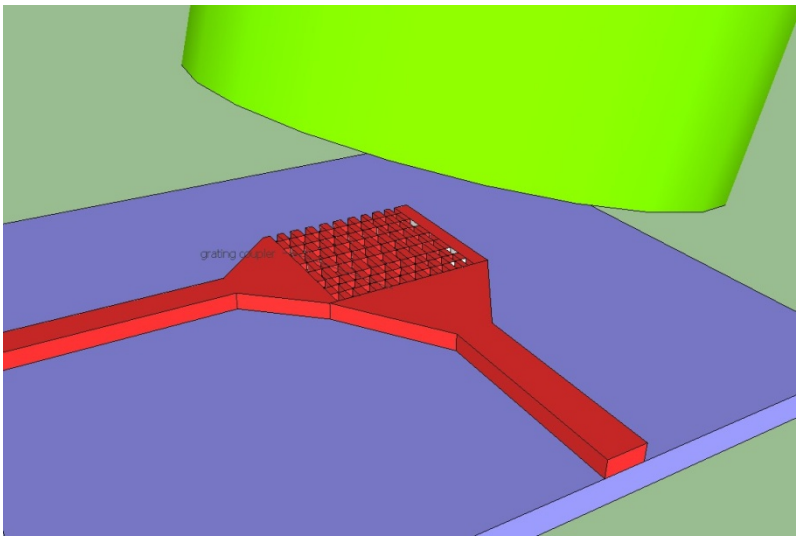

Figure 7.10: 2D polarisation diversity grating coupler.

7.2.2 Two-dimensional focusing grating couplers

This structure may be regarded as a combination of the two previous one. It consists of the intersection of two 1D focusing gratings, in order to achieve polarisation diversity.

The main advantage of this kind of structure is that the dimensions of the device can be drastically reduced, since the output taper is already included in the grating part itself.

7.3 Reported efficiencies

The following table puts together the efficiencies that have been reported for the reviewed structures.

Type of grating	Group	Efficiency
Bottom mirror [37, 38]	IMEC	69%
Top mirror [39]	University of California	95% (theoretical)
Metal grating [40]	IMEC	60% (theoretical) 34% (measured)
Slanted grating [41, 42]	Osaka University, IMEC	59% (theoretical) 16% (measured)
Chirped grating [43, 44]	University of Hong Kong	34% (measured)
Rear reflector [23]	IMEC	>70%(theoretical) 33% (measured)
Slot-waveguide based grating [24]	Valencia NTC	61% (theoretical)
1D focusing grating [20]	Luxtera	70% (measured)
2D polarisation diversity grating [45]	IMEC	23% (measured)
2D focusing gratings [46]	IMEC	27%

Table 7.1: Grating coupler reported efficiencies.

Of all those already existing structures, the ones that are of interest to us are those that can be fabricated in SOI wafers, in order to take advantage of the CMOS technology. That includes top and bottom mirrors, rear reflectors and slot waveguide based gratings which are made of CMOS compatible materials. Metal gratings are not in this category.

Chirped and slanted gratings are of great interest in the research field, but the required fabrication techniques are not suitable for mass production yet.

1D focusing gratings have already been tested in commercial applications. Polarisation diversity gratings have also been well studied and tested, so they arise as a good solution to the coupling problem.

Chapter 8

Waveguide design and simulation

In this section of the thesis the structures under study are designed and simulated. These are the large single mode waveguide, the strip nano waveguide and the grating coupler from fibre to waveguide. Then the obtained results are discussed for every structure.

Historically rib waveguides with dimensions comparable to the waveguide have been used. In the way towards miniaturisation, a change to strip waveguide is done, because this kind of structures provides higher light confinement. In the next sections simulations for both kinds of waveguides are performed, and their losses when direct butt coupled to fibre are found.

8.1 Large single mode waveguides

This kind of structure has already been presented in Chapter 3. It consists of a rib waveguide with dimensions that are large in comparison to the wavelength. Soref and Petermann studied this kind of structures for λ = 1.3 μm. [11]

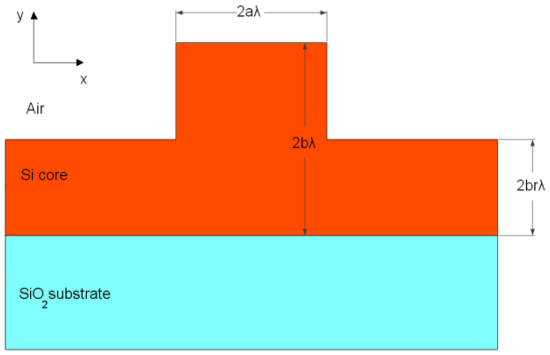

Figure 8.1: Rib waveguide cross section after [11].

8.1.1 Structure and simulation description

Square rib waveguides are considered, that is, with a = b, and vary their dimensions, following the next scheme:

(A) Core width = Core height = 4 μm
(B) Core width = Core height = 2 μm
(C) Core width = Core height = 1 μm
(D) Strip waveguide with: Core width = 0.5 μm Core height = 0.22 μm

These structures are simulated for TE polarisation and λ = 1.55 μm, and the mode mismatch between the directly coupled input Gaussian beam and the propagated mode is calculated by means of the overlap integral presented in equation 5.3. The core width is also varied to obtain their single mode region. The index and propagation profiles for every structure are shown as well. The cross sections are simulated with the FMM algorithm presented in Chapter 5. [49,50]

The following values for the effective indexes are taken: n_{Si} = 3.48, n_{SiO2} = 1.46, n_{air} = 1.

The inner-outer ratio (r) is initially r = 0.625.

(A) Core width = Core height = 4 μm

The index profile for this structure is shown in Figure 8.2.

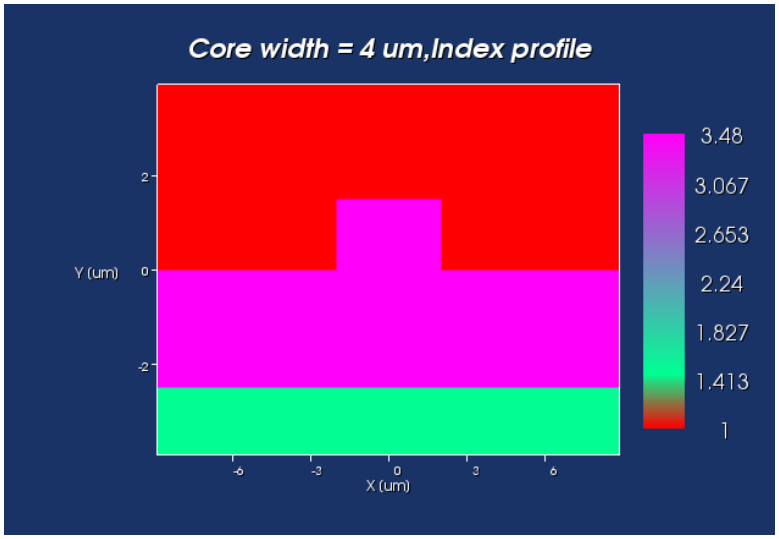

Figure 8.2: Index profile for core width = core height = 4 μm.

Then a Gaussian beam is launched in the core central region, to see how the fundamental mode propagates. The propagation profile is shown in Figure 8.3.

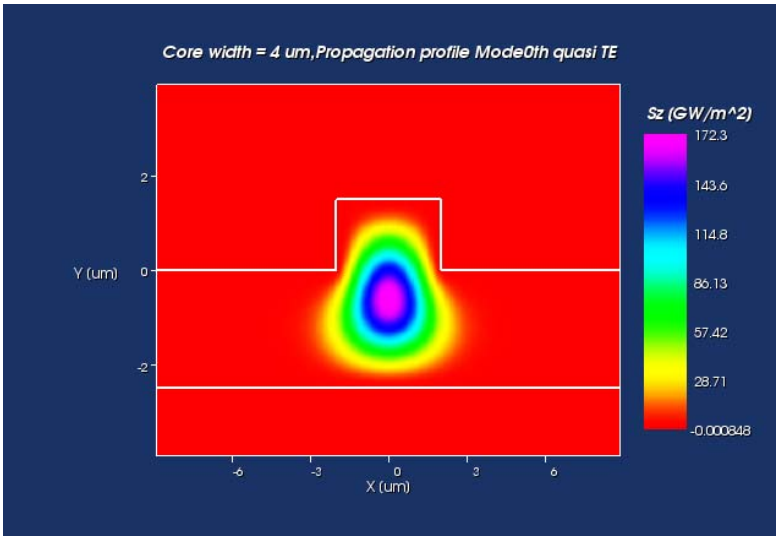

Figure 8.3: Propagation profile for core width = core height = 4 μm.

As discussed in Chapter 2, the single mode behaviour is ensured by setting $0.5 \leq r < 1$, because in this way the higher-order modes leak to the lateral slab regions.

Single mode region

The single mode region for TE modes has been studied by varying the core width and the inner-outer radio to r = 0.5 and r = 0.8. This is shown in Figure 8.4.

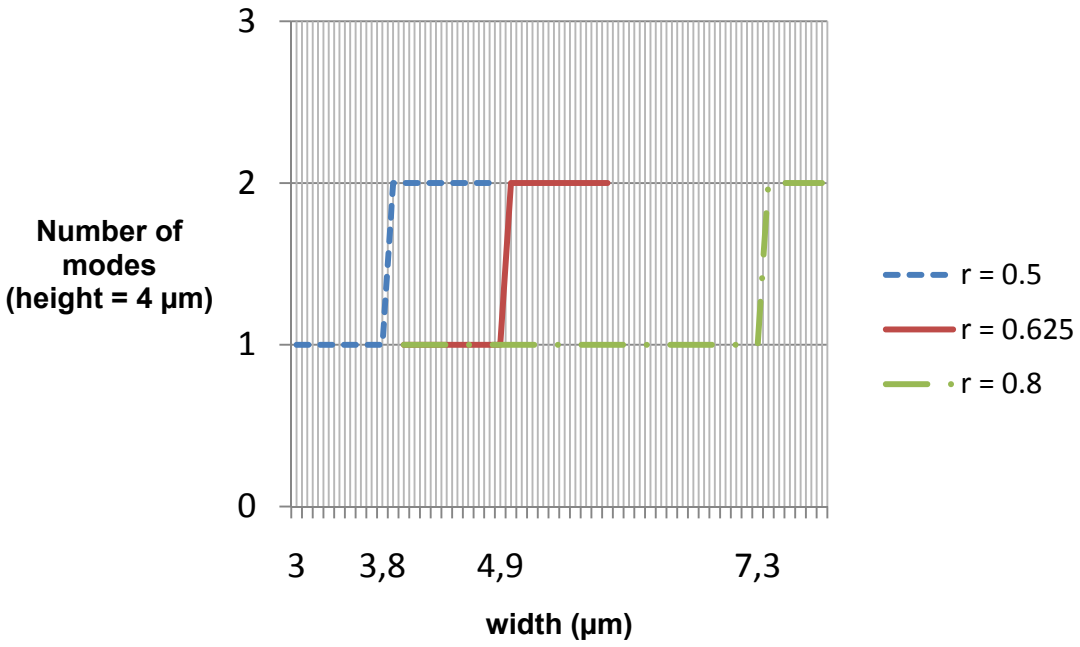

Figure 8.4: Single mode region for core width = core height = 4 μm.

The widths in which the change from single mode to multimode behaviour is found are explicitly highlighted. For example, for r = 0.625 the waveguide is single mode up to width = 4.9 μm, and for the next values (from 5.0 μm), it is multimode.

For r = 0.5 the slab region is smaller, so the lateral leakage is not so high as in the other cases, so the higher order modes do not leak as easily to the lateral slabs and the waveguide is monomode for a smaller range of waveguides.

For r = 0.8 the opposite situation happens: the lateral leakage is bigger, and so is the range of waveguide widths for monomode behaviour.

(B) Core width = Core height = 2 μm

In this step the dimensions are reduced to half their initial value. The index profile is shown in Figure 8.5:

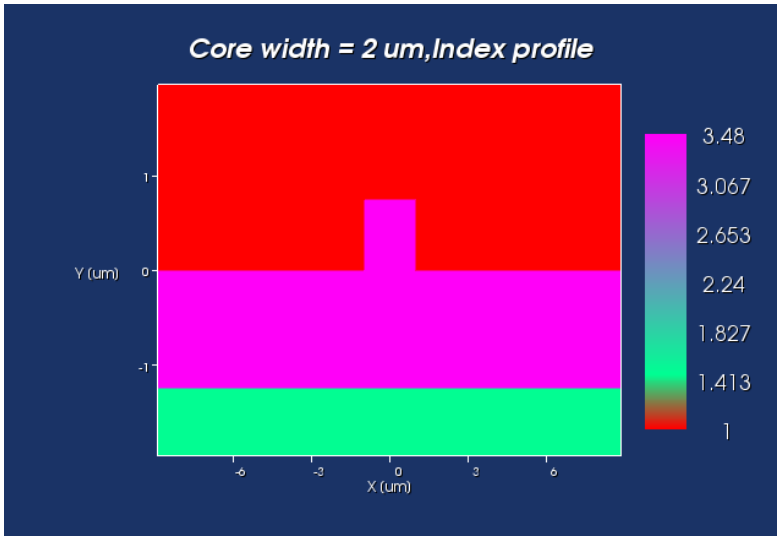

Figure 8.5: Index profile for core width = core height = 2 μm.

The propagation profile of the fundamental mode is shown in Figure 8.6.

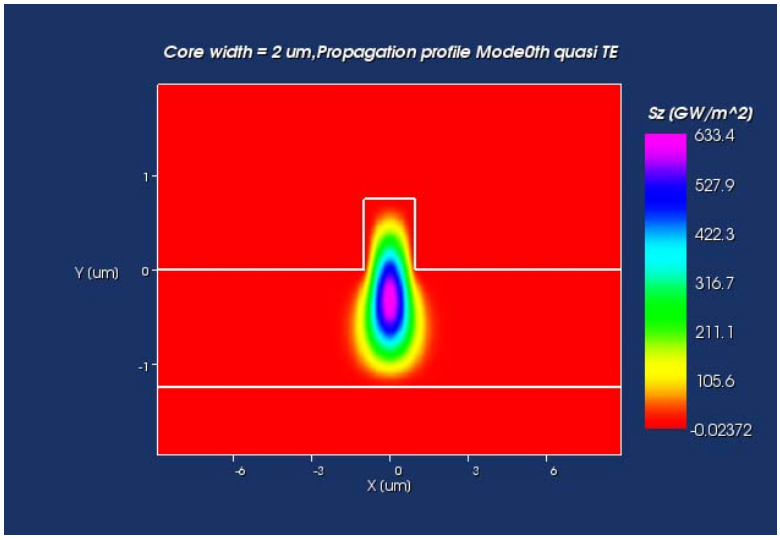

Figure 8.6: Propagation profile for core width = core height = 2 μm.

Single mode region

As in the previous section, the single mode region has been found, and is shown in Figure 8.7

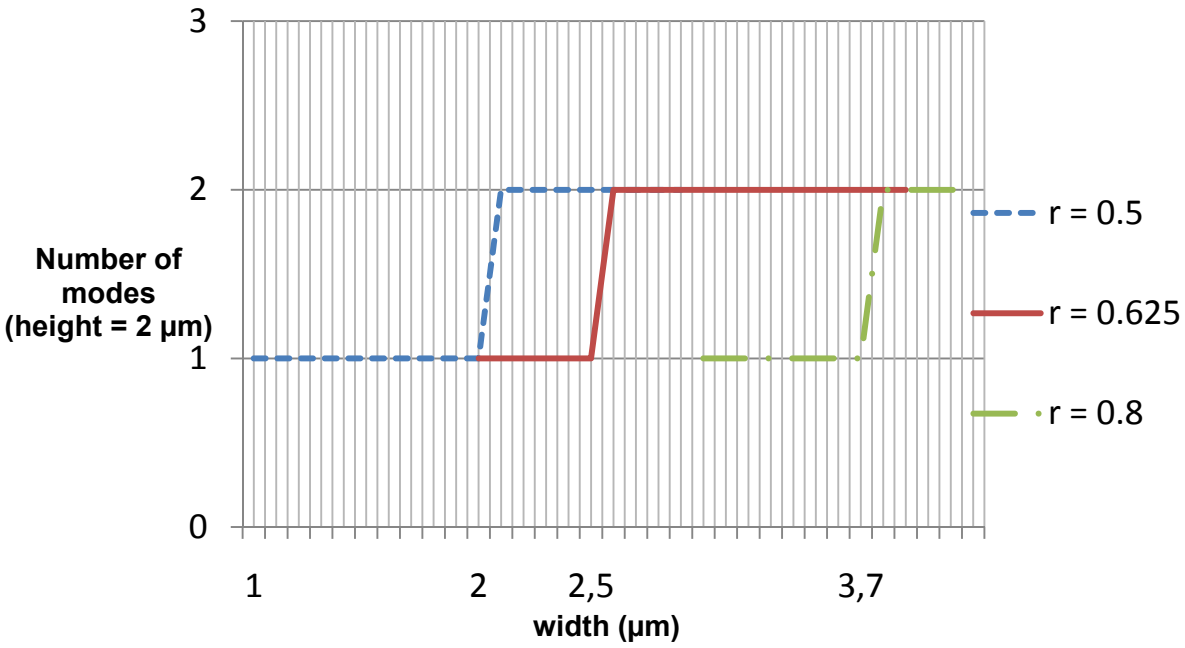

Figure 8.7: Single mode region for core width = core height = 2 µm.

(C) Core width = Core height = 1 µm

In the last step of the dimension reduction for square rib waveguides, we take the dimensions to 1 µm.

The index profile is shown in the Figure 8.8.

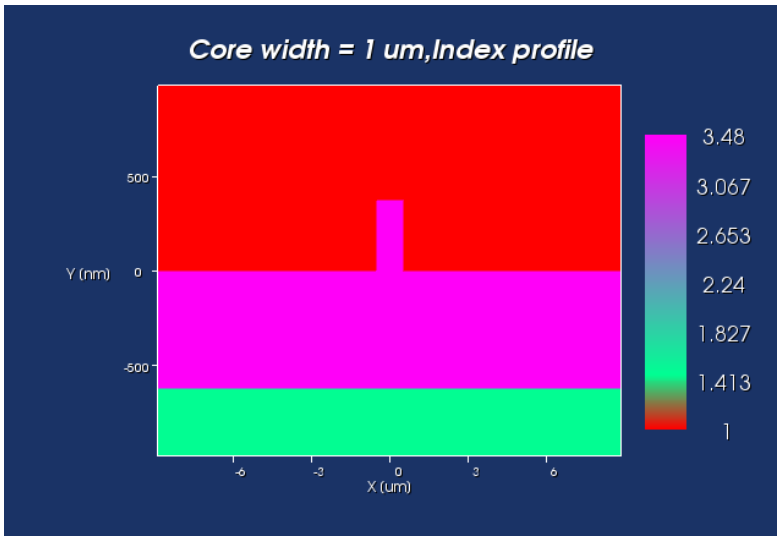

Figure 8.8: Index profile for core width = core height = 1 µm.

And the propagation profile in Figure 8.9.

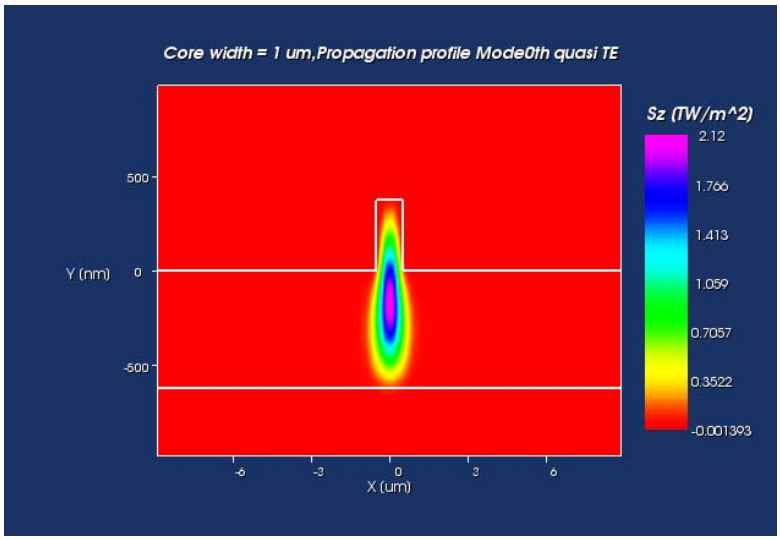

Figure 8.9: Propagation profile for core width = core height = 1 µm.

Single mode region

The single mode specific widths are also found in this section, and shown in the Figure 8.10.

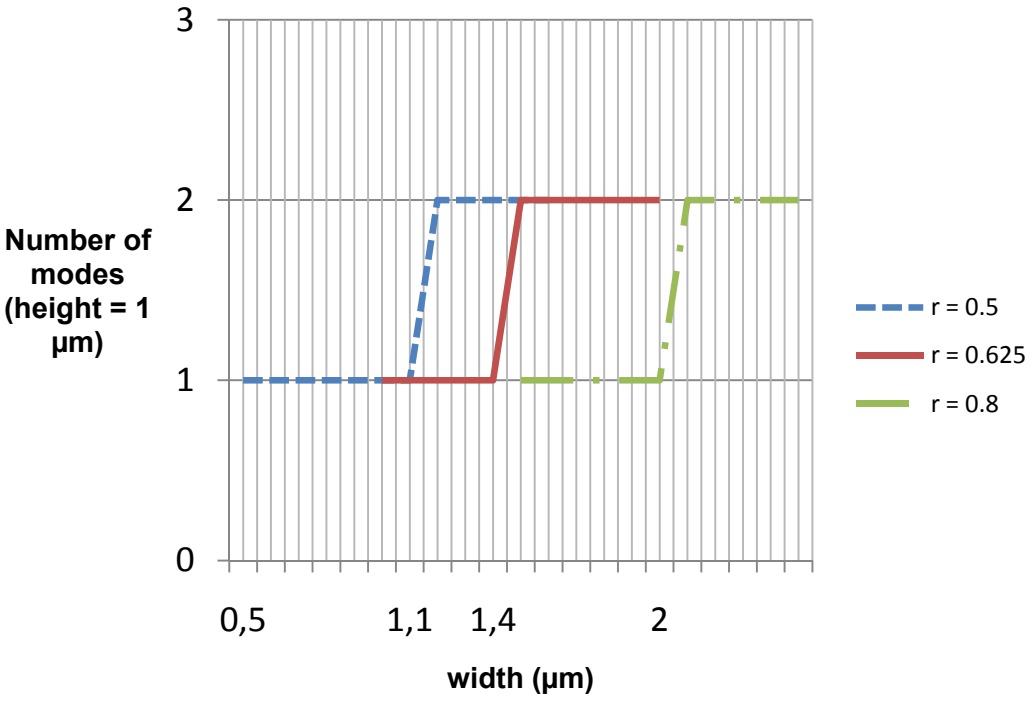

Figure 8.7: Single mode region for core width = core height = 1 µm.

(D) Strip waveguide: Core width = 0.5 μm, Core height = 0.22 μm

The last step towards miniaturisation is bringing the dimensions of the waveguide in the order of nanometers. For this reason, a strip waveguide is used. The core height of 0.22 μm is chosen because the available SOI wafers silicon layers have this thickness.

The index profile is shown in Figure 8.11.

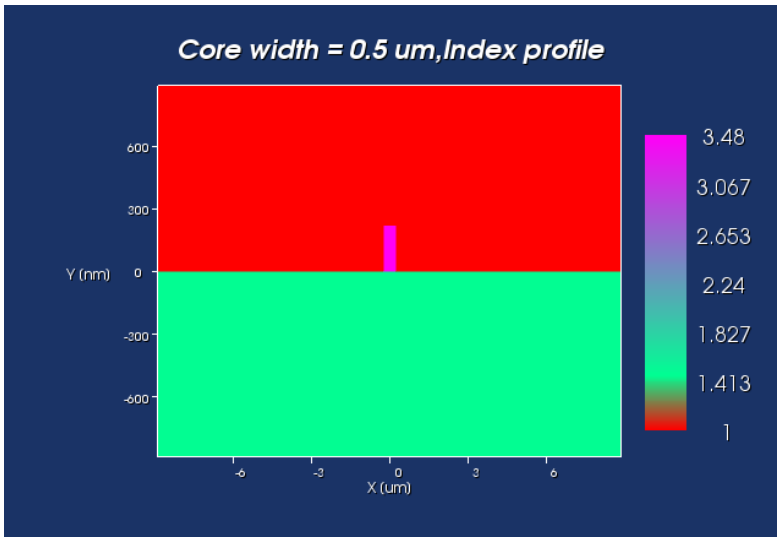

Figure 8.11: Index profile for a strip waveguide with core width = 0.5 μm, core height = 0.22 μm.

As well as the propagation profile, in Figure 8.12.

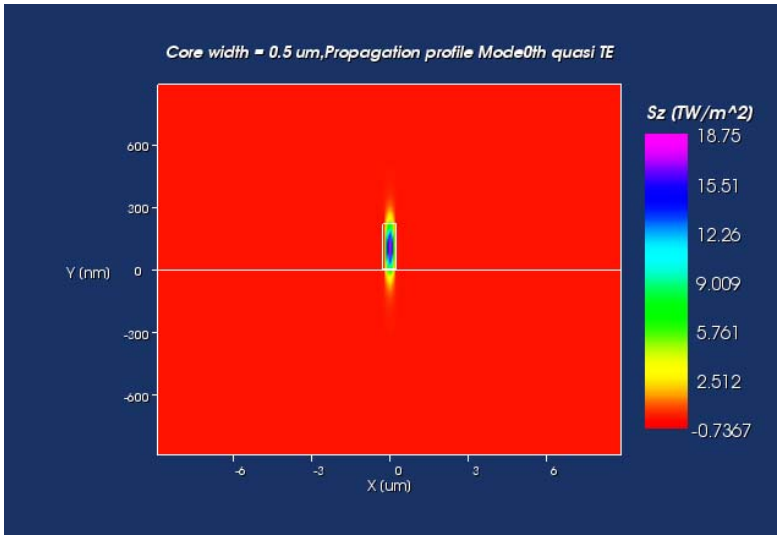

Figure 8.12: Propagation profile for a strip waveguide with core width = 0.5 μm, core height = 0.22 μm.

Single mode region

The single mode operating region is found and shown in Figure 8.13.

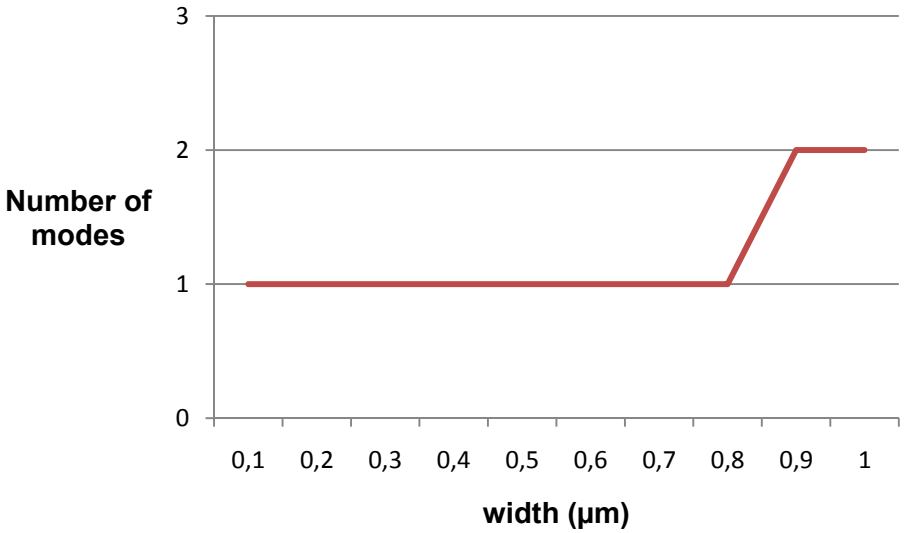

Figure 8.13: Single mode region for a strip waveguide with core width = 0.5 µm, core height = 0.22 µm.

The structure is multimode for widths bigger than 0.8 µm.

8.1.2 Mode mismatch loss

To see how effective is the direct coupling of the rib waveguide structures to a lensed fibre with MFD = 5 μm, the mode mismatch loss between the input Gaussian beam and the propagated mode is calculated by means of the overlap integral presented in equation 5.3. The results presented in table 8.1 are obtained.

	Rib waveguide			Strip waveguide
	A	B	C	D
Width [μm]	4.0	2.0	1.0	0.5
Height [μm]	4.0	2.0	1.0	0.22
Slab height [μm]	2.5	1.25	0.625	0
Mode mismatch loss [dB] (MFD=5 μm)	3.2	4.92	6.91	15.65
Minimal mode mismatch loss [dB]	3.2	4.5	4.8	14.5

Table 8.1: Mode mismatch losses for the different waveguide dimensions.

In this calculation the interface loss resulting from the butt coupling from fibre to waveguide has not been taken into account. This loss is calculated in equation 5.4 and is estimated to be around 9 dB when the coupling is performed on the silicon core. It can be easily avoided with an anti-reflection coating.

It can clearly be seen that, as the dimensions decrease, the mode mismatch losses significantly increase, showing that direct butt coupling to fibre is not a very effective technique. For this reason, other ways to couple nano strip waveguides to optical fibres have to be investigated. In the following sections we will take a look at the strip nano waveguide and its vertical coupling to fibre by means of a grating coupler.

8.2 Nano strip waveguides

In the next step towards miniaturisation of the waveguide dimensions, the structure that emerges as the best suited to achieve a good lateral confinement is the nano strip waveguide. It is composed of a SiO_2 cladding (or BOX) with a Si square core on top.

8.2.1 Structure and simulation description

The nano strip waveguide cross section is shown in Figure 8.14.

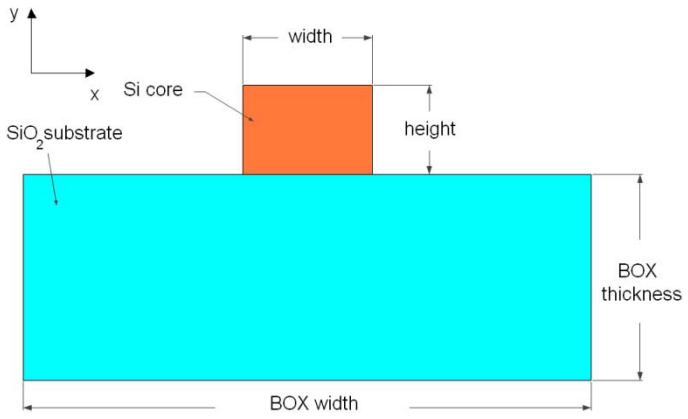

Figure 8.14: Strip nano waveguide cross section.

The BOX thickness is fixed to 2 μm and the core height to 0.34 μm, in order to use an already commercially available SOI wafer. With this core height both polarisations can be supported, as it will be shown in the next sections.

The following values for the effective indexes are taken: n_{Si} = 3.48, n_{SiO2} = 1.46, n_{air} = 1, like for the large single mode rib waveguides. Both polarisations and λ = 1.55 μm will be taken into account.

The Si core width is varied within the range 100 – 600 nm, and the coupling losses when the fibre is butt coupled to the core will be found for every width, as well as the single mode region and some performing characteristics of interest, like the effective index of the fundamental mode or the confinement factor. The cross section is simulated with the FMM method, as in the case of large single mode waveguides. [49,50]

8.2.2 Single mode region

The single mode region is shown in the Figure 8.15.

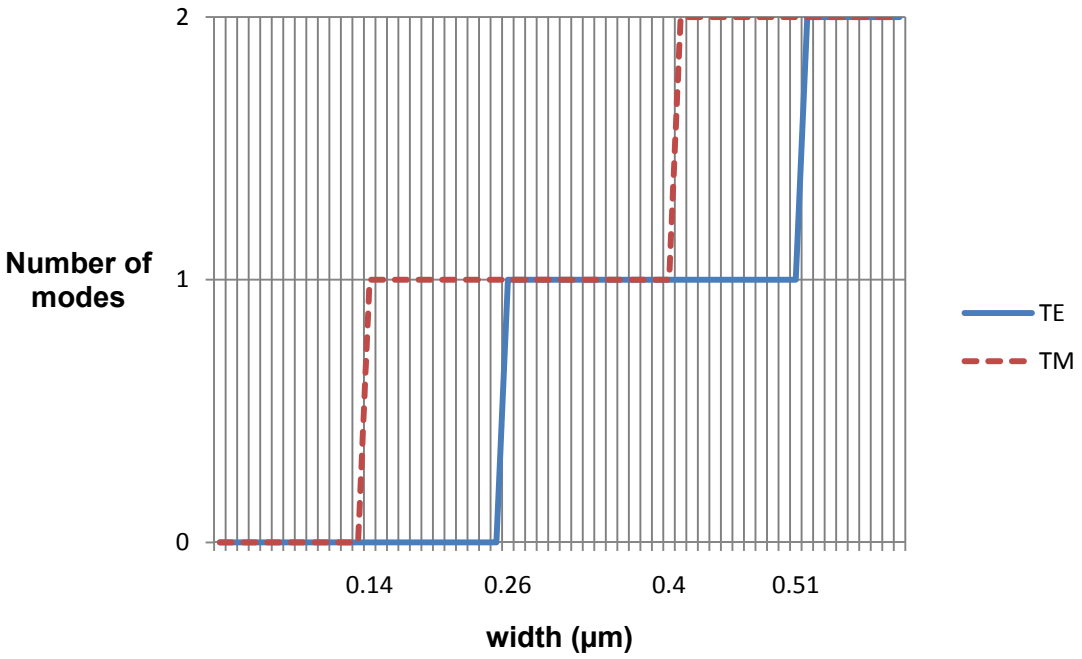

Figure 8.15: Single mode region for the strip nano waveguide.

For TM polarisation, no mode is propagated under 0.14 µm, and the waveguide is monomode for widths up to 0.4 µm. For TE polarisation, no mode is propagated under 0.26 µm, and the single mode behaviour is kept until 0.51 µm. This gives a single mode region for both polarisations between 0.26 and 0.4 µm.

If the waveguide width is chosen around the centre of this range the waveguide is robust to fabrication errors. In Chapter 2 it has been explained that the fabrication tolerances are about 10 nm, so the waveguide will not experiment significant changes in its performance.

8.2.3 Propagation profiles

The fundamental mode propagation profiles for the widths in the range 100 nm to 600 nm are shown in the Figures 8.16 and 8.17, for both TE and TM polarisations, respectively.

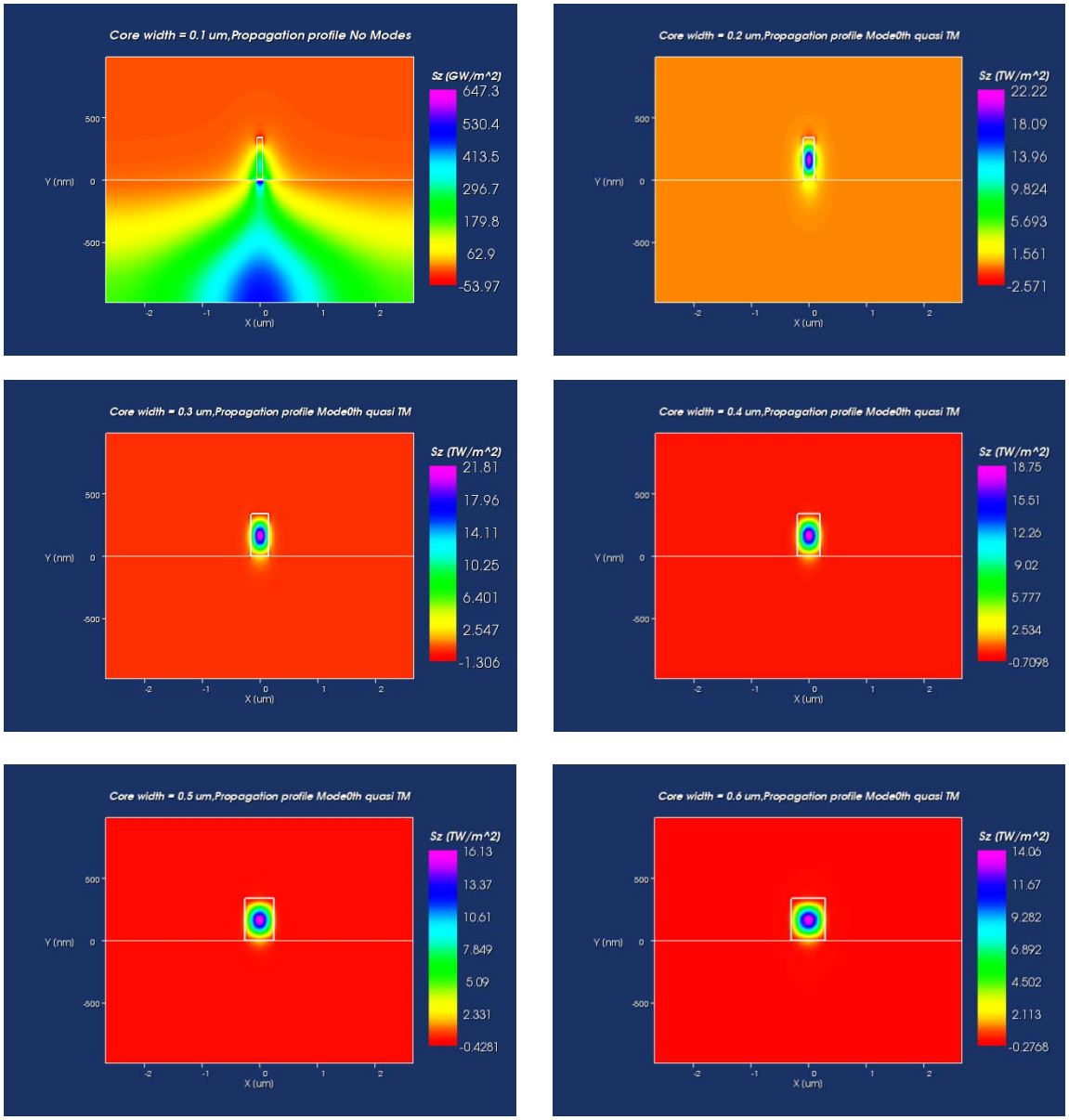

Figure 8.16: Propagation profiles for TM polarisation for core width in the range 100 nm to 600 nm.

In the case of TM polarisation, it has been shown that mode propagation starts at 0.14 μm, so it can be seen that the propagation for a 200 nm core width is still not completely confined in the core, and for 300 nm and so on the confinement is much better.

For TM polarisation the field dominant component is in the vertical component, so for the given height, “narrow” core shapes favour this polarisation.

On the other hand, TE polarisation starts at core widths that are more similar to the core height, giving place to “wide” core shapes. In our simulations, TE modes start to propagate at 0.25 μm, so for a 300 nm core width the field is stll starting to couple in the core, and for wider cores the confinement is much better.

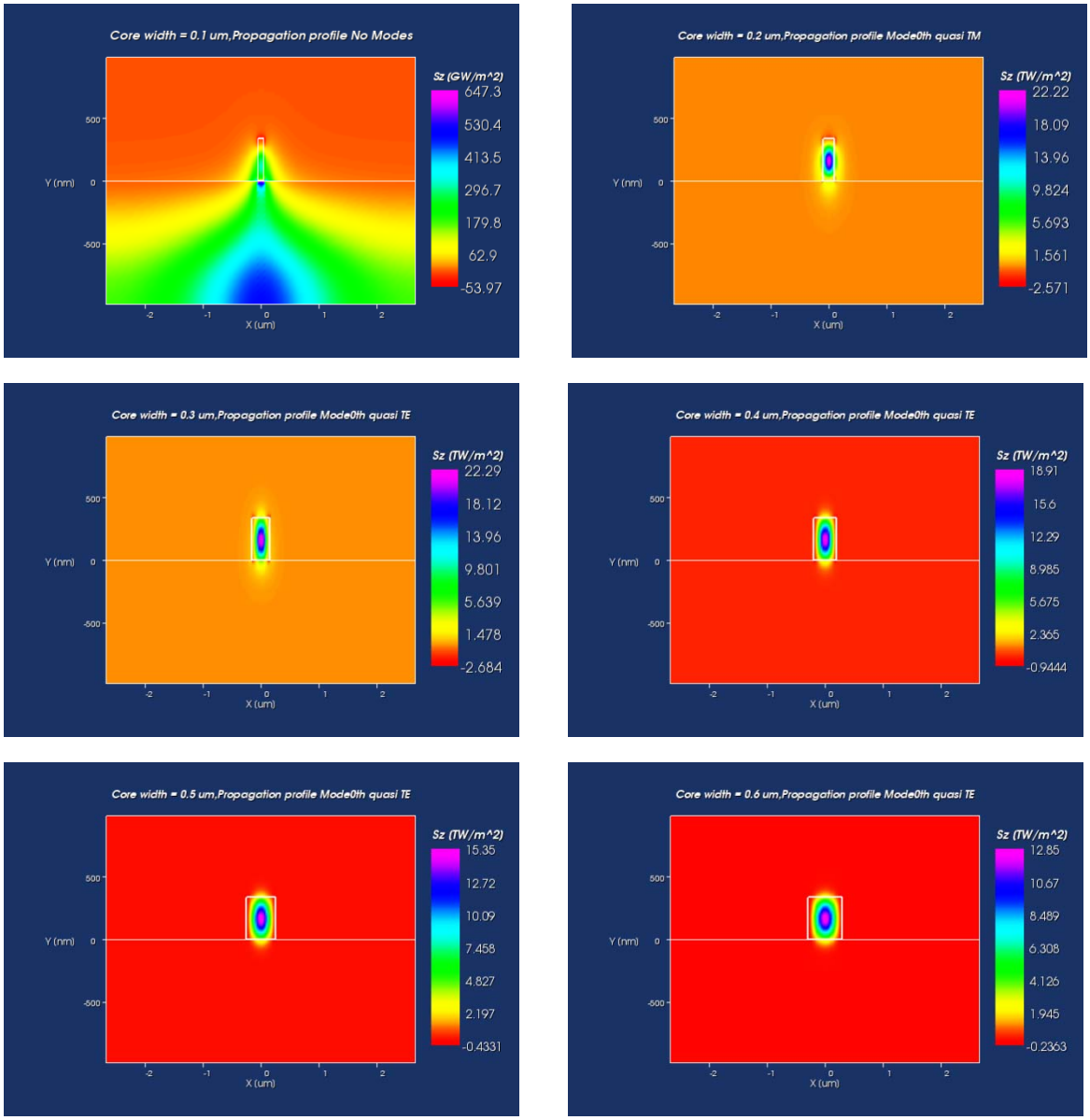

Figure 8.17: Propagation profiles for TE polarisation for core width in the range 100 nm to 600 nm.

8.2.4 Effective index

The effective indexes for the fundamental mode for every core width are shown in the Figure 8.18.

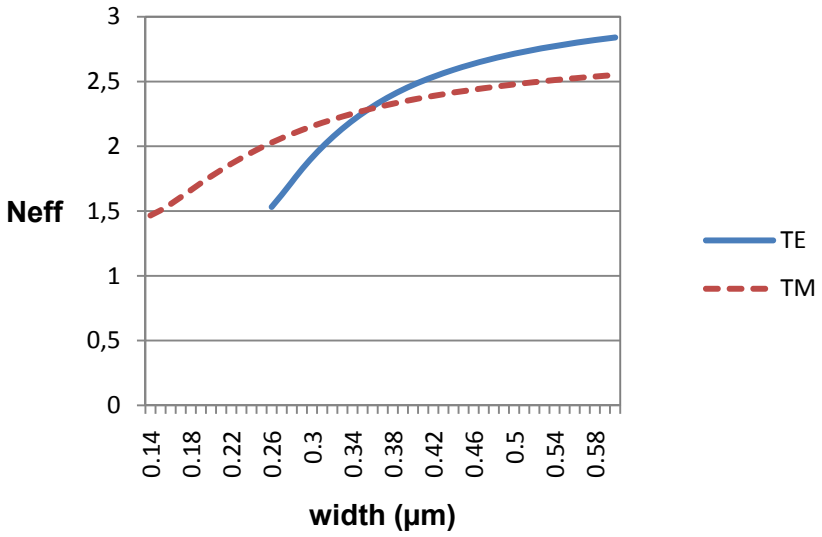

Figure 8.18: Effective index of the fundamental mode for both polarisations.

Propagation with effective indexes under the lowest refractive index of the structure (n_{Si} = 1.46) is not possible, so all the values are over this.

The TM mode propagation starts earlier, so the effective indexes are lower. Then the TE mode propagation starts, but there is a zone in which only TM propagation is allowed.

8.2.5 Confinement factor

The confinement factor of the field in the core and in the substrate has been calculated by means of the integral presented in equation 5.7 for both polarisations.

This calculation gives us an idea of how much power stays in the core and how much power couples into the core.

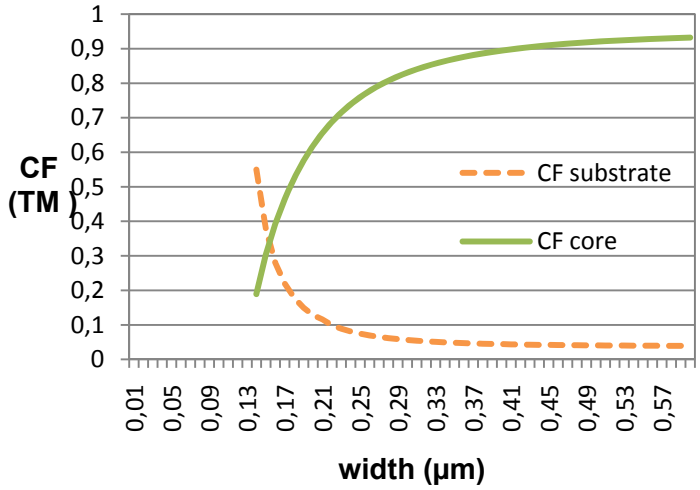

Figure 8.19: Confinement factor in the substrate and in the core for TM polarisation.

Figure 8.19 shows when the waveguide core is too narrow, much power still stays in the core, although there is TM propagation, and when it gets wider, power couples with much more intensity to the core, being the confinement factor in the core almost 1 in the end.

The same calculation has been performed for the TE polarisation. The results are presented in Figure 8.20.

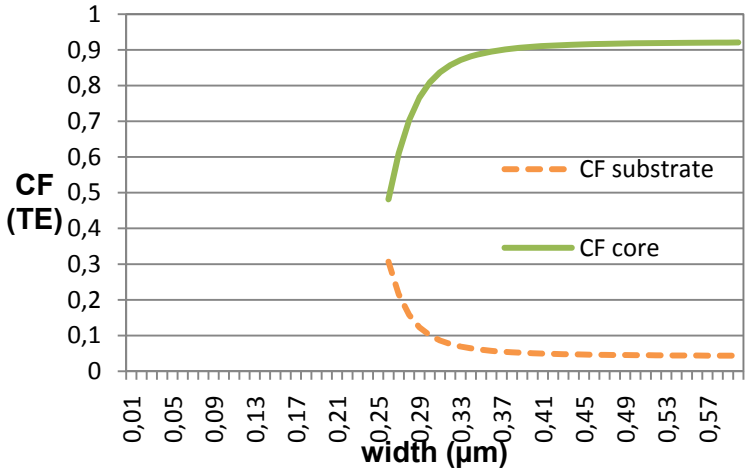

Figure 8.20: Confinement factor in the substrate and in the core for TE polarisation.

It shows that the wider the waveguide core is, the better the mode couples to the core.

Around the width that is chosen in our design (around 0.35 µm) light is well confined in the core.

8.2.6 Coupling losses

The coupling losses for the nano strip waveguide have been calculated with the overlap between the propagated mode and the fibre Gaussian field with MFD = 5 μm by means of equation 5.3 for core widths in the range from 100 nm to 600 nm. The results are presented in Figure 8.21.

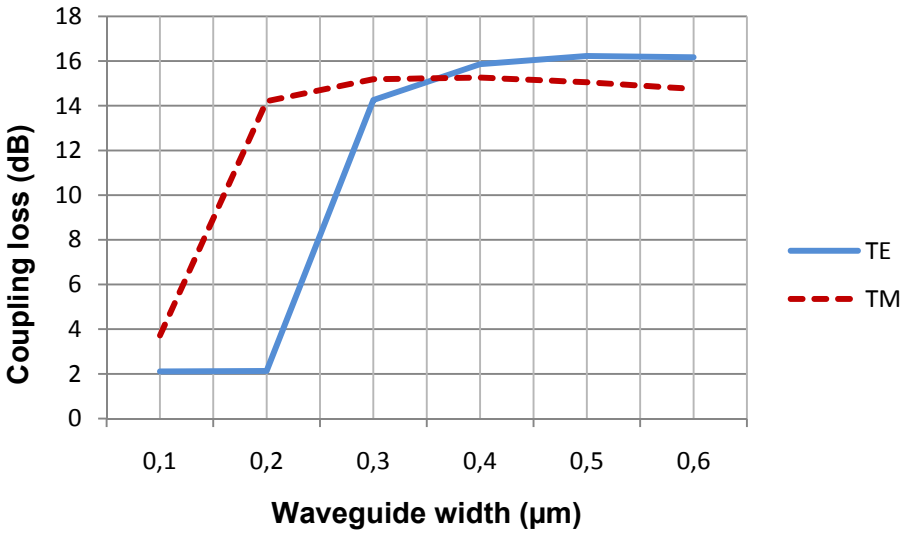

Figure 8.21: Coupling losses for TM and TE polarisation.

The interface loss has not been taken into account, because it can be avoided with an anti-reflection coating. This loss is calculated by means of equation 5.4 and is estimated to be around 3 dB when the coupling is performed on the SiO_2 layer.

This calculations show once again that direct butt coupling from fibre to waveguide is not a good technique, because coupling losses of about 15 dB are too high. This makes necessary to find a solution to better couple both devices. In the next Chapter a grating coupler for vertical coupling to fibre is studied.

Chapter 9

Grating coupler design and simulation

In this Chapter, grating coupler structures for both TE and TM polarisation are simulated, in order to find their optimal design parameters. [49, 50]

9.1 Structure description and design process

As described in Chapter 4, the grating coupler structure is composed of a corrugated silicon waveguide on top of a SiO_2 cladding or BOX. The height of the waveguide is 340 nm and the BOX thickness is equal to 2 μm. These settings correspond to a commercially available wafer. The number of periods is fixed to 22 to make sure that the corrugated surface is properly illuminated by the fibre. The width of the grating is 11 μm. A taper is placed at the output of the grating to reduce the mode dimensions from these 11 μm to the width of the strip nano waveguide, which is around 0.35 μm.

A side view of the grating is shown in Figure 9.1.

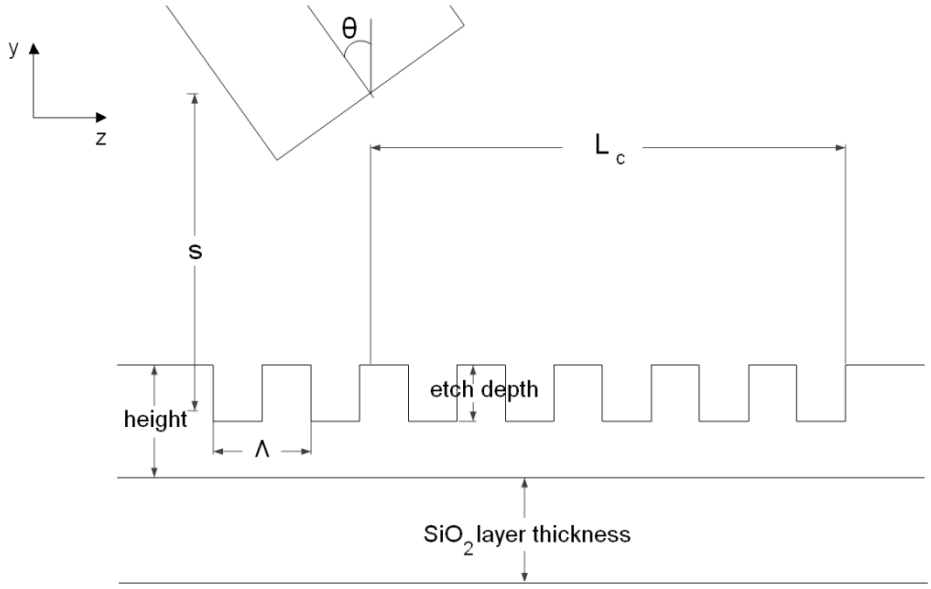

Figure 9.1: Grating coupler side view and optical fibre.

The fibre output field is approximated by a Gaussian field of MFD = 10 μm, as explained in Chapter 5. This field is either TE or TM polarized, with λ = 1.55 μm. The coupling angle, or angle of incidence, is fixed to 8º, to break symmetry (further details can be found in Chapter 5).

The field is launched at an horizontal distance to the end of the grating equal to the coupling length of equation 4.3, which is equal to 3.68 μm for both polarisations, and the vertical distance to the centre of the waveguide (s) is equal to 1 μm.

The Gaussian field is launched at this point, and then the power that reaches the output of the grating is measured, in order to obtain the efficiency. The whole structure is simulated with the FDTD algorithm exposed in Chapter 5, with a grid size of dx = dz = 0.01 μm. [49, 50]

The process followed to optimize the grating coupler is the following:

1- The optimal theoretical period is found by means of equation 4.4. The etch depth and filling factor are initially fixed to a given value, so a n_{eff} and a theoretical optimal period, Λ, are found. This n_{eff} depends on the polarisation.
2- The period is simulated around the theoretical optimal value in order to find the simulation optimal period. As the grid size is 10 nm, the period is varied in steps of 20 nm, so the half period varies in steps of the same size as the grid.
3- Once the optimal simulation period is found, the etch depth is varied to try to optimize the overlap at the output. The etch depth is varied in steps of 10 nm as well.
4- An spectral analysis is performed, to obtain the bandwidth of the structure.
5- The incidence angle is varied to obtain the alignment tolerances.

For every parameter, the margins in which the efficiency is reduced in either 1 dB or 3 dB are given, and noted as increments (Δ). In those cases in which the results are not symmetric with respect to the maximum, the smallest margin is given. Only the values that are bigger than the resolution of the simulation are taken into account.

9.2 TE grating coupler

A grating coupler for TE polarisation is designed in this section. Initially the etch depth is fixed to 100 nm and the filling factor to 0.5. With these parameters n_{eff} = 3.00606 and the period Λ_{theor} = 0.54 μm are obtained.

9.2.1 Optimal simulation period

As described in the previous section, the optimal theoretical period is found to be Λ_{theor} = 0.54 μm. Then a vary run on the period is performed in order to find the optimal period according to the simulation. This optimal period is found to be the same as the theoretical one, giving an efficiency around 18%, as shown in Figure 9.2.

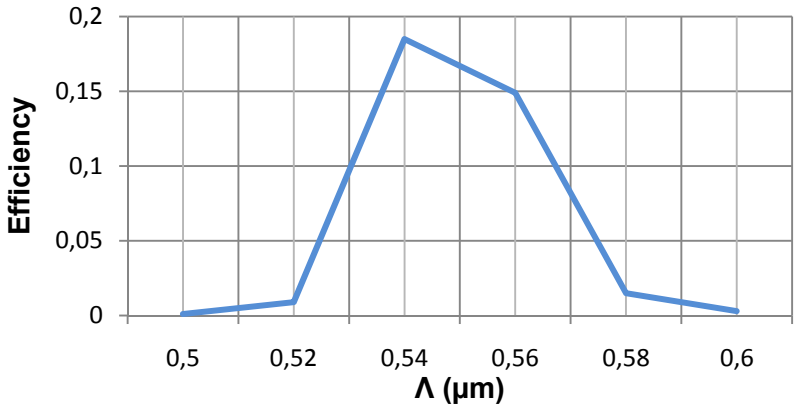

Figure 9.2: Optimal simulation period of the TE grating coupler.

The increment of the period that reduces the efficiency by 3 dB is $\Delta\Lambda_{3dB}$ = ± 10 nm.

9.2.2 Etch depth vary

Once the optimal simulation period is found, the etch depth (ed) of the grating is varied in order to optimize the efficiency of the structure. This etch is varied from 50 nm to 200 nm. The optimal etch depth is found to be 100 nm (its initial value). The result plot is shown in Figure 9.3.

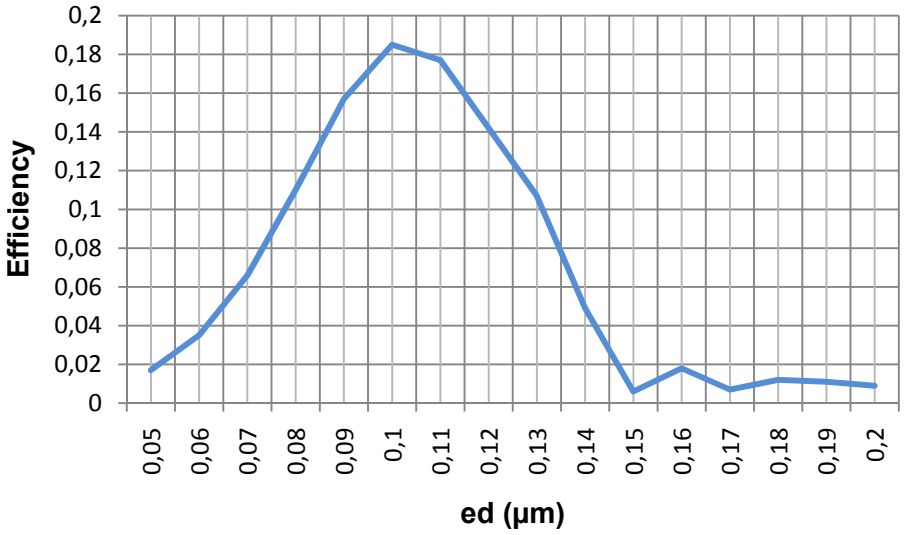

Figure 9.3: Optimal etching depth of the TE grating coupler.

If the grating is too shallow (the etch depth is too small) little light is coupled, and if the grating is too deep (the etch depth is too big) the same happens, because reflection increases, due to the fact that the incident beam does not “see” the silicon layer. So there is an optimal etching depth, that in our case is found to be 100 nm.

The increments in etching depth that reduce the efficiency by less than 1 dB and 3 dB with respect of the optimal value are, respectively, Δed_{1dB} = ± 10 nm and Δed_{3dB} = ± 20 nm.

9.2.3 Spectral response

In order to find the spectral response for both polarisations of the simulated structure, the wavelength is varied in the range 1.5-1.6 μm. The resulting plot is shown in Figure 9.4.

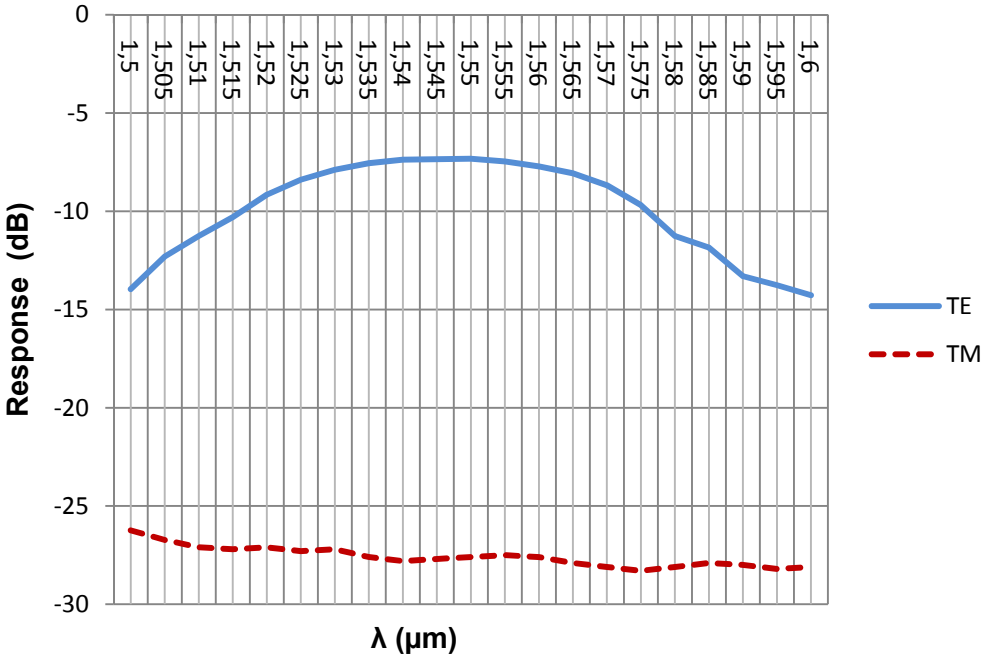

Figure 9.4: Spectral response of the TE grating coupler for both polarisations.

The losses at the central frequency of 1.55 μm are around 7 dB. The 1 dB bandwidth is found to be $\Delta\lambda_{1dB}$ = 40 nm. The 3 dB bandwidth is $\Delta\lambda_{3dB}$ = 60 nm. The response in the C-Band (1535 – 1570 nm), which is of much interest in most telecommunication applications, presents constant losses of under 1 dB respect to the peak value.

The TE–TM extinction ratio is found to be 20 dB in the central wavelength.

9.2.4 Alignment tolerances

The launch parameters, which are the angle of incidence and the horizontal and vertical coupling lengths, are varied in order to see how these variations would affect the coupling of the structure in case of misalignments.

The angle of incidence of the launched field (θ) is varied in order to find the alignment tolerances of the structure, that is, to what extent the output efficiency will decrease when the incidence angle is not the optimal one. This angle has been varied from 4º to 12º in steps of one degree.

The resulting plot is shown in Figure 9.5.

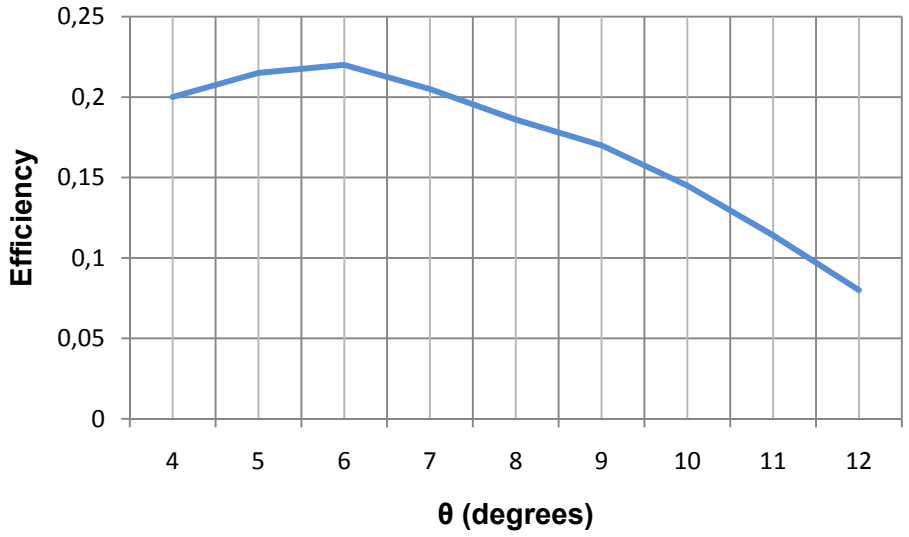

Figure 9.5: Angle tolerances of the TE grating coupler.

These results show that the grating coupler is quite robust to misalignments of the fibre. The design optimal angle was 8º. Slightly better efficiencies are achieved for 6º and 7º. The increment of the angle of incidence that reduces the efficiency by 3 dB with respect of the design angle is $\Delta\theta_{3dB} = \pm 3º$.

The coupling length in the z direction (L_c) is also varied in the range from 0 µm to 10 µm. The resulting plot is shown in Figure 9.6.

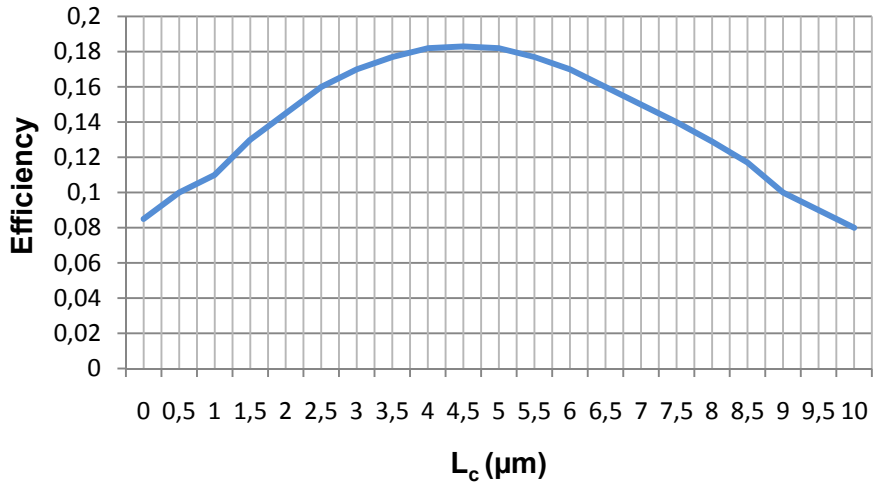

Figure 9.6: Coupling length in the z direction tolerances of the TE grating coupler.

The efficiency values in the whole simulated range stay bigger as half the maximal value, being $\Delta L_{c\ 1dB}$ = 5 µm, and $\Delta L_{c\ 3dB}$ = 10 µm. This optimal value was theoretically achieved for $L_{c,\ opt}$ = 3.68 µm. The efficiency stays more or less constant to coupling lengths up to 5 µm.

The coupling length in the y direction (s) is also varied in the range 0.5 µm to 5 µm, as shown in Figure 9.7.

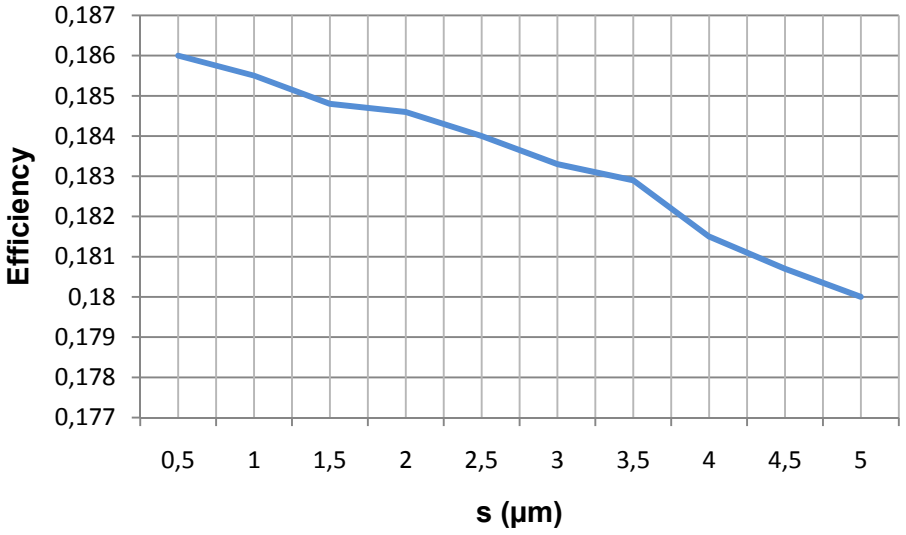

Figure 9.7: Coupling length in the y direction tolerances of the TE grating coupler.

The initial value was 1 µm. The efficiency value does not significantly change in all the range, showing that the device is robust to misalignments in the y direction.

9.2.5 Propagation and index profiles

Once the Te grating coupler has been simulated and its design parameters optimized, it is possible to obtain its index profile and a 2D plot of the propagation. Both plots are shown in Figures 9.8 and 9.9.

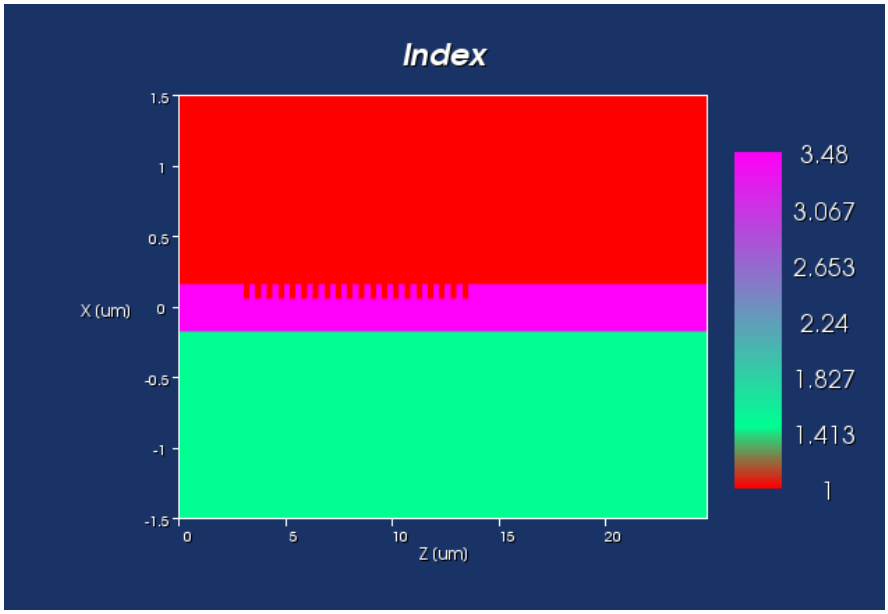

Figure 9.8: Index profile of the TE grating coupler.

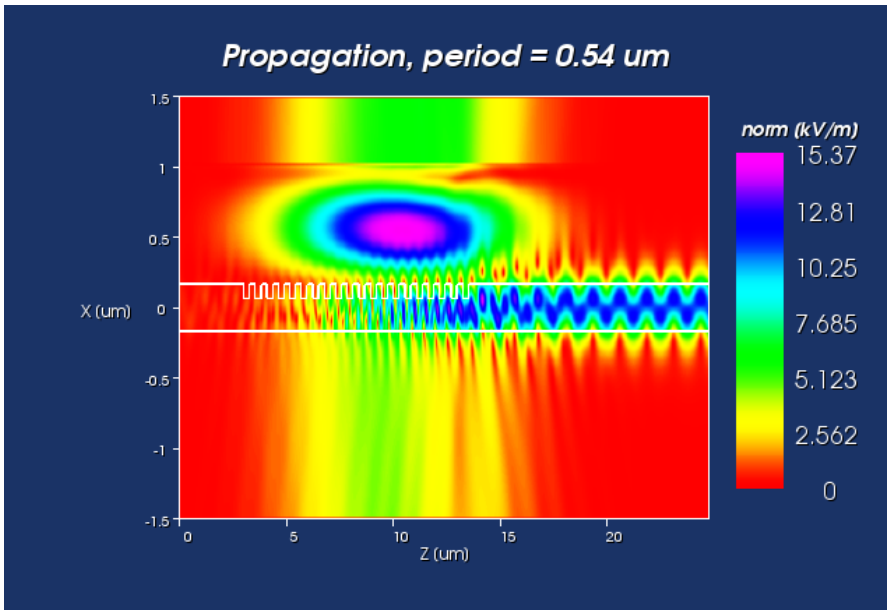

Figure 9.9: 2D propagation plot of the TE grating coupler.

In the propagation plot the E field is represented. It can be appreciated that some power couples to the output guide, and some other power leaks to the substrate.

9.3 TM grating coupler

A grating coupler for TM polarisation is designed in this section. Initially the etch depth is fixed to 70 nm and the filling factor to 0.5. With these parameters n_{eff} = 2.55844 and the period Λ_{theor} = 0.64 µm are obtained. It is important to notice that these parameters are different from those obtained in the case of TE polarisation.

9.3.1 Optimal simulation period

The design process is the same as in the case of the TE grating coupler. First of all, the optimal period according to the simulation is found. In this case, the optimal simulation period is found to be Λ_{theor} = 0.66 µm, and the efficiency around 8%, as shown in Figure 9.10.

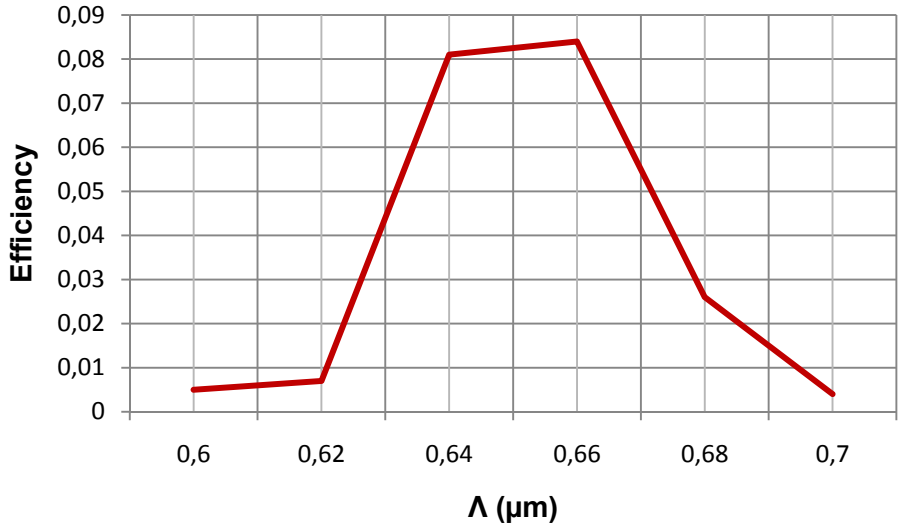

Figure 9.10: Optimal simulation period of the TM grating coupler.

The increment of the period that reduces the efficiency by 3 dB is $\Delta\Lambda_{3dB}$ = ± 10 nm.

9.3.2 Etch depth vary

The etching depth (ed) is varied from 50 nm to 200 nm as well, and the optimal in this case is found to be 80 nm. The resulting plot is shown in Figure 9.11.

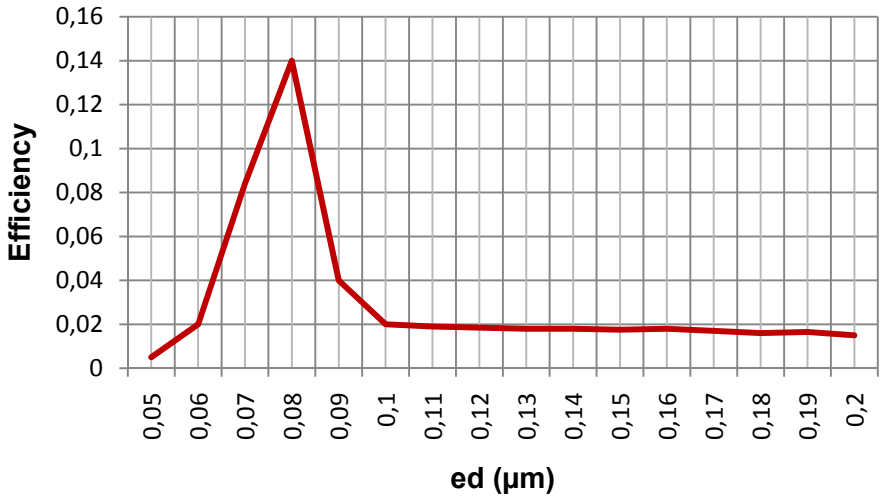

Figure 9.11: Optimal etching depth of the TM grating coupler.

As in the case of TE polarisation, there is an optimal etching depth that provides optimal coupling. In this case it is slightly smaller than for TE polarisation.

The increment of the etching depth that reduces the efficiency by less than 3 dB with respect of the optimal value is Δed_{3dB} = ± 10 nm.

9.3.3 Spectral response

In order to find the spectral response for both polarisations of the simulated TM grating coupler, the wavelength is varied in the range 1.5-1.6 μm. The resulting plot is shown in Figure 9.12.

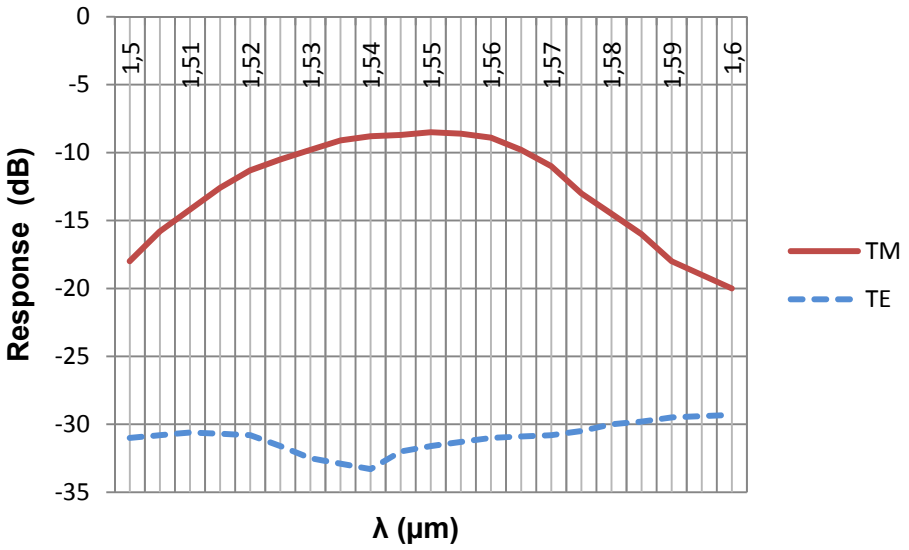

Figure 9.12: Spectral response of the TM grating coupler for both polarisations.

The losses at the central frequency of 1.55 μm are around 8.5 dB. The 1 dB bandwidth is found to be $\Delta\lambda_{1dB}$ = 30 nm. The 3 dB bandwidth is $\Delta\lambda_{3dB}$ = 50 nm. The response in the C-Band presents a constant flat shape, with maximal losses of around 2 dB respect to the peak value.

The TE–TM extinction ratio is found to be 23 dB in the central wavelength.

9.3.4 Alignment tolerances

In this section the main launch parameters are varied to see the effects of misalignments, just like in the case of the TE grating coupler.

The angle of incidence of the launched field (θ) is varied in order to find the alignment tolerances of the structure, that is, to what extent the output efficiency will decrease when the incidence angle is not the optimal one. This angle has been varied from 4º to 12º in steps of one degree.

The resulting plot is shown in Figure 9.13.

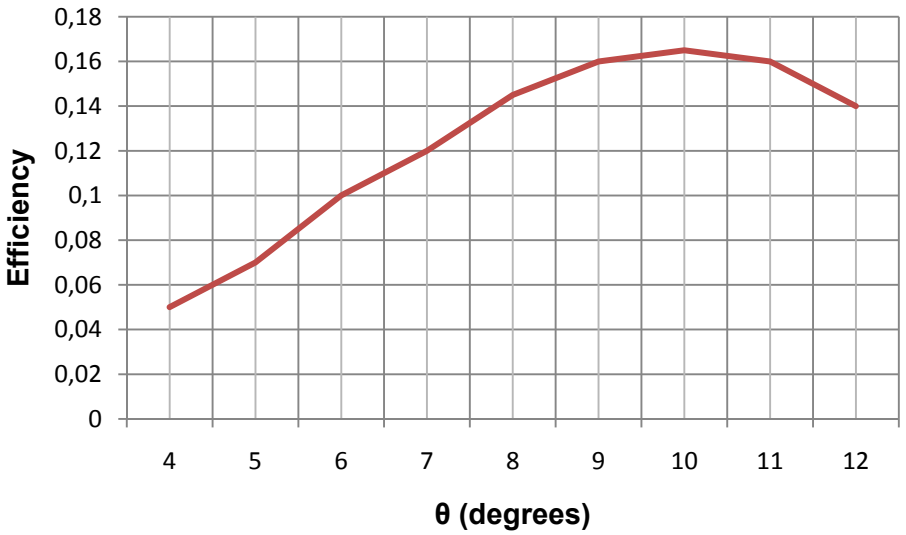

Figure 9.13: Angle of incidence tolerances of the TM grating coupler.

These results show that the grating coupler is quite robust to misalignments of the fibre. The grating was optimized for 8º, but in this case the maximal is slightly shifted as well, to achieve bigger efficiencies for 9º and 10º. The efficiency levels are relatively good for angles in the simulated range, and give an increment of the incidence angle for losses under 3 dB of $\Delta\theta_{3dB} = \pm 3º$. These results should be tested experimentally.

The coupling length in the z direction (L_c) is varied, as shown in Figure 9.14.

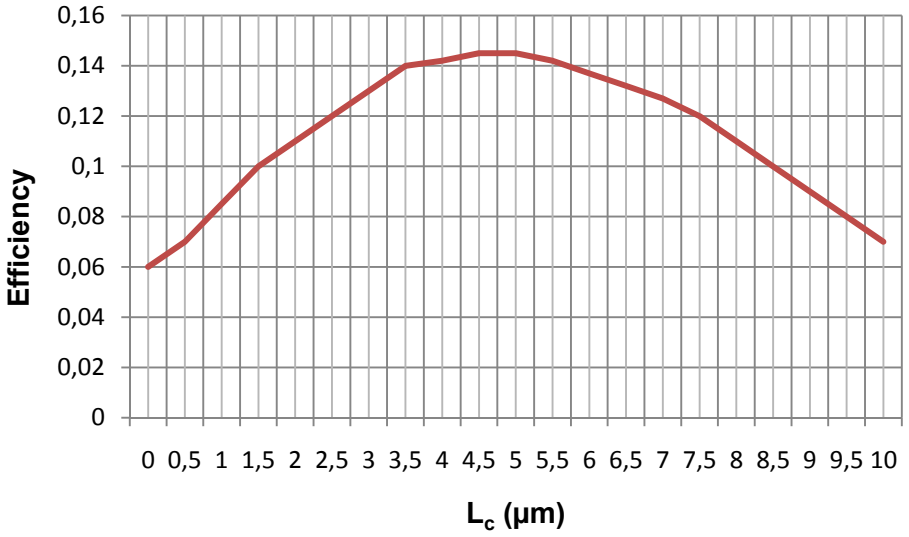

Figure 9.14: Coupling length in the z direction tolerances of the TM grating coupler.

The optimal theoretical horizontal coupling length was equal to $L_{c,\,opt}$ = 3.68 µm. The plot shows that the values between 3.5 µm and 5 µm provide efficiencies that are relatively similar and close to the optimal. The resultant increments of Lc are $\Delta L_{c\ 1dB}$ = 6 µm, and $\Delta L_{c\ 3dB}$ = 9 µm

The vertical coupling length (s) is varied too, as seen in Figure 9.15.

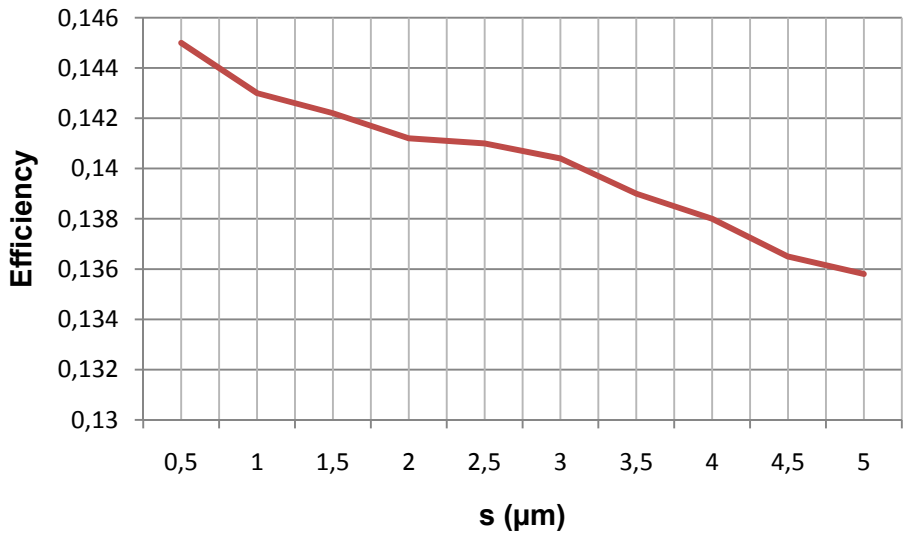

Figure 9.15: Coupling length in the y direction tolerances of the TM grating coupler.

The initial value was 1 µm. The efficiency values do not significantly decrease as the distance in the y direction increases.

9.3.5 Propagation and index profiles

Once the Te grating coupler has been simulated and its design parameters optimized, it is possible to obtain its index profile and a 2D plot of the propagation. Both plots are shown in Figures 9.16 and 9.17.

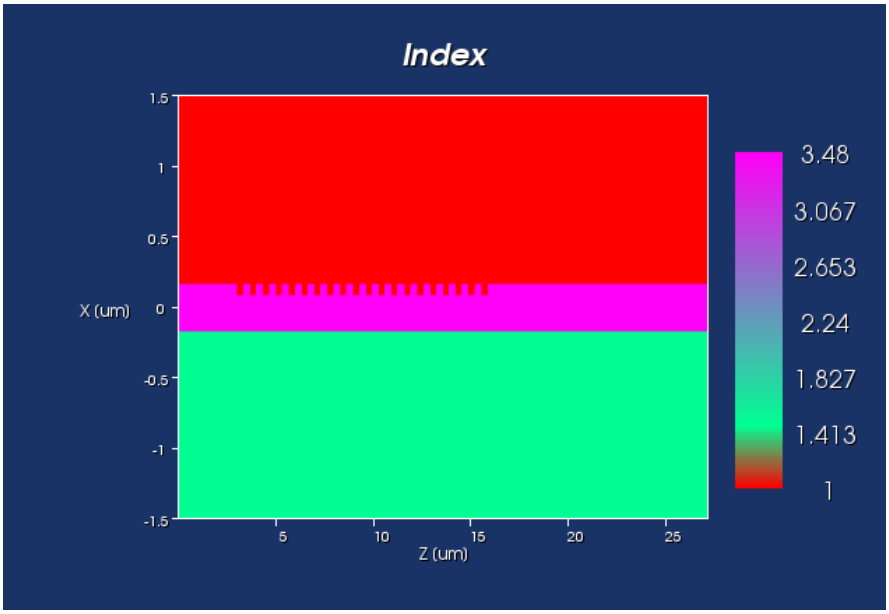

Figure 9.16: Index profile of the TM grating coupler.

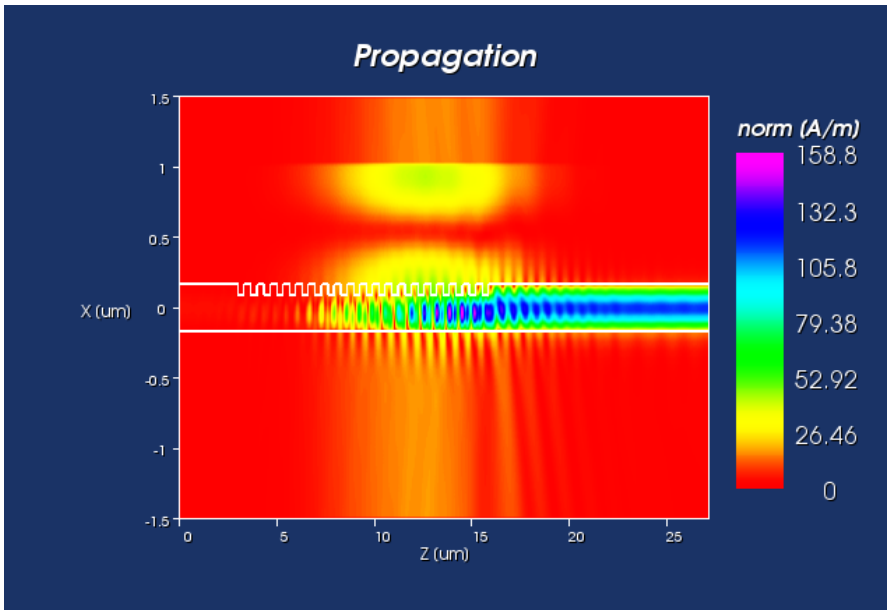

Figure 9.17: 2D propagation plot of the TM grating coupler.

For the TM propagation, the H field is represented. There is also power leakage to the substrate.

9.4 Crosstalk effects

In a totally integrated 3D packaging, it would be possible to have multi layered IC's, with waveguides and devices stacked or arrayed. Then the issue of crosstalk becomes of great importance. In this section we will study the effects that the power that leaks out of a grating coupler into the substrate may have in a waveguide that is directly underneath. A scheme of the situation is shown in Figure 9.18.

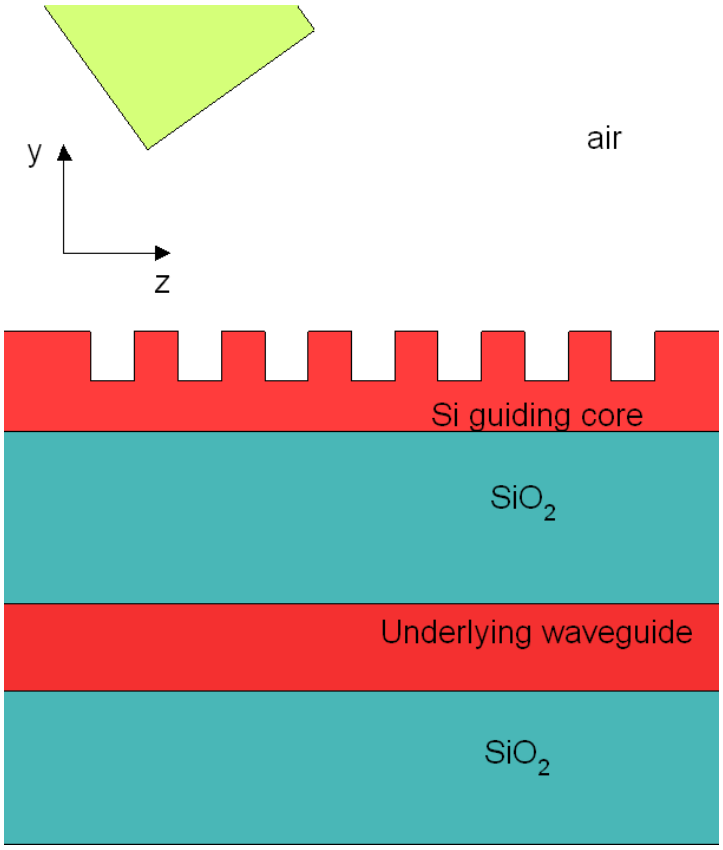

Figure 9.18: Crosstalk effects scheme.

First of all the crosstalk of two waveguides that are separated by a 2 μm SiO_2 cladding is simulated by launching a mode in the upper one and seeing if it couples to the lower one.

Then, the whole grating structure is simulated with the lower waveguide to see if there is any power that couples to it.

The study of the crosstalk effects is done for both polarisations.

9.4.1 Crosstalk effects for TE polarisation

As explained in the previous section, a mode is launched in the upper guide to see if some power couples to the lower one. A capture of the propagation is shown in Figure 9.19.

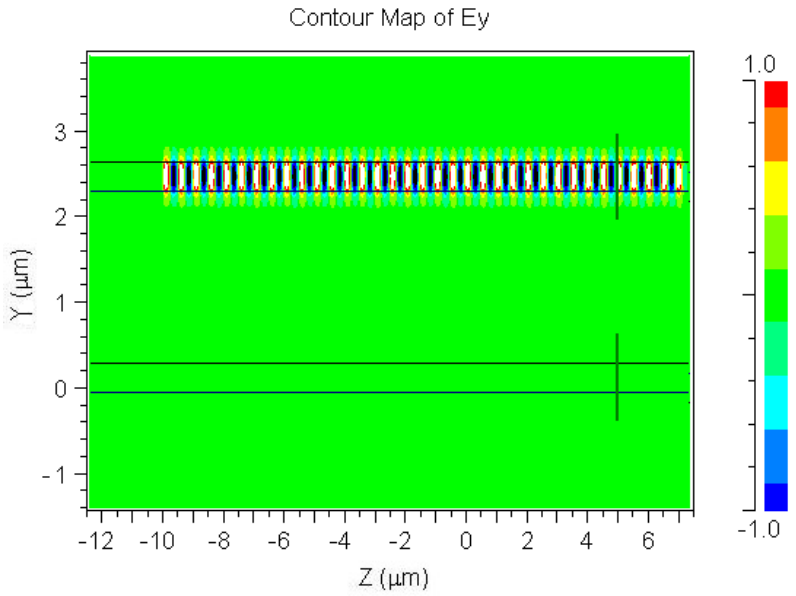

Figure 9.19: Mode propagation for TE.

It can be seen that all the power stays well confined in the upper guide, and no power couples to the lower one.

Then the structure with the grating is simulated, as shown in Figure 9.20. The plot represents the YZ plane and E field.

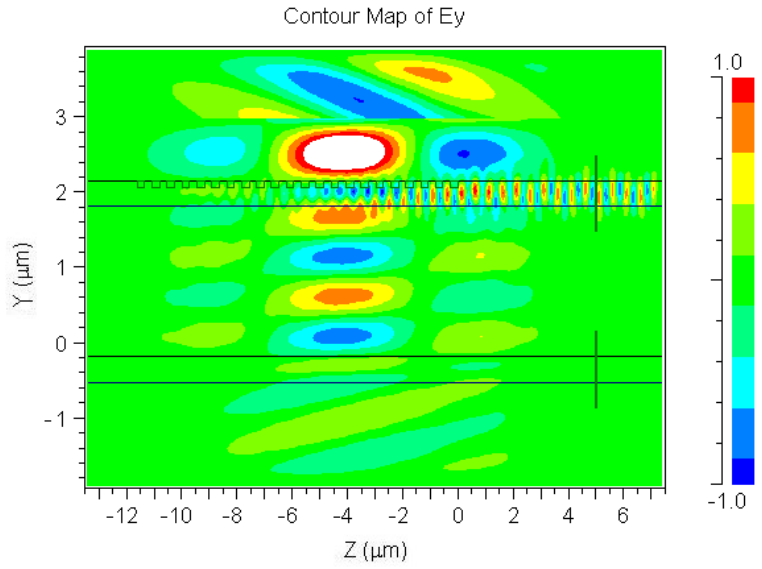

Figure 9.20: Crosstalk plot for TE grating coupler.

Power leaks down to the lower waveguide and crosses it without coupling to the output.

9.4.2 Crosstalk effects for TM polarisation

The same process is followed to find the crosstalk effects for the TM polarisation. A capture of the propagation is shown in Figure 9.21.

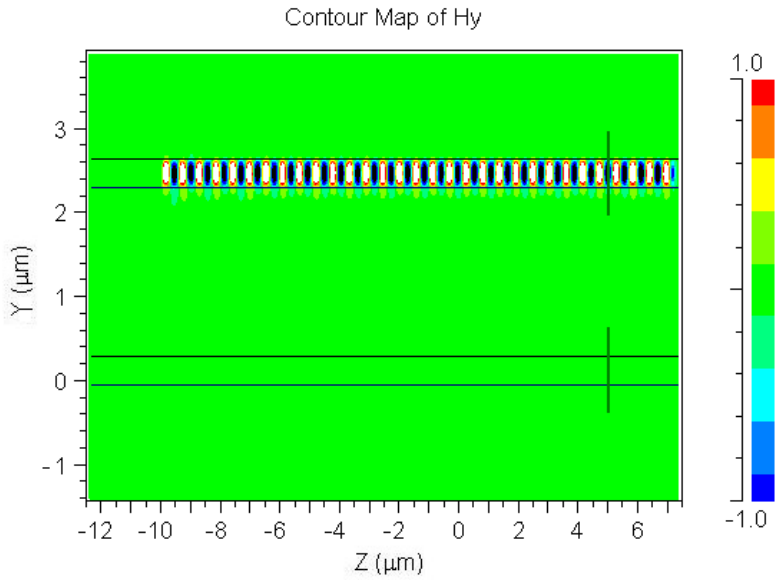

Figure 9.21: Mode propagation for TM.

The power remains well confined in this case as well.

Then the structure with the grating is simulated, as shown in Figure 9.22. It shows the YZ plane and H field.

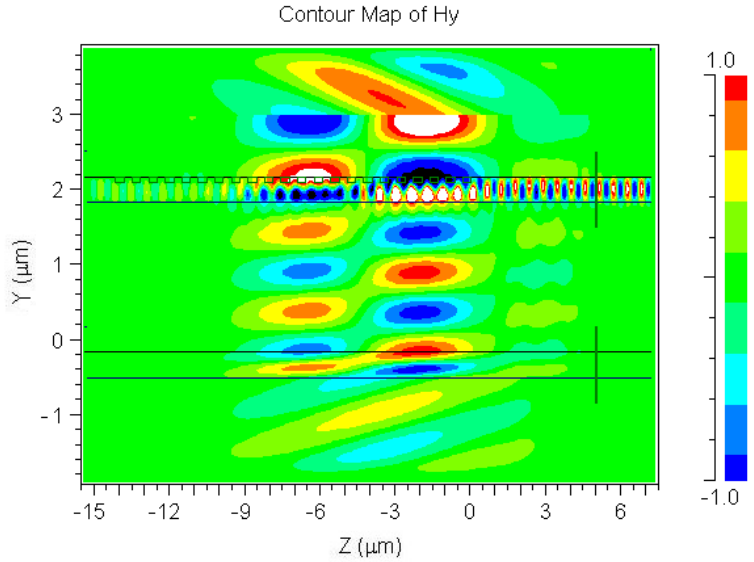

Figure 9.22:Crosstalk plot for TM grating coupler.

The power that is not coupled to the upper waveguide leaks down to the substrate without coupling to the lower waveguide. It can be concluded that there will not be any crosstalk effects for both polarisations.

9.5 Summarized results

Table 9.1 shows the main optimal design parameters of the grating couplers for both polarizations. Increments of the parameters that provide reductions in the efficiency of 1 dB or 3 dB are noted as $\Delta_{\text{-1dB}}$ and $\Delta_{\text{-3dB}}$ respectively.

Parameter	TE	TM
Silicon core height [μm]	0.34	0.34
SiO_2 layer thickness [μm]	2	2
Incidence angle (θ) [degrees]	8	8
Coupling length in the z direction (L_c) [μm]	3.68	3.68
Coupling length in the y direction (s) [μm]	1	1
Number of periods (N)	22	22
Grating width [μm]	11	11
Filling factor (ff)	0.5	0.5
Launched Gaussian field MFD [μm]	10	10
Effective index of the fundamental mode (n_{eff})	3.00606	2.55844
Theoretical optimal period (Λ_{theor}) [μm]	0.54	0.64
Simulated optimal period (Λ) [μm]	0.54	0.66
Period 3 dB increment ($\Delta\Lambda_{3dB}$) [nm]	±10	±10
Optimal etching depth [μm]	0.1	0.08
Etching depth 1 dB increment (Δed_{1dB}) [nm]	±10	-
Etching depth 3 dB increment (Δed_{3dB}) [nm]	±20	±10
Loss at central frequency [dB]	7	8.5
Central wavelength (λ) [nm]	1550	1550
1 dB bandwidth ($\Delta\lambda_{1dB}$) [nm]	40	30
3 dB bandwidth ($\Delta\lambda_{3dB}$) [nm]	60	50
Polarisation extinction ratio [dB]	20	23
Angle of incidence 3 dB tolerance ($\Delta\theta_{3dB}$) [degrees]	±3	±3
Coupling length in the z direction 1 dB tolerance ($\Delta L_{c\ 1dB}$) [μm]	±5	±6
Coupling length in the z direction 3 dB tolerance ($\Delta L_{c\ 3dB}$) [μm]	±10	±9

Table 9.1: Design parameters of the grating couplers for both polarisations

Chapter 10

Conclusions and future prospects

In this thesis, SOI single mode waveguides and grating couplers from fibre were designed and simulated. In this section the most relevant results and some future prospects that may help to improve the present structures are presented and discussed.

10.1 Conclusions

Optical interconnects are regarded as the key point to overcome the limitations of conventional electronic IC's. These interconnects have to be integrated in those chips. In this context, the System-in-Package (SiP) and the Silicon on Insulator (SOI) technologies arise as the optimal technologies to provide this integration.

In this thesis, single mode SOI nano waveguides have been designed and simulated, and their coupling to conventional optical fibres by means of a grating coupler has been studied.

Firstly, large single mode rib waveguides that had been studied since a long time ago have been studied. The direct butt coupling of optical fibres to those waveguides has been simulated, showing that the losses were too high, and making it necessary to find alternative solutions to the propagation and coupling of light in silicon.

To solve this issue, propagation using nano waveguides seems to be a suitable solution, providing high miniaturization and strong confinement of light. Our simulations show that, for the given commercially available wafer, a single mode propagation region for both polarisations exists, for core widths of several hundred of nanometers, providing good propagation characteristics.

Then, the problem of how to couple these waveguides to optical fibres has to be solved. This Thesis focuses in the design and simulation of a grating coupler for both TE and TM polarisations. Efficiencies of -7 dB and -8.5 dB are obtained respectively, with large bandwidths. Further improvements of these structures are presented in the next section. Although these losses can be highly improved, the main disadvantage that gratings still present with respect to other commercially available couplers, like tapered waveguides, is that the coupling scheme is more complicated and not so robust. The misalignment tolerances were also simulated.

Crosstalk, which is another important issue regarding integration into 3D environments, is also studied, showing that stacked waveguides and couplers do not suffer from crosstalk, which may make their performance worse.

Further measurements and experiments should be performed to test the behavior of these devices in real environments.

10.2 Future prospects

In the way to total photonic integration in silicon, more and more electro-optical and optical devices are being developed and presented. These include detectors, modulators, couplers and many others. The biggest challenge, however, still remains the production and integration of light emitting devices, such as lasers.

The last goal of this path would be having totally photonic-operated networks and IC's.

Concerning the nano waveguides that are studied in this work, the next steps will lead to further miniaturization and integration. To achieve these objectives the fabrication technologies and techniques have to be improved and fully developed. Plasmonics is a emerging technology that has made its appearance lately and promises new and exciting possibilities.

Regarding grating couplers, there are some improvements that have already been applied in order to reduce the losses that these kind of devices present, such as bottom mirrors or rear reflectors. These can be introduced in the basic structures that are presented in this Thesis to achieve better performances. Other structures, such as the 2D polarisation independent grating couplers, can be fabricated.

References

[1] T.Tekin, M.Töpper, H. Reichl., "PICSiP: New System-in-Package Technology Using A High Bandwidth Photonic Interconnection Layer For Converged Microsystems", Proc. SPIE, Vol.7366, 736618, 2009.

[2] W.Chen, W.R. Bottoms, K.Pressen, J.Wolf, "The next step in assembly and packaging: system level integration-SiP", International Technology Roadmap for Semiconductors http://www.itrs.net/Links/2007ITRS/LinkedFiles/AP/AP_Paper.pdf, 2009.

[3] N.M. Jokerst, M.A. Brooke, Sang-Yeon Cho, S. Wilkinson, M. Vrazel, S. Fike, J. Tabler, Yoong Joon Joo, Sang-Woo Seo, D. Scott Wills, and A. Brown., "The Heterogeneous Integration of Optical Interconnections Into Integrated Microsystems", IEEE Journal of Selected Topics in Quantum Electronics, vol.9, no.2, pp. 350-360, March/April 2003.

[4] Wei Koh, "System-in-Package (SiP) Technology Applications", 6th International Conference on Electronic Packaging Technology, pp. 61-66, September 2005.

[5] B.L. Weiss and R.A. Soref, "Introduction to the Issue on Silicon-Based Optoelectronics", IEEE Journal of Selected Topics in Quantum Electronics, Vol. 4, no. 6, November/December 1998.

[6] B. Jalali and S. Fathpour, "Silicon Photonics", Journal Of Lightwave Technology, Vol. 24, No. 12, pp. 4600-4615, December 2006.

[7] G.A. Keeler, "Optical Interconnects To Silicon CMOS Integrated Optoelectronic Modulators And Short Pulse Systems", Stanford University, PhD Thesis, December 2002.

[8] R.Soref, "The Past, Present and Future of Silicon Photonics", IEEE Journal Of Selected Topics In Quantum Electronics, Vol. 12, No. 6, pp. 1678-1687, November/December 2006.

[9] G.T.Reed and A.P.Khights, "Silicon photonics: an introduction", John Wiley&Sons,Ltd, 2004.

[10] W.Bogaerts, R.Baets,P.Dumon, V.Wiaux, S.Beckx, D.Taillaert, B.Luyssaert, , J.Van Campenhout, P.Bienstman and D.Van Thourhout, "Nanophotonic Waveguides in Silicon-on-Insulator Fabricated With CMOS Technology", Journal Of Lightwave Technology, Vol. 23, no. 1, pp. 401-412, January 2005.

[11] R.A. Soref, J. Schmidtchen, and K. Petermann, "Large Single-Mode Rib Waveguides in GeSi-Si and Si-on-SO2" , IEEE Journal Of Quantum Electronics. Vol. 27. no. 8, pp. 1971-1974, August 1991.

[12] S.P. Pogossian, L. Vescan, and A. Vonsovici, "The Single-Mode Condition for Semiconductor Rib Waveguides with Large Cross Section", Journal Of Lightwave Technology, Vol. 16, No. 10, pp. 1851-1853, October 1998.

[13] Qian Wang and Seng Tiong Ho, “Modal Analysis of Silicon Photonic Wire and TM pass Nanowaveguide Polarizer”, PhotonicsGlobal@Singapore, 2008. IPGC 2008. IEEE, pp. 1-4, December 2008.

[14] Yu. A. Vlasov and S.J. McNab, “Waveguiding in Silicon-on-Insulator Photonic Crystal and single mode strip waveguides”, The 17th Annual Meeting of the IEEE Lasers and Electro-Optics Society, Vol.2, pp. 809-810, November 2004.

[15] Yu. A. Vlasov and S.J. McNab, “Losses in single-mode silicon-on-insulator strip waveguides and bends”, Optical Society of America, 2004.

[16] T.Tsuchizawa, K.Yamada, H.Fukuda, T.Watanabe, J.Takahashi, M.Takahashi,T.Shoji, E.Tamechika, S.Itabashi and H.Morita, “Microphotonics Devices Based on Silicon Microfabrication Technology”, IEEE Journal Of Selected Topics In Quantum Electronics, Vol. 11, no. 1, pp.232-240, January/February 2005.

[17] L. Vivien, F. Grillot, E. Cassan, D. Pascal, S. Lardenois, A. Lupu, S. Laval, M. Heitzmann, J.-M. Fédéli, “Comparison between strip and rib SOI microwaveguides for intra-chip light distribution”, Optical Materials 27 (2005), pp.756–762, October 2004.

[18] C. Angulo Barrios, V. R. Almeida,R. Panepucci and M. Lipson, “Electrooptic Modulation of Silicon-on-Insulator Submicrometer-Size Waveguide Devices”, Journal Of Lightwave Technology, Vol. 21, no. 10, pp. 2332-2339,October 2003.

[19] D. Van Thornhout, P.Dumon, W.Bogaerts, G.Roelkens, D.Taillaert, G.Priem, R.Baets, “Recent Progress in SOI Nanophotonic Waveguides”, ECOC 2005 Proceedings, Vol.2, pp.241-244, 2005.

[20] C. Gunn, “Fully Integrated VLSI CMOS and Photonics”, IEEE Symposium on VLSI Technology 2007, pp.6-9, June 2007.

[21] V.R. Almeida, R.R. Panepucci, M.Lipson, “Nanotaper for compact mode conversion”, Optics Letters, Vol. 28, no. 15, pp.1302-1304, August 2003.

[22] Zheng Wang, “Design and simulation of spot-size converter for photonic integrated System-in-Package”, TU Berlin, Research Center of Microperipheric Technologies, Master Thesis, 2010.

[23] D.Taillaert, “Grating couplers as Interface between Optical Fibres and Nanophotonic Waveguides”, Ghent University, PhD Thesis, June 2004.

[24] J. V. Galan, P. Sanchis, J. Blasco, and J. Marti, “Study of High Efficiency Grating Couplers for Silicon-Based Horizontal Slot Waveguides”, IEEE Photonics Technology Letters, Vol. 20, no. 12, pp.985-987, June 2008.

[25] Laurent Vivien, Daniel Pascal, Sebastien Lardenois, Delphine Marris-Morini, Eric Cassan, Frédéric Grillot, Suzanne Laval, Jean-Marc Fédéli, and Loubna El Melhaoui, “Light Injection in SOI Microwaveguides Using High-Efficiency Grating Couplers”, Journal Of Lightwave Technology, Vol. 24, no. 10, pp.3810-3815, October 2006.

[26] Xuejun Xu, Shaowu Chen, Jinzhong Yu and Xiaoguang Tu, “An investigation of the mode characteristics of SOI submicron rib waveguides using the film mode matching method”, J. Opt. A: Pure Appl. Opt. 11 (2009) 015508 (7pp), December 2008.

[27] Aasmund Sv Sudbø, “Film mode matching: a versatile numerical method for vector mode field calculations in dielectric waveguides”, Pure Appl. Opt. 2 (1973) 211-233, September 1992.

[28] K.Kawano and T. Kitoh, “ Introduction to Optical Waveguide Analysis: Solving Maxwell’s Equations and the Schrödinger Equation”, John Wiley & Sons, 2001.

[29] S.T. Chu and S.K. Chaudhuri, “Finite Difference Time-Domain Method for Optical Waveguide Analysis”, Progress in Electromagnetic Research, Pier 11, 255-300, 1995.

[30] Rose M. Joseph and Allen Taflove, “FDTD Maxwell’s Equations Models for Nonlinear Electrodynamics and Optics”, IEEE Transactions On Antennas And Propagation, Vol. 45, No. 3, pp. 364-374, March 1997.

[31] J.P. Berenger, “A Perfectly Matched Layer for the Absorption of Electromagnetic Waves”, Journal of Computational Physics 114, pp. 185-200, 1994.

[32] A. G. Rickman, G. T. Reed, and F. Namavar, “Silicon-on-Insulator Optical Rib Waveguide Loss and Mode Characteristics”, Journal Of Lightwave Technology, Vol. 12, no.10, pp.1771-1776, October 1994.

[33] A. F. Evans and D. G. Hall ,“Propagation loss measurements in silicon-on-insulator waveguides formed by the bond and etch back process”, University of Rochester, July 1991.

[34] M Bruel, B Aspar and A-J Auberton-Herv´e (1997) ‘Smart-Cut: A new silicon on insulator material technology based on hydrogen implantation and wafer bonding’, Jpn J. Appl. Phys., Vol. 36, pp. 1636–1641, November 1997.

[35] L. Zimmermann, M. Schnarrenberger, T. Mitze, J. Bruns, K. Petermann, „Study of Reactive Ion Etched (RIE) Facets of Silicon-on-Insulator (SOI) Rip Waveguides”, IEEE International SOI Conference 1998 Proceedings, pp. 15-16, October 1998.

[36] K.K. Lee, D.R. Lim, Hsin-Chiao Luan, A. Agarwal, J. Foresi and L.C. Kimerling, “Effect of size and roughness on light transmission in a Si/SiO2 waveguide: Experiments and model”, Applied Physics Letters, Vol. 77, no. 11, pp. 1617-1619, September 2000.

[37] F.Van Laere, G.Roelkens, M.Ayre, J.Schrauwen, D.Taillaert, D. Van Thourhout, T.F. Krauss, and R.Baets, “Compact and Highly Efficient Grating Couplers Between Optical Fibre and Nanophotonic Waveguides”, Journal Of Lightwave Technology, Vol. 25, no. 1, pp.151-156, January 2007.

[38] F. Van Laere, G. Roelkens, J. Schrauwen, D. Taillaert, P. Dumon, W. Bogaerts, D. Van Thourhout and R. Baets, “Compact grating couplers between optical fibres and Silicon-on-Insulator photonic wire waveguides with 69% coupling efficiency”, Optical Society of America, 2006.

[39] A. Narasimha and E. Yablonovitch, “Efficient optical coupling into single mode Silicon-on-Insulator thin films using a planar grating coupler embedded in a high index contrast dielectric stack”, Optical Society of America, 2002.

[40] S.Scheerlinck, J.Schrauwen, F.Van Laere, D.Taillaert, D.Van Thourhout and R.Baets, “Efficient, broadband and compact metal grating couplers for silicon-on-insulator waveguides”, Optical Society of America, 2007.

[41] Masayuki Matsumoto, “Analysis of the Blazing Effect in Second-Order Gratings”, IEEE Journal Of Quantum Electronics, Vol. 28. no.10, pp. 2016-2023, October 1992.

[42] F.Van Laere, M.V. Kotlyar, D.Taillaert, D.Van Thourhout, T.F. Krauss, and R.Baets, “Compact Slanted Grating Couplers Between Optical Fibre and InP–InGaAsP Waveguides”, IEEE Photonics Technology Letters, Vol. 19, no. 6, pp.396-398, March 2007.

[43] X. Chen, C. Li and H. K. Tsang, “Characterization of Silicon-on-Insulator Waveguide Chirped Grating for Coupling to a Vertical Optical Fibre”, IEEE 978-1-4244-1918-0/08, 2008.

[44] Xia Chen, Chao Li, and Hon Ki Tsang, “Fabrication-Tolerant Waveguide Chirped Grating Coupler for Coupling to a Perfectly Vertical Optical Fibre”, IEEE Photonics Technology Letters, Vol. 20, no. 23, pp. 1914-1916, December 2008.

[45] F.Van Laere, T.Stomeo, D.Taillaert, G.Roelkens, D.Van Thourhout, T.F. Krauss, and R.Baets, “Efficient Polarisation Diversity Grating Couplers in Bonded InP-Membrane”, IEEE Photonics Technology Letters, Vol. 20, no. 4, pp. 318-320, February 2008.

[46] F.Van Laere, W.Bogaerts, P.Dumon, G.Roelkens, D.Van Thourhout and R.Baets, “Focusing Polarisation Diversity Grating Couplers in Silicon-on-Insulator”, Journal Of Lightwave Technology, Vol. 27, no. 5, pp. 612-618, March 2009.

[47] L.Vivien, G.Maire, G.Sattler, D.Marris-Morini, E.Cassan, S.Laval, “A high efficiency silicon nitride grating coupler”, IEEE 1-4244-0935-7107, 2007.

[48] Chubing Peng and W.A Challener, “Input-grating couplers for narrow Gaussian beam: influence of groove depth”, Optical Society of America, 2004.

[49] RSoft Design Group,Inc, FullWave manual.

[50] User manual Phoenix Software, Phoenix BV.